Dynamique de spin dans les structures semi-conductrices de basses dimensions

Mateusz Goryca

University of Warsaw

Université de Grenoble

Mateusz Goryca

Spin dynamics in low-dimensional semiconductor structures

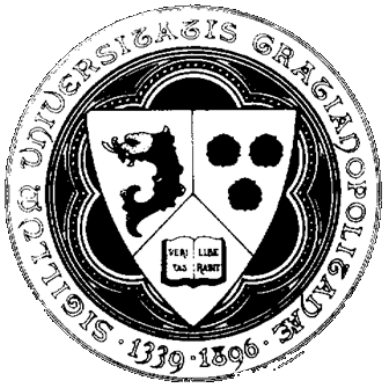

PhD thesis supervised by

dr hab. Piotr Kossacki and dr Marek Potemski

30.11.2011

I dedicate this thesis to Professor Jan Gaj.

Acknowledgements

Here I would like to thank all the people who helped and supported me during my doctoral study. First of all, I would like to thank my PhD supervisors - Piotr Kossacki and Marek Potemski. I highly appreciate their support and care during my study, their advice and discussions. Thank you Piotr for forcing me into making an effort to understand physics.

I thank all my colleagues form research groups of Prof. Jan Gaj at the University of Warsaw and Dr. Marek Potemski at Grenoble High Magnetic Field Laboratory. In particular I thank Tomek Kazimierczuk for priceless help in the experimental work and fruitful discussions about results and interpretation. I thank Paulina Płochocka for great help with the high magnetic field experimental setup and long measurements. I also thank her and Duncan Maude for fantastic hospitality in Grenoble. I appreciate help and patience of Ivan Breslavetz, without whom the experimental work would be much more painful than it was.

It is my pleasure to thank Dr. Denis Scalbert and Dr. hab. Adam Babiński for agreement to be the referees of my manuscript and Prof. Joël Cibert and Prof. Andrzej Wysmołek for the acceptance to participate in my jury.

I thank Dr. Piotr Wojnar form Polish Academy of Sciences and Prof. Joël Cibert for the samples and helpful discussions about physics.

I would like to thank Andrzej Golnik, Tomek Jakubczyk, Wojtek Pacuski, Asia Papierska, Jan Suffczyński and all other colleagues form University of Warsaw for creating great atmosphere in the lab. I also thank Clément Faugeras, Aurélien Nicolet and Benjamin Piot from

Grenoble High Magnetic Field Laboratory for their hospitality and a lot of help with French paperwork.

I would like to thank all my other friends from University of Warsaw and Grenoble High Magnetic Field Laboratory, who were not involved in my research, but with whom I have spent this great time: Monika Bajda, Asia Bartoszek, Ania Korbecka, Jan Kunc, Petr Neugebauer and all the others.

I would also like to express my gratitude to my loving parents for their constant support.

Thank you!

Abstract / Résumé / Streszczenie

Abstract

This work is devoted to the studies of spin dynamics of magnetic Mn^{2+} ions embedded in low-dimensional CdTe-based nanostructures. The particular emphasis is focused on the system of single CdTe quantum dots with single Mn^{2+} ions, which give an insight into unperturbed interactions of magnetic ion with its semiconductor environment. A method of all-optical manipulation and readout of the spin state of a single magnetic ion is presented. The experiment exploits the spin-conserving exciton transfer between neighbouring quantum dots to inject polarized exitons into the dot with the Mn^{2+} ion and to orient its spin. The dynamics of the orientation process is measured in a time-resolved experiment and described with a simple rate equation model. One of possible orientation mechanisms - the dark excitons recombination - is discussed and shown experimentally. The optical orientation of the Mn^{2+} ion is also used to investigate the spin-lattice relaxation of an isolated magnetic ion in low and high magnetic field.

The work also addresses phenomena occurring in low and zero magnetic field in large systems of magnetic moments - quantum wells and quantum dots containing Mn^{2+} ions. New experimental technique of fast magnetic pulses is used to investigate the Mn^{2+} electronic spin dynamics in the absence of magnetic field with nanosecond resolution. After the pulse of magnetic field, a fast decay of the magnetization is observed. The experimental findings are described in terms of hyperfine coupling with the nuclear spin of the Mn^{2+} ions. The effect is highly sensitive to the presence of an anisotropy, particularly the one introduced by hole gas and by strain. Application of the external magnetic field suppresses the fast dynamics in diluted magnetic quantum

wells and well known, slow spin-lattice relaxation is observed. Surprisingly, quantum dots with many Mn^{2+} ions show fast spin dynamics even after application of external field, up to 0.5 T. The fast process may origin from the spin-spin interaction between the magnetic ions, especially if their spatial distribution within the dot is not uniform.

The work is organized in following way:

- In chapter 1 I briefly present a short introduction into the subject: description of basic properties of diluted magnetic semiconductors ($Cd_{1-x}Mn_xTe$ in particular) and low-dimensional semiconductor structures - quantum wells and quantum dots - containing magnetic ions. Current level of knowledge on spin dynamics in such systems is presented. The aim of this work is also defined.
- Chapter 2 contains description of the samples used in this work. Both the growth techniques and the basic properties of quantum wells and quantum dots are presented.
- Chapter 3 presents standard experimental techniques, commonly used in optical studies of semiconductor nanostructures. Micro photoluminescence, single photon correlation and spectroscopy in high magnetic field are discussed.
- A new experimental technique of fast magnetic pulses is presented in chapter 4. The pulses of magnetic field are generated by a miniature magnetic coil placed directly on a sample surface.
- Chapter 5 describes the experiment of optical spin manipulation of a single Mn^{2+} ion embedded in the CdTe quantum dot. The dynamics of the orientation process was measured in a time-resolved experiment and described with a simple rate equation model.
- One of possible Mn^{2+} orientation mechanisms is discussed in chapter 6. The dark excitons optical transitions, which are allowed due to the presence of a magnetic impurity in the dot, can

efficiently induce the Mn^{2+} polarization.

- Chapter 7 describes investigation of the spin relaxation for systems of single and many magnetic ions, in both high and low magnetic field. In the case of a single Mn^{2+} ion in a quantum dot it was possible to measure pure spin-lattice relaxation, unperturbed by the spin-spin interaction. In the case of diluted magnetic quantum wells a fast spin dynamics in the complete absence of the magnetic field was observed.
- The last chapter 8 contains the summary of the work. Perspectives of future research in the fields discussed in this work are briefly presented.

Résumé

Ce travail présente l'étude de la dynamique de spins d'ions Mn^{2+} insérés dans des structures de CdTe de faibles dimensions. L'accent est plus particulièrement mis sur des boîtes quantiques individuelles de CdTe contenant un ion Mn^{2+} unique, ce qui permet d'accéder aux interactions non perturbées de l'ion magnétique avec son environnement semi-conducteur. Nous présentons une méthode purement optique de manipulation et de lecture des états de spin de l'ion magnétique unique. Les expériences utilisent le fait que les états de spin se conservent lors d'un transfert excitonique entre proches boîtes quantiques, pour injecter un exciton polarisé dans la boîte contenant l'ion Mn^{2+} afin d'orienter son spin. Les dynamiques de processus de réorientation sont observées lors de mesures résolues en temps, puis analysées via un modèle simple d'équations de taux. Un des mécanismes possible de réorientation, la recombinaison d'excitons sombres, est présenté expérimentalement, puis discuté. L'orientation optique de l'ion Mn^{2+} est aussi utilisée pour étudier les relaxations spin-réseau d'un ion magnétique isolé sous faibles et sous forts champs magnétiques.

Ce travail décrit aussi les phénomènes présents pour des champs magnétiques nuls ou faibles dans des systèmes de moments magnétiques plus grands (puits et boîtes quantiques contenant plusieurs ions Mn^{2+}). Une nouvelle technique expérimentale, basée sur des impulsions magnétiques rapides, nous permet d'étudier la dynamique de spin des ions Mn^{2+} en l'absence de champ magnétique et ce, avec une résolution temporelle de l'ordre de la nanoseconde. Nous observons une rapide décroissance de la magnétisation après une impulsion magnétique. Le phénomène est décrit en terme de couplage hyperfin avec le spin nucléaire des ions Mn^{2+}. Cet effet est particulièrement sensible à toute anisotropie, notamment celles introduites par un gaz de trous ou par le contrainte du réseau. L'application d'un champ magnétique externe supprime les dynamiques rapides dans les puits quantiques magnétiques dilués et des phénomènes plus commun de relaxation

lente spin-réseau sont alors observés. Il est toutefois surprenant que les boîtes quantiques avec un grand nombre d'ions Mn^{2+} présentent ces dynamiques de spin rapides même après application d'un champ magnétique allant jusqu'à 0.5 T. Ce processus rapide pourrait venir des interactions spin-spin des ions Mn^{2+}, en particulier si leur distribution spatiale n'est pas régulière à l'intérieur de la boîte.

Cette étude est organisée de la manière suivante:

- Le Chapitre 1 présente une brève introduction au sujet: la description des propriétés fondamentales des semiconducteurs dilués magnétiques (en particulier les alliages de $Cd_{1-x}Mn_xTe$) et des structures semiconductrices de basse dimensionnalité - puits et boîtes quantiques - contenant des impuretés magnétiques. L'état de l'art concernant la dynamique de spin dans de tels systèmes est présenté. Le but de cette étude est ensuite défini.
- Le Chapitre 2 est consacré à la description des échantillons utilisés dans cette étude. Les techniques de croissance ainsi que les propriétés des puits et des boîtes quantiques sont présentées.
- Le Chapitre 3 présente les techniques expérimentales, couramment utilisées pour les études de spectroscopie optique de nanostructures semiconductrices. Les techniques de micro-photoluminescence, de corrélation de photons et de spectroscopie sous champ magnétique intense sont discutées.
- Une nouvelle technique expérimentale basée sur des impulsions magnétiques rapides est présentée au Chapitre 4. Les impulsions magnétiques sont générées par une bobine miniature placée directement sur la surface de l'échantillon.
- Le Chapitre 5 decrit les expériences de manipulation optique du spin d'un ion Mn^{2+} unique situé dans une boîte quantique de CdTe. La dynamique de spin ainsi que le processus d'orientation du spin ont été mesuré par une expérience résolue en temps et sont décris par un modèle simple d'équations bilans.

- Un mécanisme possible d'orientation du spin des ions Mn est discuté au chapitre 6. Les transitions optiques des excitons obscurs, qui sont autorisées à cause de la présence d'une impureté magnétique dans la boîte quantique, peuvent efficacement induire une polarisation de l'ion Mn^{2+}.
- Le Chapitre 7 décrit l'étude de la relaxation de spin dans des sytèmes d'ions uniques ou contenant plusieurs ions magnétiques, en condition de faible ou de fort champ magnétique appliqué. Dans le cas de l'ion Mn^{2+} unique dans une boîte quantique, il a été possible de mesurer directement la relaxation spin-réseau, non perturbée par l'interaction spin-spin. Dans le cas de puits quantiques dilués magnétique, une dynamique de spin rapide a été observé en absence de champ magnétique appliqué.
- Le dernier Chapitre 8 présente un résumé de ce travail, ainsi que les possibles perspectives.

Streszczenie

Niniejsza praca poświęcona jest badaniom dynamiki spinów magnetycznych jonów Mn^{2+} w niskowymiarowych strukturach wykonanych z CdTe. Szczególną uwagę poświęcono systemowi pojedynczych kropek kwantowych zawierających pojedyncze jony Mn^{2+}. Kropki takie oferują wyjątkową możliwość szczegółowego badania oddziaływań pojedynczego jonu magnetycznego z jego półprzewodnikowym otoczeniem. Zaprezentowano metodę optycznej manipulacji i odczytu stanu spinowego pojedynczego jonu magnetycznego. Eksperyment wykorzystuje transfer ekscytonu pomiędzy sąsiadującymi kropkami, podczas którego spin jest zachowany, do umieszczenia spolaryzowanych ekscytonów w kropce z jonem Mn^{2+} i do zorientowania spinu tego ostatniego. Dynamika procesu orientacji została zbadana w eksperymencie czasowo-rozdzielczym i opisana prostym modelem. Przedyskutowano i zaprezentowano doświadczalnie jeden z możliwych mechanizmów orientacji - optyczną rekombinację tzw. ciemnych ekscytonów. Optyczna orientacja spinu Mn^{2+} została również użyta do zbadania relaksacji spin-sieć izolowanego jonu w niskim i wysokim polu magnetycznym.

W pracy poruszono również zjawiska zachodzące w niskim i zerowym polu magnetycznym w dużych systemach jonów magnetycznych - studniach i kropkach kwantowych zawierających jony Mn^{2+}. Nowa technika eksperymentalna, wykorzystująca szybkie impulsy pola magnetycznego, została użyta do zbadania dynamiki elektronowego spinu jonów Mn^{2+} przy braku zewnętrznego pola magnetycznego z nanosekundową rozdzielczością. Zaobserwowano szybką relaksację namagnesowania po impulsie pola. Wyniki doświadczalne opisano uwzględniając sprzężenie nadsubtelne ze spinem jądrowym jonów Mn^{2+}. Zaobserwowany efekt jest czuły na obecość anizotropii, spowowodanej na przykład obecnością gazu dziurowego lub naprężeń. Przyłożenie zewnętrznego pola magnetycznego blokuje szybką relaksację namagnesowania w studniach kwantowych, a obserwowana jest dobrze poz-

nana relaksacja spin-sieć. Co zaskakujące, w kropkach kwantowych zawierających wiele jonów Mn^{2+} szybka relaksacja jest obserwowana nawet po przyłożeniu zewnętrznego pola do 0,5 T. Ten szybki proces może być spowodowany oddziaływaniem spin-spin pomiędzy jonami magnetycznymi, szczególnie jeśli ich rozkład przestrzenny w kropce nie jest jednorodny.

Układ pracy jest następujący:

- W rozdziale 1 przedstawiono krótkie wprowadzenie do tematyki poruszanej w niniejszej pracy: opis podstawowych własności półprzewodników półmagnetycznych (*ang.* Diluted Magnetic Semiconductors), w szczególności $Cd_{1-x}Mn_xTe$, oraz niskowymiarowych struktur półprzewodnikowych - studni i kropek kwantowych - zawierających jony magnetyczne. Przedstawiono obecny stan wiedzy na temat dynamiki spinów w takich strukturach, jak również określono cel niniejszej pracy.
- Rozdział 2 zawiera opis spróbek użytych w pracy. Opisano zarówno techniki wzrostu, jak i podstawowe własności studni i kropek kwantowych.
- W rozdziale 3 przedstawiono standardowe techniki pomiarowe, szeroko stosowane w optycznych badaniach nanostruktur półprzewodnikowych. Opisano techniki mikro-fotoluminescencji, korelacji pojedynczych fotonów oraz spektroskopii w wysokim polu magnetycznym.
- Nowa technika eksperymentalna, wykorzystująca szybkie impulsy pola magnetycznego, została zaprezentowana w rozdziale 4. Impulsy pola magnetycznego są generowane za pomocą miniaturowej cewki umieszczonej bezpośrednio na powierzchni próbki.
- W rozdziale 5 opisano eksperyment optycznej manipulacji spinem pojedynczego jonu Mn^{2+} w kropce kwantowej wykonanej z CdTe. Dynamika procesu orientacji została zbadana w eksperymencie czasowo-rozdzielczym i opisana prostym modelem.

- Jeden z możliwych mechanizmów orientacji spinu Mn^{2+} przedyskutowano w rozdziale 6. Optyczna rekombinacja tzw. ciemnych ekscytonów, dozwolona dzięki obecności domieszki magnetycznej w kropce, może efektywnie indukować znaczącą polaryzację jonu Mn^{2+}.
- W rozdziale 7 opisano badania relaksacji spinowej w systemach z pojedynczym oraz z wieloma jonami magnetycznymi, zarówno w wysokim jak i niskim polu magnetycznym. W przypadku pojedynczego jonu Mn^{2+} w kropce kwantowej możliwe było zbadanie czystej relaksacji spin-sieć, niezaburzonej poprzez oddziaływanie spin-spin. W przypadku studni kwantowych wykonanych z półprzewodnika półmagnetycznego zaobserwowano szybką relaksację przy braku zewnętrznego pola magnetycznego.
- Ostatni rozdział 8 zawiera podsumowanie pracy. Możliwości dalszych badań w obszarach w niej poruszanych zostały krótko przedstawione.

Contents

List of Figures

Acronyms and abbreviations

Roman Symbols

CW continuous wave (*e.g.* excitation)

DMS Diluted Magnetic Semiconductuctors

EPR Electron Paramagnetic Resonance

MBE Molecular Beam Epitaxy

ML monolayer

PLE Photoluminescence Excitation

QD quantum dot

QW quantum well

RHEED Reflection High Energy Electron Diffraction

SK Stranski-Krastanov growth technique

SLR spin-lattice relaxation

X neutral exciton

X^+ positively charged exciton

X^- negatively charged exciton

X_d dark exciton

XX biexciton

Chapter 1

Introduction

The ability to incorporate magnetic atoms into semiconductor structures offers a tempting possibility to integrate information storage and information processing microelectronic devices. A completely new research area called "spintronics" has evolved around this concept [1, 2]. Perspectives of devices operating on single spins are particularly inspiring. Although today the incorporation of single magnetic atoms is not fully controllable, the constant progress in technology of fabrication of semiconductor nanostructures gives hope for a possibility to dope the nanostructures in controllable manner in the future. Expected advantages for miniaturization and superior speed of future spintronic devices, as well as potential use of magnetic ions embedded in semiconductor lattice as spin qubits, attract attention of many research laboratories around the world.

From the point of view of possible applications, the knowledge about the spin dynamics of magnetic ions in the semiconductor crystal is crucial. The mechanisms responsible for this dynamics have been studied for years. Many experiments supplied substantial knowledge concerning the physical properties of different diluted magnetic semiconductors. Although many dynamic features of magnetic ions in a semiconductor crystal are well understood, the development of new magnetic nanostructures (in particular quantum dots) and new experimental techniques opened new areas of research. For instance, the ability to produce quantum dots with exactly one magnetic ion embedded, inside created unmatched opportunity to investigate properties of a truly isolated ion, not interacting with any other magnetic moments. The development of the technique of fast magnetic

pulses allowed, in turn, measurements of the spin dynamics in the absence of any magnetic field. In reference to these issues, this work reports experimental results and their interpretation related to the mechanisms governing the spin dynamics - orientation and relaxation - of the manganese ions embedded in the CdTe crystal.

Particular emphasis has been focused on system of single CdTe quantum dots with single Mn^{2+} ions, which give a peerless insight into the interactions of magnetic ion with semiconductor environment. Phenomena occurring in low and zero magnetic field in larger systems of magnetic ions, which have not been investigated before, are also addressed.

In this chapter, I briefly review the current level of knowledge on $Cd_{1-x}Mn_xTe$-based quantum wells and quantum dots and the spin dynamics of magnetic atoms in these system. In the end, I define the aim of this work.

1.1 Diluted Magnetic Semiconductors

Diluted Magnetic Semiconductuctors (DMS), also known as Semimagnetic Semiconductors are semiconductor materials in which part of the original cations has been substituted by ions with non-vanishing magnetic momentum (*e.g.* Mn, Cr, Co, Fe, *etc.*) [3]. The magnetic system does not form an organised sublattice. The density of the magnetic ions in the host material is small and they are randomly located at the cation sites. As a result such a system may be considered as containing two interacting subsystems. The first one is a diluted ensemble of localised magnetic moments. The second subsystem is a system of delocalized carriers with well known properties, typical for semiconductor host crystal. The crystal electronic and structural properties remain almost unchanged by the doping with magnetic atoms. This makes diluted magnetic semiconductors perfect for studying the basic mechanisms of the interactions between the spins of the band carriers and the localised spins as well as other mechanisms governing the spin dynamics of the magnetic ions (*e.g.* spin-lattice or spin-spin interactions). The delocalisation of the carriers is so vast that their wavefunctions cover many randomly distributed magnetic ions. This allows the use of a virtual crystal approximation, in which a fraction of the average spin value (proportional to the content of the magnetic ions in the host crystal) is attributed to each cation

site. Moreover, the interaction of the carriers with these fractional spins can be described within assumptions of so-called mean field approximation: all spin operators of localized magnetic moments can be replaced by their thermodynamic mean value.

Originally, the weak doping of the semiconductor with magnetic ions was intended to enhance the response of the material to external magnetic field. One of the most spectacular examples of such enhancement are the giant Zeeman splitting of the electronic bands and, resulting from the band splitting, giant Faraday rotation of the polarization plane of light passing the DMS crystal. The prefix "giant" describing these effects is related to the magnitude of enhancement, being equal to several orders of magnitude when compared to ordinary semiconductors without magnetic ions at a given external magnetic field [3, 4].

Among the DMS materials, the most common are II-VI compounds (*e.g* CdTe, ZnTe, CdSe) with transition metal ions (*e.g.* Mn, Co or Fe) substituting their original cations. In II-VI family, $Cd_{1-x}Mn_xTe$ appears as particularly suitable for studies of low-dimensional structures.

First of all the II-VI materials (and CdTe in particular) posses excellent optical properties. CdTe has a direct band gap at the Γ point of the Brillouin zone (see section 1.1.1). The band gap width for the bulk CdTe is equal to 1.606 eV (at helium temperature) [5] and lowering its dimensionality leads to the increase of the gap. This makes the CdTe nanostructures a perfect subject of the optical spectroscopy, as the light emission and absorbtion occurs in the visible region. The optical experiments are also facilitated by the fact that decades of development of the crystal growth techniques and the state of the art control over the growth parameters on different substrates result in a superb optical quality of the samples. The wide bang gap, relatively high exciton (X) binding energy and significant exciton oscillator strength enable light emission and facilitates optical experiments at higher temperature, when compared to III-V materials.

Secondly, the great flexibility of the $Cd_{1-x}Mn_xTe$ material is due to the isoelectronic character of manganese in CdTe, offering the possibility of independent magnetic doping and electrical biasing of nanostructures [6, 7]. Moreover, the advancements in crystal growth, particularly in Molecular Beam Epitaxy (MBE) allowed zinc blende structure crystals of $Cd_{1-x}Mn_xTe$ to be grown in almost en-

tire composition range (x in the range of $0-100\%$) without significant change of crystal properties of the material [8, 9]. This, along with superb optical properties of the CdTe makes the $Cd_{1-x}Mn_xTe$ an excellent candidate for growth of diluted magnetic nanostructures. Such structures offer a broad range of optical methods which yield direct information on the properties of magnetic system embedded in the semiconductor crystal.

1.1.1 Magnetooptical properties of $Cd_{1-x}Mn_xTe$

As mentioned above, CdTe (and as a consequence diluted $Cd_{1-x}Mn_xTe$) has a direct band gap at the Γ point of Brillouin zone. The structure of the electronic bands, typical for semiconductors with a zinc-blende crystal lattice, is shown schematically in Figure 1.1. The conduction band is twofold spin degenerate at k=0 (two $\pm 1/2$ spin subbands), while the valence band is fourfold degenerate. The latter consists of two subbands with total angular momentum $J = 3/2$: the one of so-called heavy holes, with the spin projection onto the growth axis $J_z = 3/2$ and the subband of light holes with $J_z = 1/2$. "Heavy" and "light" describing the holes refer to the effective mass along the quantization axis. The holes with total angular momentum $J = 1/2$ form a split-off band, which is separated from the maximum of the valence band at $k = 0$ by the spin-orbit coupling Δ_{SO}. For CdTe, Δ_{SO}=930 meV [10] which is large enough to neglect the influence of this band on the phenomena discussed in this work.

As mentioned in previous section, one of the most characteristic effects observed in DMS materials is a giant Zeeman splitting of the electronic bands. It results from the exchange interaction between the (s,p) band electrons and the d electrons of the Mn^{2+} ions, which have $3d^5$ electronic shell configuration (the interaction is often shortly called the $(s,p)-d$ exchange). The consequence of the electronic band splitting caused by the magnetization of the Mn system, is splitting of the exciton transition (recombination of the bound electron-hole pair) into six components. Photons emitted in four of these transitions (two in each circular polarization) are visible in Faraday configuration, when the magnetization of the Mn system is parallel to the light propagation direction. Two remaining transitions lead to emission of linearly polarized photons visible in Voigt configuration

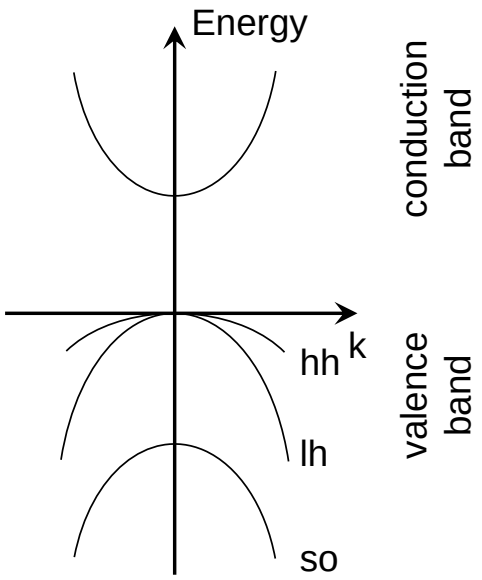

Figure 1.1: A schematic diagram of the band structure of the CdTe. *hh* refers to heavy holes, *lh* to light holes and *so* to the split-off band (see description in text).

(magnetization perpendicular to the light propagation). The selection rules of these transitions are shown in Figure 1.2.

The magnetization of the $Cd_{1-x}Mn_xTe$ material is given by the mean value of the Mn^{2+} spin $\langle S \rangle$ and the Mn fraction x. If the external magnetic field is applied along the z axis, the mean value of the spin projections onto perpendicular axes is equal to 0 and the magnetization M can be written as:

$$\mathrm{M} = -g_{Mn}\mu_B N_0 x \langle S_z \rangle \tag{1.1}$$

where g_{Mn} is Mn Lande factor ($g_{Mn} = 2$), μ_B is Bohr magneton, N_0 is a number of cation sites per unit volume and $\langle S_z \rangle$ is a mean value of the spin projection of a Mn^{2+} ion (therefore $x\langle S_z \rangle$ is a mean magnetization per one cation site) [11]. In the case of very diluted material (x <1%), where the interactions between Mn^{2+} ions can be neglected, the $\langle S_z \rangle$ in temperature T and external magnetic field B is given by:

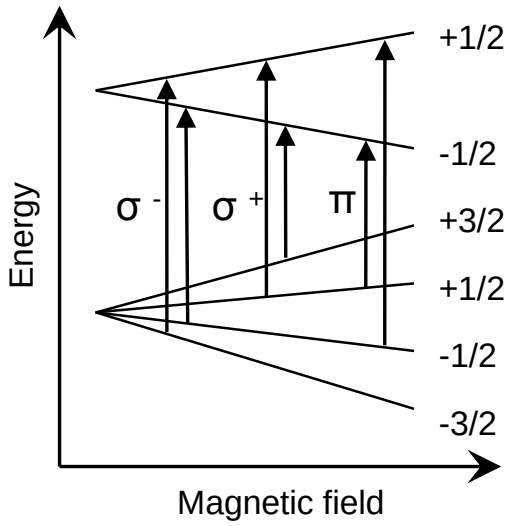

Figure 1.2: A schematic diagram of the selection rules for excitonic transitions in $Cd_{1-x}Mn_xTe$ with non-vanishing magnetization. The conduction band is described with the electron spin, the valence band with the hole spin.

$$\langle S_z \rangle = -\frac{5}{2} B_{\frac{5}{2}} \left(\frac{5}{2} \frac{g_{Mn} \mu_B B}{k_B T} \right) \tag{1.2}$$

where $\frac{5}{2}$ is the total electronic spin of the Mn^{2+} ion, k_B is the Boltzmann constant and B_J is the Brillouin function:

$$B_J(x) = \frac{2J+1}{2J} \coth\left(\frac{2J+1}{2J} x \right) - \frac{1}{2J} \coth\left(\frac{1}{2J} x \right) \tag{1.3}$$

The antiferromagnetic $d-d$ interaction between the Mn^{2+} ions in material with higher Mn content makes the situation more complex. The most closely spaced pairs of the Mn^{2+} ions are completely resistant to moderate magnetic field, as the interaction between the ions is much stronger than their interaction with the field (the exchange constant for nearest-neighbour Mn^{2+} spins J_{NN} is approximately equal to 540 μeV [12], while the Zeeman energy $g_{Mn}\mu_B$ $\approx$116 μeV$\cdot$T^{-1}). This,

as well as the reduction of the averaged spin in triangles and higher complexes of Mn^{2+} ions, can be described by introducing the effective Mn fraction in the $Cd_{1-x}Mn_xTe$ material, x_{eff} [4, 13]. This fraction of the Mn^{2+} ions is aligned by the magnetic field. However, even weakly interacting (more distant) ions are more resistant to the field than the isolated ones. This results from non-negligible $d-d$ interaction. This effect can be simulated by using an effective temperature of the Mn system, $T_{eff} = T + T_0$ [4, 13]. Thus the formula describing the magnetization takes following form:

$$\mathrm{M} = \frac{5}{2} g_{Mn} \mu_B N_0 x_{eff} B_{\frac{5}{2}} \left(\frac{5}{2} \frac{g_{Mn} \mu_B B}{k_B (T + T_0)} \right) \tag{1.4}$$

Due to very large number of possible relative positions of the Mn^{2+} ions in the host crystal, it is not efficient to derive the expression for x_{eff} and T_0 for a given Mn content in the $Cd_{1-x}Mn_xTe$ material. However, in Refs. [14] and [15] following empirical expressions were found to describe experimental data with good accuracy:

$$x_{eff}(x) = x \left(0.261 e^{-43.34x} + 0.723 e^{-6.19x} + 0.00715 \right) \tag{1.5}$$

$$T_0(x) = x \frac{35.37 \text{ K}}{1 + 2.752x} \tag{1.6}$$

All above parameters have been deduced from the Zeeman splitting measurements performed on bulk $Cd_{1-x}Mn_xTe$ [13]. The approximations are valid for moderate Mn fraction x<67%, liquid helium temperatures and moderate magnetic field (B<5 T). Under other conditions, particularly for lower temperatures, a spin glass phase was observed [16, 17, 18, 19]. For higher magnetic field, the correction related to close neighbours is necessary. In all experiments described in this work structures with very low Mn content were used, so that in most cases we can consider the Mn^{2+} ions as isolated.

The important fact from the point of view of investigation of the magnetic

system is that the splitting of all bands increase linearly with the magnetization of the material. Thus the splitting of the excitonic transitions measured in different polarizations also depends linearly on the magnetization. This can be used to optically probe the state of the magnetic system. In particular, the splitting of the heavy hole states in Faraday configuration is given by:

$$\Delta E = N_0(\beta - \alpha)x\langle S_z\rangle \tag{1.7}$$

where α and β are electron-Mn and hole-Mn exchange integrals. Values of $N_0\alpha$ and $N_0\beta$ were determined experimentally. For $Cd_{1-x}Mn_xTe$ they are equal 0.22 eV and 0.88 eV, respectively [4].

The degeneracy between heavy and light holes can be lifted by reducing the symmetry of the system. For example, it can be achieved by application of uniaxial pressure or confinement in a quasi-2D layer. This is the case of thin CdTe structures, like quantum wells (see section 1.2) or self-organized lens-shaped quantum dots (section 1.3) embedded in barriers with different lattice constant (ZnTe, for example). In all structures discussed in this work, the lowest valence subband is the heavy hole one.

1.2 Quantum wells

Quantum well (QW) is a two-dimensional structure confining particles within barriers of potential. In practice, this idea is realized most commonly in epitaxially grown semiconductors. The simplest way to obtain a quantum well is to embed a thin layer (usually less than 100 atomic layers) of one semiconductor between the barriers of a different material with larger energy band gap. The obtained confinement is the cause of most of the properties which differ quantum wells from bulk semiconductors.

When a thin layer of one semiconductor is embedded in a different material, the way the valence and conduction bands in the two materials will line up in respect to each other is not easy to predict in general case. In principle there are two possible types of band alignment for a quantum well. In the first one, called

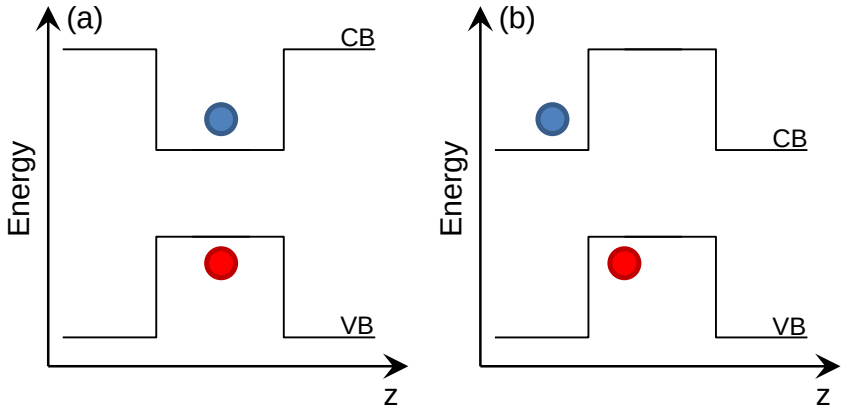

Figure 1.3: A schematic diagram of the band structure of a *Type I* (a) and *Type II* (b) quantum well and the spatial confinement of the carriers. Blue points represent electrons, the red ones represent holes.

Type I structure, both electrons and holes have lower energy in the material of the quantum well. This kind of band structure is schematically shown in Figure 1.3a. In second type, called *Type II* structure, different charge carriers have minimum energy in different materials. Figure 1.3b shows this type od structure.

All 2D structures discussed in this work are made of $Cd_{1-x}Mn_xTe$ embedded in $Cd_{1-x}Mg_xTe$ or $Cd_{1-x-y}Mg_xZn_yTe$ material. The compositions are chosen in such a way that the energy gap of the barrier is larger than the energy gap of the $Cd_{1-x}Mn_xTe$. The band offset between the two materials is such that *Type I* alignment is formed. As a result both types of the charge carriers are confined in the layer possessing smaller band gap and their free movement is limited only to the plane of this layer.

As mentioned in section 1.1.1, 2D carrier confinement and the strain caused by the lattice mismatch of the quantum well and the barrier material lift the degeneracy of the valence band. For biaxial compressive strain (smaller lattice constant of the barrier compared with the quantum well material), the lowest energy holes are heavy holes with total angular momentum projection $J_z = \pm 3/2$. Relatively large valence band splitting in all samples discussed in this work justifies considering all valence subbands other than the heavy hole one as irrelevant for investigated properties, except for the case discussed in chapter 6.

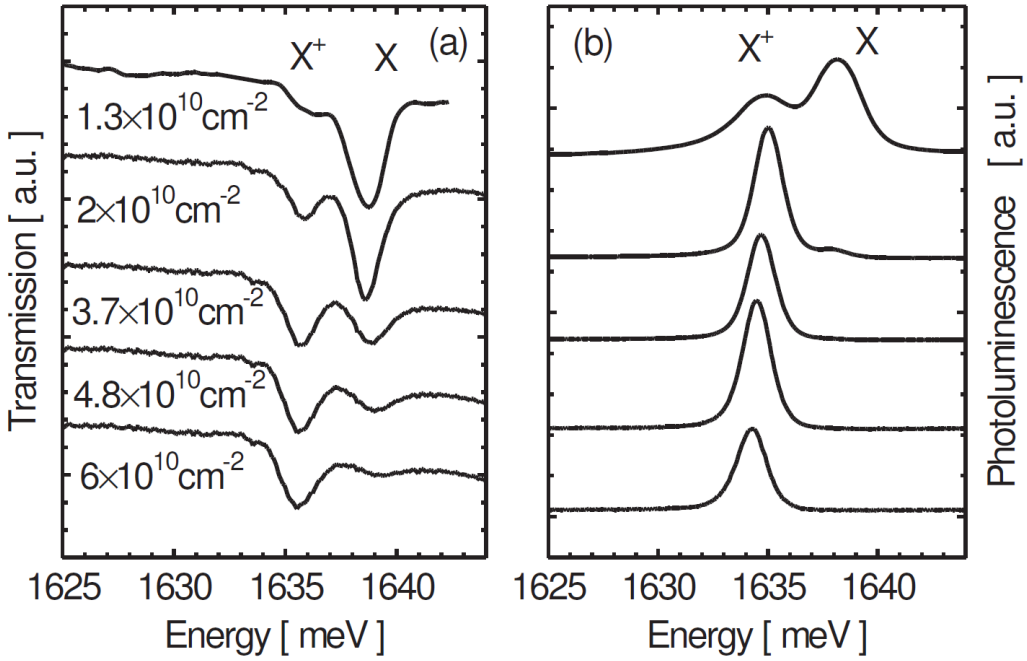

Figure 1.4: Optical spectra ((a) - absorption and (b) - photoluminescence) of an 8 nm wide $Cd_{0.998}Mn_{0.002}Te$ quantum well with indicated densities of two-dimensional hole gas. Lines related to both neutral (X) and positively charged (X^+) excitons are clearly visible. (from Ref. [24])

The carrier confinement in quantum wells (as in other low-dimensional structures) enhances the Coulomb interaction between electrons and holes. As a result the exciton binding energy increases. This is true not only for neutral excitons (bound electron-hole pair), but also for the trions, *i.e* charged excitons, for which the increase is even larger than for neutral ones. These exciton complexes consist of either two holes and one electron (positive trion, X^+), or two electrons and one hole (negative trion, X^-). As a result of the increase of the binding energy in the optical spectra of quantum wells (both in absorption and emission) lines related to both neutral and charged excitons are observed and are dominant close to the band gap edge [20, 21, 22, 23]. This is clearly seen in Figure 1.4. The figure also shows the possibility to tune the carrier density in the quantum well by using illumination of energy above the barrier band gap. This mechanism is discussed in section 2.2.

1.3 Quantum dots

Quantum dots (QDs) are nanometer-size semiconductor structures in which the carriers are confined in all three spatial directions. As a result the energy spectrum of the carriers is quantized in shells of discrete levels. Due to the analogy with the energy spectrum of atoms, quantum dots are often called "artificial atoms". Properties of the carriers in the quantum dots result from the combination of the semiconductor bulk properties (*e.g.* effective mass of the carriers) and the spatial confinement.

For a long time, the most intensively studied self-organised quantum dots were those made of III-V binary compounds: arsenides (e.g. InAs/GaAs) [25, 26, 27] and phosphides (e.g. InP/GaP). [28, 29]. More recently, II-VI materials gained a large interest as the advancements in growth techniques allowed fabrication of II-VI high quality quantum dots with fairly controllable parameters. Tellurides (e.g. CdTe/ZnTe) [30, 31] and selenides (e.g. CdSe/ZnSe) [32, 33] are among the most intensively investigated II-VI quantum dots. The CdTe dots are particularly suitable for optical spectroscopy, as the excitonic transitions in such dots occur in the visible range of the electromagnetic spectrum.

Similarly to the case of quantum wells, the flat lens shape of the dots (see section 2.3) lifts the degeneracy of the valence band. The heavy holes with angular momentum projection $J_z = 3/2$ are the lowest energy ones. When such a hole is confined in the quantum dot together with the electron (spin $S = 1/2$), four different excitonic states can be formed. The difference between these states is the spin orientation of the two carriers. Two of these states, with the hole and electron spin oriented antiparallely, are optically active. Their total angular momentum equals 1. These are called bright neutral excitons. The other two states, called dark excitons, possess total angular momentum equal 2 and are usually not optically active. They might be optically observed when their wave function is mixed with other (bright) states. This occurs for example when the magnetic ion is present in the quantum dot. Such situation is described in chapter 6.

Except neutral excitons, other more complex excitonic states might be observed if the barrier potential is high enough. These include charged excitons (two electrons and one hole or two holes and one electron), biexcitons (XX, two

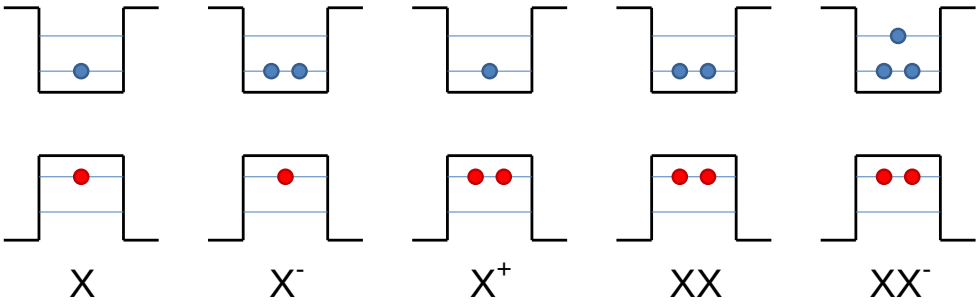

Figure 1.5: A schematic diagram of a few lowest energy charge states of a CdTe quantum dot: neutral exciton (X), charged excitons (X^+ and X^-), neutral biexciton (XX) and negatively charged biexciton (XX^-). Blue points represent electrons, the red ones represent holes. Thin horizontal lines in the potential well represent *s*- and *p*-like shells.

electrons and two holes), charged biexcitons *etc.* (see Figure 1.5). The optical transition of each of these states occur in slightly different energy, as the Coulomb interaction between the carriers changes the total energy of the system. In CdTe quantum dots the energies of these transitions, and therefore corresponding lines in the luminescence spectrum, follow a well known pattern, shown in Figure 1.6. The origin of the lines has been confirmed by many experiments, including single photon correlation and charge tuning of the dots by external electric field [34, 35, 36, 37].

1.3.1 Diluted magnetic quantum dots

Quantum dots made of diluted magnetic semiconductors combine properties of these interesting materials with consequences of zero-dimensionality. One of the most pronounced differences in the description of these objects and other DMS structures with higher dimensionality is the fact that in quantum dots usually only a single, strongly localized carrier or exciton is interacting with magnetic ions embedded in the dot. As a consequence the overlap of the carrier (or exciton) and the magnetic ions wave functions is larger, thus their interaction is stronger when compared to quantum wells or bulk material with similar content

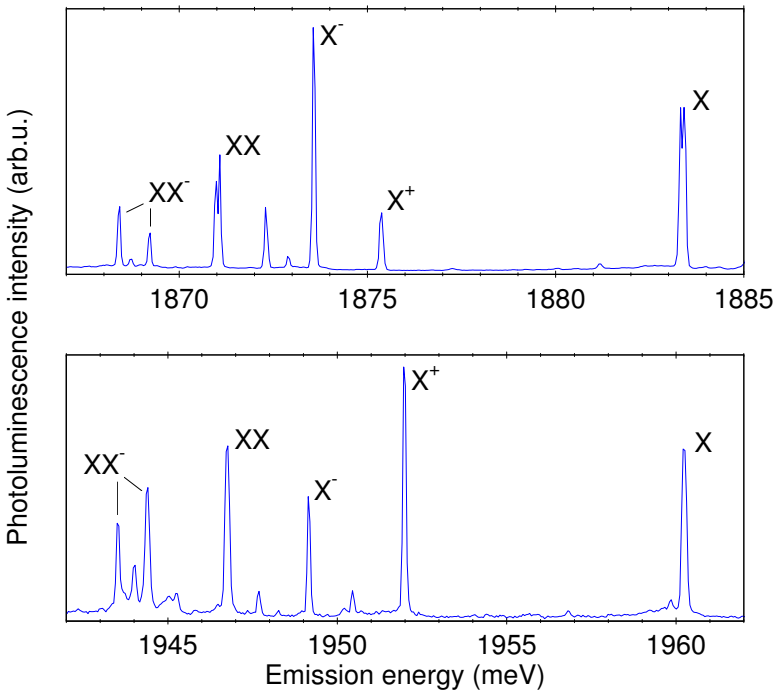

Figure 1.6: Typical photoluminescence spectra of individual CdTe/ZnTe quantum dots with indicated lines related to specific excitonic transitions: neutral exciton (X), charged excitons (X^+ and X^-), neutral biexciton (XX) and negatively charged biexciton (XX^-). Details of line identification methods can be found in Refs. [34, 35, 36, 37].

of magnetic ions. Many interesting experiments exploiting this strong interaction have been demonstrated, including the use of magnetic doped nanocrystals as a voltage-controlled spin filter [38] or observation of quasi-zero-dimensional magnetic polarons (*i.e.* correlated carrier and magnetic ion spins) in individual quantum dots [39].

DMS quantum dots have been proposed as building blocks for spin-base quantum logic gates [40, 41, 42] and are considered as a miniature cells of memory devices [43, 44, 45, 46]. However, the use of quantum dots with magnetic ions in such application requires a detailed knowledge on the spin dynamics of the magnetic moments in such systems. This issue is one of the key points addressed in this work.

For the reasons already discussed in previous sections, the $Cd_{1-x}Mn_xTe$ material seems to be perfect for investigation of phenomena occurring in diluted magnetic quantum dots, especially for optically-oriented experiments. Two types of such quantum dots have been investigated in this work. The first one contained moderate amount of magnetic atoms, between tens and one hundred atoms per one dot in average. The second type was prepared in the way that it was possible to select single quantum dots with single magnetic ions. The latter type is discussed in the next section. In case of the former type, only large ensembles of such dots were investigated. The luminescence spectrum of such ensemble shows a very broad band consisting of millions of lines, each related to a specific quantum dot. The huge number of lines makes it impossible to resolve them. However, even the broad band can be used to monitor the magnetization of the Mn^{2+} ions embedded in the quantum dots. When the magnetization becomes non-zero (*e.g* upon application of external magnetic field) the luminescence lines related to *s*-shell excitonic states (X, X^-, X^+, XX) of every dot follow the giant Zeeman effect and split into two circularly polarized components. As it was shown by Wojnar *et al.* [47], in case of X, X^-, and X^+ the lower energy component becomes more pronounced than the high energy one, due to non-negligible spin relaxation of the excitonic complexes confined in the dots . As a result the spectrum of every single dot becomes strongly circularly polarized. Such behaviour is clearly visible in Figure 1.7, presenting results of a micro photoluminescence experiment taken from Ref. [47]. Therefore the entire spectrum of a big ensemble of dots also becomes circularly polarized. It is especially pronounced in the low energy part of the spectrum, consisting mostly of the lines related to *s*-shell excitonic states. This is visible in the macro photoluminescence experiment, results of which are shown in Figure 1.8. Therefore the degree of circular polarization of the spectrum (or simply its intensity in low energy tail at given polarization) can be used to monitor the changes in the magnetization of the magnetic ions.

1.3.2 Quantum dots with single magnetic ions

A quantum dot with an exactly one magnetic ion is a qualitatively different system when compared to the dot with many ions. The magneto-optical effects

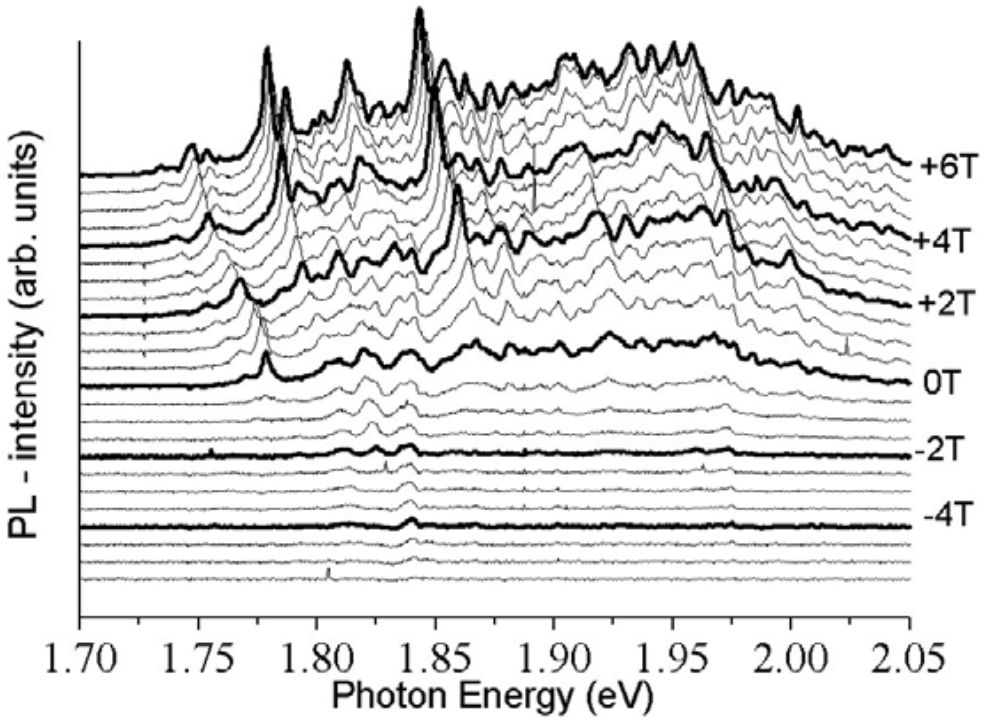

Figure 1.7: Photoluminescence spectra of a small ensamble of $Cd_{1-x}Mn_xTe/Zn_{0.8}Cd_{0.2}Te$ quantum dots with moderate content of Mn^{2+} ions (a few tens of ions per dot), measured in magnetic field in the range 0 - 6 T. Measurements were performed in liquid helium temperature in Faraday configuration. Positive values of field correspond to σ^+ polarization, negative values to σ^- polarization. A low energy shift of lines related to excitonic transitions in single quantum dots is clearly visible upon application of magnetic field. (from Ref. [47])

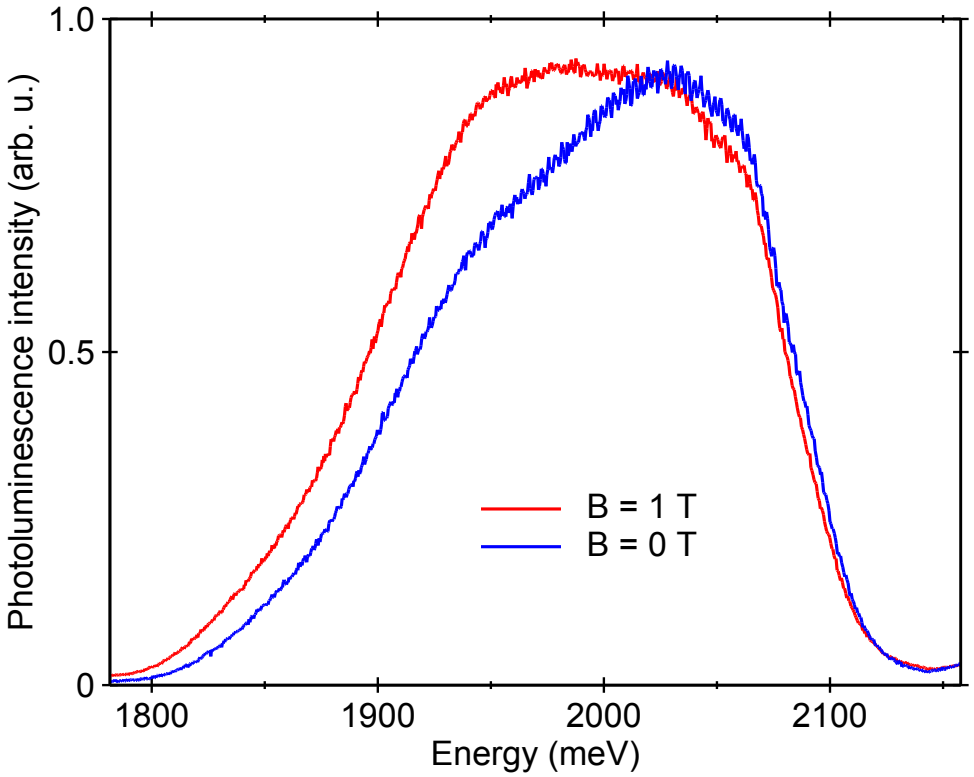

Figure 1.8: Photoluminescence spectra of a large ensemble of $Cd_{1-x}Mn_xTe/Zn_{0.8}Cd_{0.2}Te$ quantum dots with moderate content of Mn^{2+} ions (a few tens of ions per dot), measured with and without magnetic field. Measurements were performed in liquid helium temperature in Faraday configuration in σ^+ polarization.

in single Mn-doped dot, resulting from the influence of the magnetic system on the exciton confined in the dot, cannot be described as an effect of statistical behaviour of a large ensemble of magnetic moments. On the contrary, it is a result of a relatively simple interaction between two spins (the excitonic one and the one of the magnetic ion). This opens insight into properties of a single, selected Mn^{2+} ion. It gives possibility to analyze the mechanisms governing the behaviour of the magnetic atom in the semiconductor crystal unperturbed by the interaction with other magnetic moments.

Quantum dots with single Mn^{2+} ions were considered theoretically in the case of spherical nanocrystals with a strong confinement [48]. The first experimental observation of the single Mn^{2+} ions in self-organized CdTe quantum dots was done by L. Besombes and co-workers [49] and was followed by many experiments [7, 35, 50] and theoretical works [51, 52] which supplied substantial knowledge on such system. A few years later a similar observation was done by A. Kudelski and co-workers in InAs dots [53, 54]. This work is devoted to the CdTe dots. Such choice is motivated by the availability of the samples and the simplicity of CdTe based system. The lack of the orbital momentum of the Mn^{2+} ion embedded in the CdTe crystal lets us describe the magnetic CdTe quantum dot with the exciton confined inside in terms of interaction of pure spins (spins of the magnetic ion, electron and hole), which is not the case with the dots made of InAs.

Basic magnetooptical properties of the single Mn-doped CdTe quantum dots are the same as in the non-magnetic dots. The order of the transitions related to recombination of different excitonic complexes, the Zeeman splitting of the excitonic states *etc.* are typical for similar CdTe dots without magnetic impurities. A photoluminescence spectrum of a typical dot with single Mn^{2+} ion is shown in Fig. 1.9

The major difference between the spectrum of a non-magnetic CdTe quantum dot, and a dot with exactly one Mn^{2+} ion is a characteristic multifold splitting of photoluminescence lines related to each of the excitonic transitions. To understand the origin of this splitting let us focus on the case of neutral exciton state confined in the quantum dot. In such a case, the exchange interaction between the exciton and the magnetic ion changes the total energy of the system, depending on the relative orientation of the two spins (see Figure 1.10(a)). This lifts

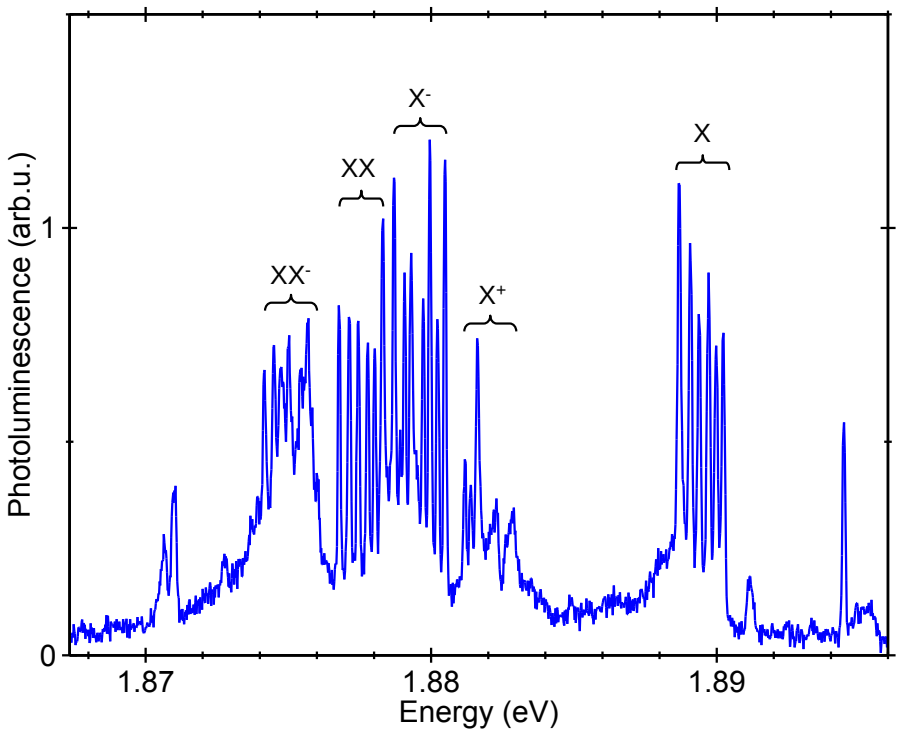

Figure 1.9: Typical photoluminescence spectrum of a single-Mn doped CdTe quantum dot with indicated lines related to recombination of specific excitonic states.

the degeneracy of the exciton-Mn system, even in zero magnetic field. Since the total spin of the Mn^{2+} ion is equal to 5/2, the number of its possible projections onto the quantization axis given by the anisotropic excitonic angular momentum (parallel to the growth axis of the sample) is equal to 6. Therefore the energy level of the ground state spits into 6 sublevels (see Figure 1.10(b)). As a result the neutral excitonic spectrum of the quantum dot consist of six sharp lines, each 2-fold degenerated and related to a specific spin state of the exciton-Mn system (see Figure 1.10(c)). If observed photons are related to the excitons with specific spin projection (+1 or −1), which defines their circular polarization, then each component of the excitonic sextuplet corresponds to a specific spin state of the Mn^{2+} ion. For example, the lowest energy line is related to the Mn^{2+} state with

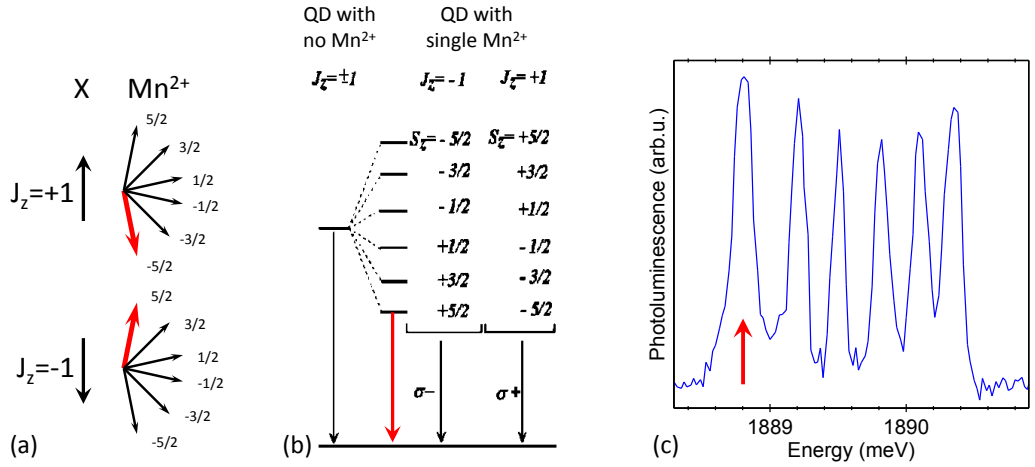

Figure 1.10: (a) A schematic diagram of possible relative orientations of the exciton and Mn^{2+} spin. Numbers indicate spin projection onto the quantization axis parallel to the growth axis of the sample. (b) Diagram of the neutral exciton energy levels and optical transitions in the non-magnetic quantum dot (left) and in the single Mn-doped dot (right). (from Ref. [49]) (c) Photoluminescence spectrum of the neutral exciton confined in the quantum dot with single Mn^{2+} ion taken without polarization resolution. Red arrows indicate the spin states and photoluminescence line related to each other.

spin projection equal to $-5/2$ if the spectrum is recorded in σ^+ polarization, and to the state with spin projection equal to $+5/2$ if the σ^--polarized spectrum is observed (see Figure 1.10).

Since the biexciton is a spin singlet state, the interaction of the Mn^{2+} ion with the carriers in such state compensate each other and therefore in the first order approximation no energy splitting is present in the initial state, prior to the recombination process [49]. However, the final state of the optical recombination of the biexciton (after emission of the photon) is the neutral exciton state, which is split into six sublevels. Thus the part of photoluminescence spectrum related to the biexcitonic transition also shows sixfold splitting, clearly visible in Figure 1.9.

More complex multiplets are related to charged excitonic states. A detailed analysis of spectra related to recombination of these states can be found in Ref. [7]. The experiments described in this work focus on neutral exciton and biexciton features.

1.4 Aim of this work

As mentioned at the beginning of this chapter, the spin dynamics of magnetic ions embedded in the semiconductor crystal might be important from the point of view of possible applications. This work explores new fields of research of this spin dynamics, which became available thanks to the development of new magnetic nanostructures and new experimental techniques. The work reports new experimental results related to mechanisms governing the spin dynamics - orientation and relaxation - of the Mn^{2+} ions embedded in the CdTe crystal. A significant part of this work is devoted to single CdTe quantum dots with single Mn^{2+} ions and phenomena occurring in low and zero magnetic field, which is interesting not only from the applicational, but also from the scientific point of view.

1.4.1 Spin orientation

The knowledge of properties of isolated magnetic ions is particularly important from the point of view of miniaturization and scalability of future information storage devices. Among such devices the concept of those with all-optical writing and readout of information seems particularly promising. The optical readout of the magnetization of the magnetic system is possible due to the *s,p-d* interaction between the optically recombining excitons and the magnetic ions. In the case of system consisting of many magnetic atoms, it leads to the giant Zeeman splitting of the excitonic states with different spin projection onto the quantization axis (see section 1.1). In the case of single magnetic impurity (*e.g.* in the Mn-doped CdTe quantum dots), the *s,p-d* interaction lifts the degeneracy of the magnetic ion-exciton complex and causes the characteristic multifold splitting of the excitonic state (see section 1.3.2). This gives the unique possibility to perform a direct optical readout of the spin state of the single magnetic ion.

The optical writing of information in the magnetic system embedded in the semiconductor crystal is, however, a more difficult challenge. The optical induction or switching of the magnetization in large magnetic systems has been demonstrated, for example in (Zn,Mn)Se [55] or (Cd,Mn)Te [6, 56] quantum wells, (Cd,Mn)Te quantum dots [57], (Hg,Mn)Te crystals [58] or thin films of

ferrimagnetic alloys [59]. The electric control over the magnetic system in semiconductor has been also shown [60], as well as the use of combined electronic and optical properties of a semiconductor doped with magnetic ions [61]. However, mechanisms used in all those experiments are not scalable down to single magnetic ions, as they all involve the spin-spin interactions between large ensembles of magnetic impurities. At the time when we started experiments described in this work, the optically induced spin orientation of a single magnetic ion had not been demonstrated. Thus the main aim of this work was to develop the procedure for such orientation. The experiment showing the possibility to use a single Mn^{2+} ion embedded in the CdTe quantum dot as a magnetic volatile memory is described in chapter 5. A similar experiment using a slightly different technique than ours was done independently by L. Besombes and co-workers [45].

The aim of this work was also to investigate the spin-related phenomena, which can help to understand the dynamics of the spin of magnetic impurities. The dark excitons optical recombination, for example, impossible to observe in non-magnetic quantum dots in the absence of magnetic field, is easily observable in single Mn-doped dots. The experiment, revealing the role of this recombination in the process of optical orientation of the Mn^{2+} spin is presented in chapter 6. The investigation of the spin-lattice relaxation (SLR) of the single Mn^{2+} ion, described in the next section, is another example of the experiment which takes advantage of the spin orientation mechanism to analyze the spin dynamics of the single magnetic impurities.

1.4.2 Spin relaxation

The spin dynamics caused by relaxation processes has been intensively studied, for years, in bulk and 2D DMS materials. The main interactions which keep the system of magnetic ions in thermodynamical equilibrium with the crystal lattice were identified as a spin-lattice interaction [62, 63] which can lead to a global change of magnetization, and spin-spin interaction [64, 65] which can act locally and lead to the spin diffusion to non-spin-conserving centres (*e.g.* clusters of more than two coupled magnetic ions [66, 67], which statistically exist within the random ions distribution). It has been also shown that hot photo-created carriers

can mediate in the energy transfer between magnetic ions and the crystal lattice [68, 69].

Although many features of the spin relaxation of a system of magnetic ions in a semiconductor crystal are well understood, there are still several aspects that remain little investigated.

First of all, due to limitations of sample growth techniques, in all previous experiments the spin dynamics of a big ensemble of magnetic ions was investigated. This was done either with diluted magnetic bulk material [63, 70, 71] or quantum wells [67, 72, 73]. However, even for very diluted materials, the distances between adjacent magnetic ions were not negligible. Therefore the spin-spin interaction between these ions had always to be considered, which made the situation more complicated. Quantum dots with single magnetic ions enable the investigation of the spin relaxation caused by pure spin-lattice interaction. The aim of this work is to investigate in detail this interaction in low and high magnetic field. Results of such experiments are presented in section 7.1.

Secondly, a great majority of the experiments focused on investigation of the interactions between magnetic ions and their vicinity were performed in the presence of a moderate magnetic field. For instance, a short heat pulse was used to change the population of the Zeeman sublevels, and the evolution of the magnetization was monitored a pick-up coil [71] or extracted from the giant Zeeman effect in reflectivity [74] or photoluminescence [73]. Faraday rotation following the creation of electron-hole pairs by a laser pulse reveals the transverse relaxation time T_2 [72, 75]. T_2 was also deduced from the width of the Electron Paramagnetic Resonance (EPR) line, in the range of Mn content where it exhibits exchange narrowing.

Because of the presence of magnetic field, the spin relaxation was always connected with the energy relaxation. A completely different situation occurs in the absence of the magnetic field when the spin-flip of the magnetic field does not require the energy transfer. The magnetization relaxation under such conditions was not a subject of any previous experiments. The aim of this work was therefore to perform a detailed investigation of the spin dynamics of magnetic ions embedded in a quantum well and in quantum dots in low and zero magnetic field. I present results of these new experiments in section 7.2.

Chapter 2

Samples

2.1 Technology

All samples used in this work were grown by Molecular Beam Epitaxy. It is a well established method, developed since late 1960s. It allows a precision growth of thin films of semiconductors and oxides. The extremely slow deposition rate (typically being of order of 10 nm per minute) allows the films to grow epitaxially and gives possibility to control the films thickness with monolayer precision. To monitor the growth of the crystal layers and their quality the reflection high energy electron diffraction (RHEED) is often used.

One of the simplest structures useful from the point of view of this work, possible to be grown by MBE, are quantum wells. A progress in the MBE technology in the 1970s allowed a controllable growth of also more complicated structures, namely the quantum dots. One of the most intensively studied type of semiconductor quantum dots are self-assembled dots formed using the Stranski-Krastanov (SK) growth technique [76, 77]. In this technique the lattice mismatch between the materials of the substrate and the quantum dots leads to the formation of strained islands on a few-monolayer thick film called a wetting layer. For that reason this mode of crystal growth is also known as "layer-plus-island".

The CdTe/ZnTe quantum dots used in this work were formed in modified SK growth mode, following the original idea of Tinjod *et al.* [31]. In this method a 2D CdTe layer is temporarily capped with layer of amorphous tellurium to induce

the transition to dots. Then the tellurium is thermally desorpted. As an effect, a sharp transition from 2D to 3D character of the surface in the RHEED image is observed. Finally, the quantum dots are capped with thin layer of ZnTe. A more detailed description of the sample growth and morphology of the dots can be found in Ref. [47].

2.2 Quantum wells

Samples containing quantum wells used in this work were grown in the CEA-CNRS Laboratory in Grenoble and in the Institute of Physics, Polish Academy of Sciences in Warsaw.

Samples from the CEA-CNRS Laboratory were grown on $Cd_{1-x}Zn_xTe$ (001) substrates with the Zn content x equal to 4% or 12%. They contain a single 8 nm-wide, p-type $Cd_{1-x}Mn_xTe$ quantum well, with 0.2% to 1.5% Mn content. The quantum well is embedded in $Cd_{0.75}Mg_{0.25}Te$ barriers in case of samples grown on the 4% Zn substrate and $Cd_{0.7}Zn_{0.08}Mg_{0.22}Te$ barriers for 12% Zn substrate. The Mg content in the barriers determines the valence band offset, while the presence of Zn controls the lattice match to the substrate. The carriers are introduced to the quantum well either by modulation doping with nitrogen (a thin N-doped layer between the quantum well and sample surface) or by the presence of surface electron traps [78]. In the latter case, a nitrogen doped layer is also placed between the quantum well and the buffer layer. This is done to screen any electrically active defects in the buffer from affecting the quantum well. In order to avoid any direct transfer of the carriers, the N-doped layer is located far from the quantum well. A schematic cross section of the samples is shown in Figure 2.1 and their parameters are presented in table 2.1. Note that carrier density given in the table strongly depends on the experimental conditions. The nominal density is estimated for liquid helium temperature with no illumination and no magnetic field applied to the sample.

The samples described above give a useful possibility to control the carrier density by additional illumination above the band gap of the barrier material. Such a feature is one of the most pronounced effects of illumination of heterostructures and was widely investigated for many systems [80, 81, 82]. In our case, the key

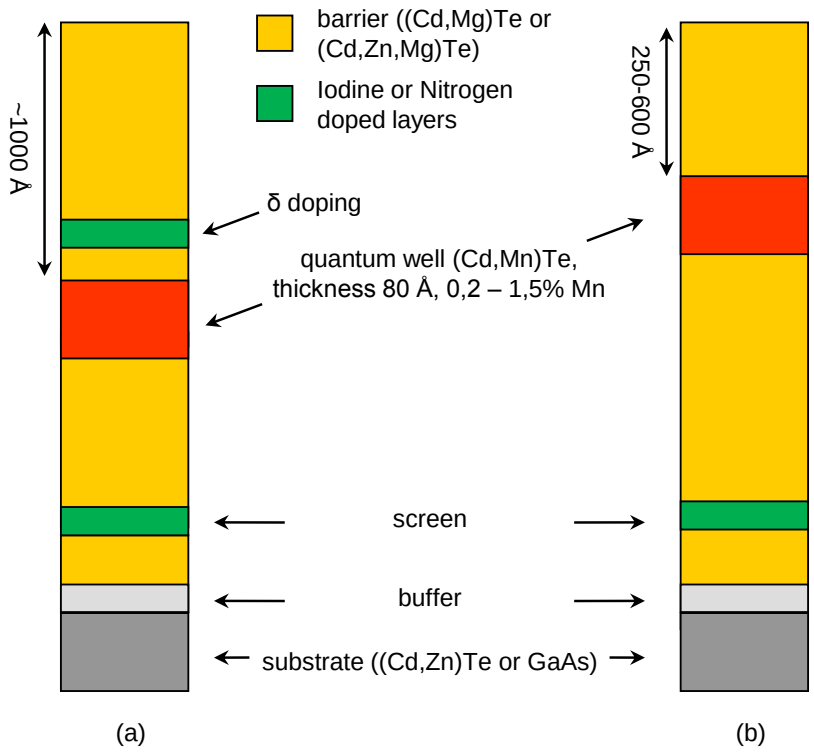

Figure 2.1: A schematic cross section of the samples containing quantum wells used in experiments described in this work. (a) refers to the samples with modulation doped barriers, (b) represents the samples in which the carriers were introduced to the quantum well by the presence of surface electron traps

Sample	Type	Mn concentration (%)	Doping	Nominal carrier density (cm^{-2}) [15, 79]
M1200	p	0.2	N	$1 \cdot 10^{10}$
M1305	p	0.4	N	$3 \cdot 10^{11}$
M1384	p	0.8	surface	$1.5 \cdot 10^{11}$
M1359	p	1.5	surface	$3.5 \cdot 10^{11}$
110597c	n	0.4	I	n/a
122905a	n	0.4	I	n/a
122905b	n	0.8	I	n/a
040397b	n	1.0	I	n/a

Table 2.1: Basic parameters of the samples containing quantum wells used in this work (n/a - not available).

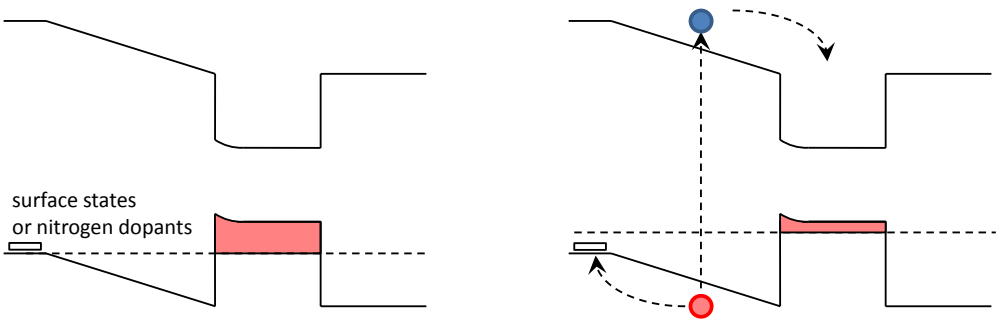

Figure 2.2: A schematic diagram of the mechanism allowing the control over the hole gas density in the quantum well in the p-type samples. The change in carrier density is obtained by illuminating the sample with light of energy above barriers band gap. Blue colour refers to electrons, the red one to the holes.

element of this mechanism is the existence of acceptor states (nitrogen dopants or surface states) in the close vicinity of the quantum well, which create the electric field in the barrier material. The schematic diagram of the mechanism is shown in Figure 2.2. When the photons with energy above the band gap create electron-hole pairs the electric field separates these carriers. The electrons migrate directly to the quantum well and neutralize the hole gas confined inside. The holes migrate towards the acceptors and then tunnel back to the quantum well. Due to limited tunnelling rate of the holes, the carrier density in the quantum well in the stationary state is lower than in the case without illumination above barrier bad gap. Using this mechanism it is possible to reduce the hole density in the quantum by several orders of magnitude, so that in the sample spectrum a line related to the neutral exciton appears. Example spectra showing this phenomenon are shown in Figure 2.3.

Samples with n-type doping were also used in this work. They were grown in the Polish Academy of Sciences in Warsaw on GaAs (001) substrates. Similarly to the p-type samples, they contain a single 8 nm-wide $Cd_{1-x}Mn_xTe$ quantum well embedded between $Cd_{1-x}Mg_xTe$ barriers. The Mn content in the quantum well varies between 0.2% and 1.5%. The carrier gas is introduced by modulation doping of barriers with iodine [83]. A schematic cross section of the samples is

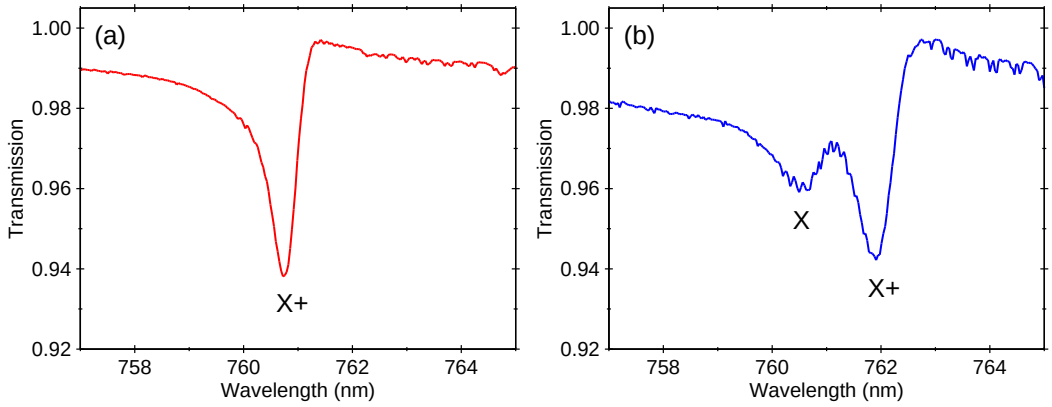

Figure 2.3: Transmission spectra of a p-type sample containing a CdTe quantum well doped with 0.8% of Mn: (a) illuminated with a long-wavelength-pass filter (high density of hole gas) (b) illuminated with a white lamp without any filter (low holes density).

shown in Figure 2.1(a) and their parameters are shown in table 2.1. Likewise in the p-type samples, there is possibility to control the carrier density by illumination. A diagram of this mechanism is shown in Figure 2.4. The photocreated electrons and holes are separated by the electric field in the region between the sample surface and the doped layer. The holes migrate towards the surface of the sample and are trapped by surface acceptors states. The electrons migrate towards the quantum well. Part of photocreated electrons is trapped in the doped layer, but part of them tunnel farther to the quantum well. As a result the electron gas density increases. More detailed description of this process can be found in Ref. [10].

2.3 Quantum dots

Samples used in this work were grown in the Institute of Physics, Polish Academy of Sciences in Warsaw. The sample structure contain four layers deposited during the growth on GaAs substrate: a CdTe buffer ($\simeq$3 μm), a ZnTe lower barrier

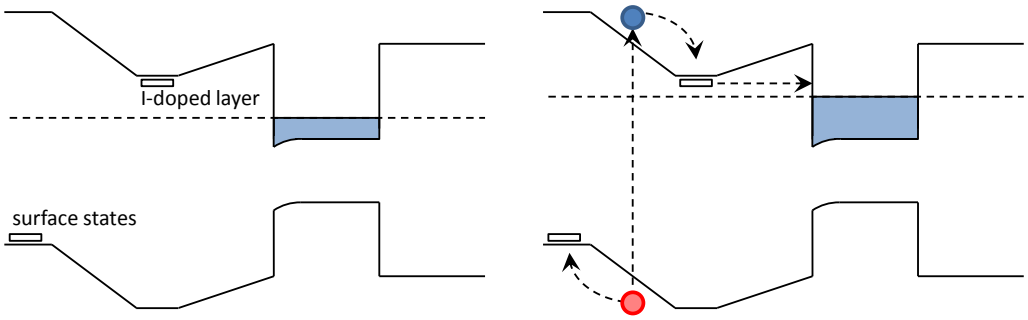

Figure 2.4: A schematic diagram of the mechanism allowing the control over the hole gas density in the quantum well in the n-type samples. Blue colour refers to electrons, the red one to the holes.

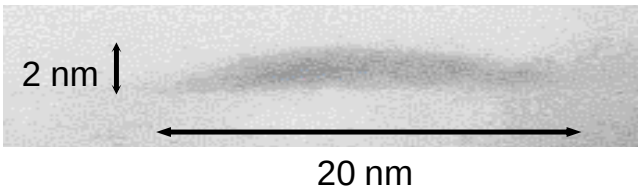

Figure 2.5: A transmission electron microscopy (TEM) image of a typical quantum dot used in this work. Courtesy of S. Kret and P. Dłużewski (Institute of Physics, Polish Academy of Sciences).

(0.7 μm), a single CdTe quantum dots plane formed from 6 monolayers (MLs) of epitaxial CdTe, and a ZnTe capping layer (100 nm). The quantum dots grown in this process are lens-shaped, with lateral size of about 10-20 nm and about 2 nm along the growth axis (see Figure 2.5). The density of the quantum dots is equal to about 5×10^9 cm^{-2} [47].

Two central out of six monolayers of the CdTe contain a low amount of Mn atoms. Two different types of samples were used in the experiments. In the first one the average Mn content in the quantum dots material is estimated to about 1%. In the second one is was much smaller, reaching the value of about 0.05%. This value of the Mn content was adjusted in such a way that it is possible to

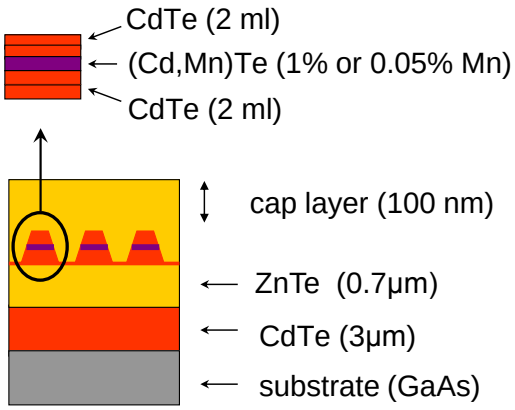

Figure 2.6: A schematic cross section of the samples containing quantum dots used in experiments described in this work.

select a significant number of dots, each containing a single Mn^{2+} ion.

A schematic cross section of the samples is shown in Figure 2.6.

Chapter 3

Standard experimental setups and techniques

Information about the spin dynamics of the magnetic atoms in experiments described in this work is obtained by using optical methods. Photoluminescence is a primary tool to collect information on the state of magnetic system, and the only one in case of manganese doped quantum dots. In case of diluted magnetic quantum wells, the transmission and reflectance measurements were also involved in conjunction with fast magnetic field pulses. This original technique is described in chapter 4. In this chapter, I describe standard experimental techniques, commonly used in optical studies of semiconductor quantum dots.

3.1 Micro photoluminescence

The majority of the experiments related to quantum dots described in this work focus on single dot phenomena. Therefore the first experimental quest is to collect light emitted by selected single quantum dot. The selection of the dot is done both spatially and spectrally. The spatial selection is done by using a microscope objective. It enables illumination and luminescence collection from an area not greater than 1 μm in diameter.

Two experimental setups with different microscopes were used in this work. In the Institute of Experimental Physics at the University of Warsaw, where the

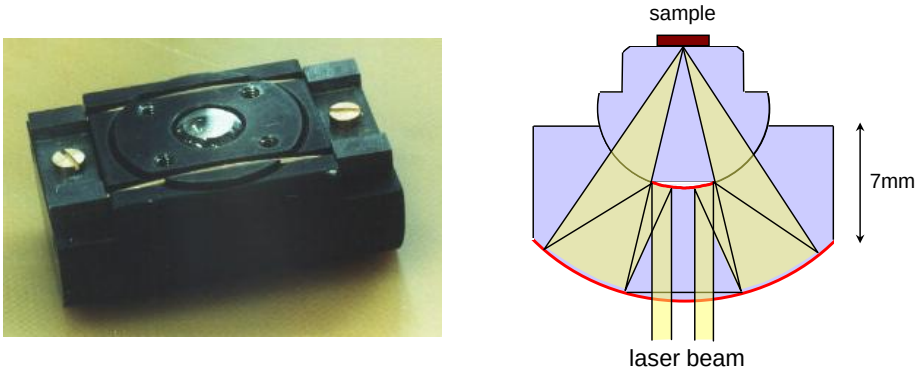

Figure 3.1: A photograph of the microscope objective used in the micro-luminescence measurements in low magnetic field in an optical cryostat and a schematic diagram of beam path inside.

sample was placed in an optical cryostat, a specially designed mirror objective with a high numerical aperture (equal to about 0.7) [84] was used. A cross section of this objective is shown in Figure 3.1. The resolution of the device is given mainly by the diffraction limit and reaches 500 nm. The sample was placed on the focal plane of the microscope, at its back surface. Such mounting guarantees excellent mechanical stability, enabling virtually infinitely long measurements of selected single quantum dot[1]. The microscope together with the sample is immersed in liquid helium bath inside the cryostat. Since the cryostat allows direct optical access to the sample, the whole setup is based on free beam optics. The laser used to illuminate the sample enters the cryostat along the optical axis of the device. The light emitted by quantum dots and collected by the microscope follows the same axis. The photoluminescence signal is then separated from the laser beam by use of a dichroic mirror outside the cryostat. Such setup enables polarization-resolved measurements, both in excitation and detection, simply by placing polarization optics in appropriate beam.

In Grenoble High Magnetic Field Laboratory, where no optical cryostat was

[1]The longest experiment on a single quantum dot performed in this setup lasted more than 4 weeks and was stopped by the user.

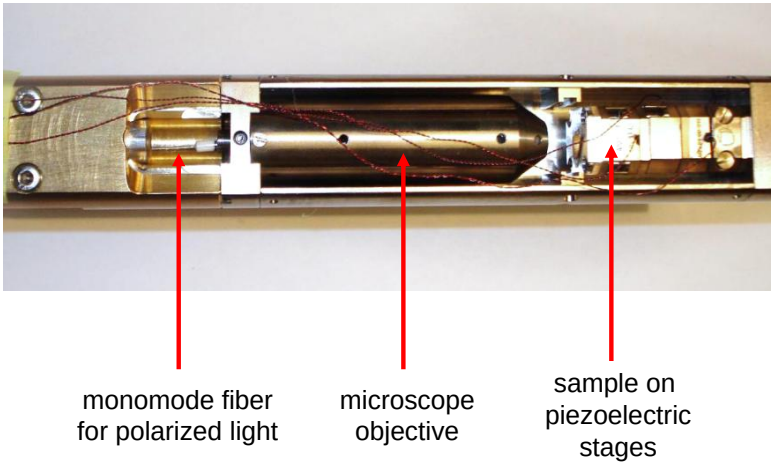

Figure 3.2: A photograph of the micro-luminescence setup comprising of a microscope objective and piezoelectric x-y-z stages with sample holder used during measurements in high magnetic field.

available, an optical fiber setup was used. A standard achromatic microscope objective is placed inside the cryostat. Both the exciting and the collected light are transmitted though a monomode fiber coupled directly to the objective. The photoluminescence signal is separated from the laser beam by a fiber-based dichroic beam splitter. The sample is placed on a precise piezoelectric x-y-z stages below the microscope. Such setup enables scanning of the sample surface with the laser spot with spatial resolution of about 100 nm. A photograph of this system is shown in Figure 3.2. The microscope objective with piezoelectric stages is placed inside the cryostat and kept in the temperature of about 10 K.

Such setup makes the polarization-resolved measurements much more difficult in comparison with the setup based on free beam optics. The monomode fiber which is about 10 m long acts as a high order, wavelength-dependent wave plate. Moreover, as the experiments are carried out in high magnetic field, a strong Faraday rotation occurs in the fibers. However, as long as there is a reference point, the use of polarization optics outside the cryostat permits the compensation of the influence of the fibers on polarization of transmitted light. In the detection part of the setup the polarization optics consits of half-wave and quarter-wave

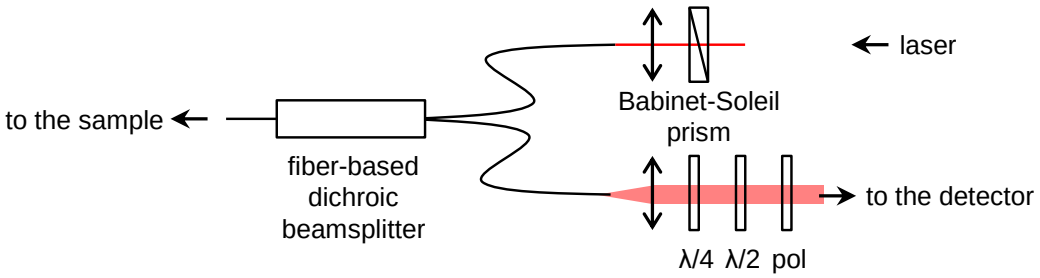

Figure 3.3: A schematic diagram of polarization optics used in the micro-photoluminescence setup utilizing optical fibers.

plates and a linear polarizer (such an idea was also presented in Ref. [85]). On the excitation side, the Babinet-Soleil compensator is used. Such a setup is schematically shown in Figure 3.3. In case of detection, the light emitted by the quantum dots itself can be used as a reference point, since in magnetic field the luminescence excitonic lines of the dots split into two circularly polarized components. Therefore it is possible to align the wave plates and the polarizer in such a way that only one of these components is transmitted. As shown in section 5.2.1, in case of resonant excitation, the excited state also splits into two states in magnetic field. Both these states are related to a specific spin projection of the exciton onto the axis given by the magnetic field (+1 or -1), thus they are resonantly coupled to oppositely circularly polarized light in Faraday configuration. Therefore the energy of the resonant excitation is strictly related to the circular polarization of light, which can be used for polarization calibration of the excitation beam. However, obtaining polarization resolution without magnetic field, both in detection and excitation, is impossible.

The light emitted by the quantum dots, after leaving the cryostat (in the first setup) or the fiber (in the second one) is collected with a monochromator equipped with a charge coupled device (CCD) camera and an avalanche photodiode. The CCD camera allows collection of time-integrated spectra of the samples. The avalanche photodiode is connected to a time-resolved photon counter. It enabled recording of temporal profiles of the photoluminescence at specific energy in the experiments where the excitation beam is modulated.

Although very small, the size of the illuminated spot did not assure excita-

tion of single quantum dot. Due to quite high dot density the number of dots actually observed with microscope objectives described above was equal to a few hundreds. The spectral selection of single quantum dots was done by finding well resolved, isolated lines in the long-wavelength tail of the spectrum of the observed ensemble of dots. A well known pattern of photoluminescence lines related to recombination of excitons in specific charge states in CdTe quantum dots [34, 36, 86, 87] facilitated the identification of lines related to the same quantum dot. The identification was confirmed by power dependence measurements and in some cases by single photon correlation experiments. In case of experiments with resonant excitation of quantum dots (see section 5.2, chapter 6 and section 7.1) the identification of luminescence lines was simplified, as the number of dost actually emitting light was smaller by more than one order of magnitude than the total number of dots in the laser spot.

The photoluminescence of the quantum dots was excited with a continuous wave laser beam, either above the band gap of the ZnTe barrier (at 475 nm or 532 nm) or using a tuneable dye laser in the range 570 - 610 nm. The polarization optics placed in the laser beam enabled selection of the desired circular polarization of exciting light. In experiments of optical manipulation of the Mn^{2+} spin (see section 5.2.4) and its relaxation (see section 7.1.2) the intensity of excitation and its polarization were modulated. This was achieved by passing the laser beam through acousto-optic and electro-optic modulators. Using the first one we were able to switch the excitation on and off. The second modulator allowed us to change the circular polarization of the laser. The switching time of both modulations was 10 ns. The modulators were driven by a set of pulse generators synchronized with a time-resolved photon counting system (*PicoQuant TimeHarp 200* or *PicoHarp 300*), which was used to record the temporal profiles of the photoluminescence signal at selected energy. A schematic diagram of the experimental setup in such configuration is shown in Figure 3.4.

3.2 Single photon correlation

Single photon correlation is a powerful technique that allows investigation of time-dependent phenomena occurring in light emitting structures. In case of quantum

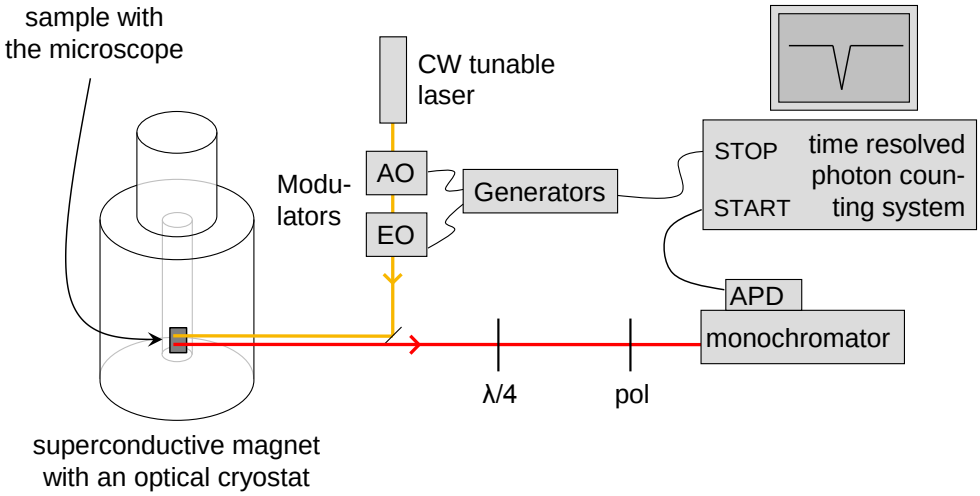

Figure 3.4: A schematic diagram of the experimental micro-photoluminescence setup enabling time-resolved measurements with intensity- and polarization-modulated excitation.

dots, it has been used for example to investigate the excitation mechanisms [34] or entanglement of photons emitted in a biexciton-exciton cascade [88, 89]. In quantum dots doped with magnetic ions (especially with exactly one magnetic ion) it gives the possibility to investigate the spin dynamics of the magnetic system. The information on the state of magnetic ions is carried by the photons emitted by the quantum dot, originating from the excitonic transitions. Therefore the temporal resolution of such experiment is limited only by the exciton lifetime.

The correlation measurements were performed in a Hanbury-Brown and Twiss (HBT) [90] configuration type setup with spectral filtering. The setup consists of two monochromators equipped with avalanche photodiodes and CCD cameras. Maximum spectral resolution of the monochromators was better than 100 μeV enabling observation of well resolved photoluminescence lines of singly Mn-doped quantum dots. The avalanche diodes were connected with "Start" and "Stop" inputs of a single photon correlation system (*PiqoQuant TimeHarp 200*). A schematic diagram of such experimental setup is shown in Figure 3.5.

The overall temporal resolution of this system was equal to about 500 ps,

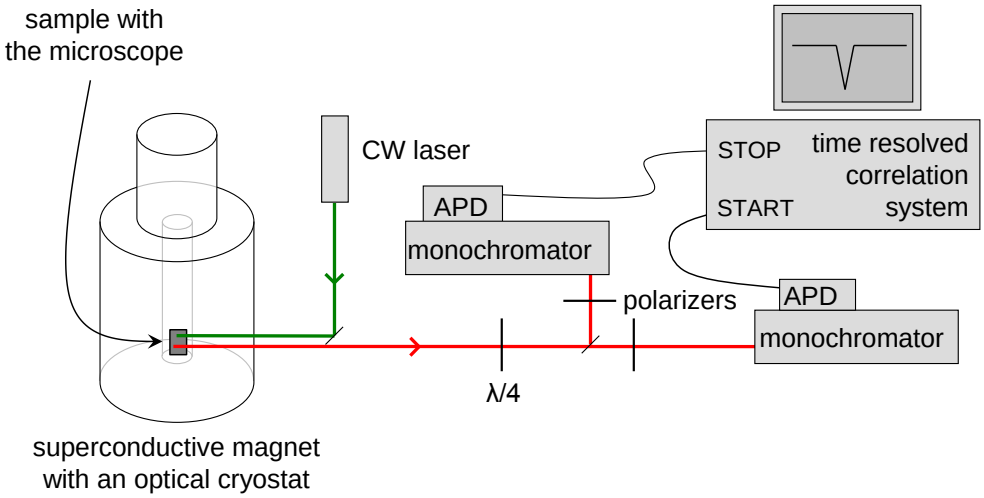

Figure 3.5: A schematic diagram of the experimental setup for single photon correlation

which is close to the exciton lifetime in the quantum dots under investigation. The maximum quantum efficiency of the photodiodes (at 560 nm) was equal to 55% and the dark count rate was not greater than 200 s^{-1}. Such parameters allow performing correlation measurements of photons emitted by a single quantum dot with a reasonable signal accumulation time (between a few and a few tens of hours). The correlation system generates histograms of correlated photon detection events versus delay between the detected photons. The use of a delay line, made of long coaxial cable, at "Stop" input of the correlation electronics allowed recoding events with a negative delay between photons, *i.e.* events when the photon at "Stop" detector arrived before the photon arrival at the "Start" one. After normalization, the histograms recorded with the card are equivalent to the normalized second order correlation function:

$$g^{(2)}(\tau) = \frac{\langle I(t)I(t+\tau)\rangle}{\langle I(t)\rangle^2} \tag{3.1}$$

where $\langle ...\rangle$ denotes the time average and $I(t)$ is the light intensity at time t. $g^{(2)}(\tau)$

gives the probability of detecting a photon at time τ, knowing that a photon has been detected at time t=0.

Photons emitted by the investigated quantum dot were divided in two beams collected by the two monochromators on a polarizing or non-polarizing beam splitter. Polarization optics (quarter-wave plates and linear polarizer) mounted on the two beams separately enabled independent control of the polarization and energy of photons detected by the two detectors in use.

3.3 Spectroscopy in high magnetic field

The experimental setup with superconducting split-coil magnet available in the Institute of Experimental Physics at the University of Warsaw enabled measurements in magnetic field up to 7 T. Experiments in higher field (dark exciton spectroscopy described in chapter 6 and measurements of the Mn^{2+} ion spin relaxation described is section 7.1) were carried out in Grenoble High Magnetic Field Laboratory. Two different magnets were in use: a superconductive one, producing field up to 14 T and a 20 MW resistive magnet capable of producing field up to 28 T. Both magnets have the same bore diameter equal to 35 mm, thus they are compatible with the same type of the cryostat. This allowed the use of the same probe with the optical setup during experiments on both magnets.

Chapter 4

Pulsed magnetic field technique

Experimental techniques presented in the previous chapter are among widely used optical methods of investigating physical phenomena in semiconductors. They do not, however, give insight to many of the properties of the magnetic system. In particular, the possibility to investigate the spin dynamics in absence of any applied magnetic field is strongly limited. Spin dynamics of the Mn^{2+} ions in $Cd_{1-x}Mn_xTe$ has been studied, for years, almost exclusively in the presence of a magnetic field. Typical measurements involve a short heat pulse used to drive the sample out of thermal equilibrium, the evolution of the magnetization being measured with a pick-up coil [71] or extracted from the giant Zeeman effect in reflectivity [74] or photoluminescence [73]. Faraday rotation following the creation of electron-hole pairs by a laser pulse reveals the transverse relaxation time T_2 [72, 75]. T_2 was also deduced from the width of the Electron Paramagnetic Resonance (EPR) line, in the range of Mn content where it exhibits exchange narrowing (above 10%).

In Ref. [70], the magnetization of a bulk $Cd_{1-x}Mn_xTe$ sample, in the presence of a static field, was changed by the collinear, AC field of a coil, and monitored by Faraday rotation. The spin-lattice relaxation time was clearly identified and exhibits a dramatic decrease at low field. In principle, this method can be used down to zero field but the frequency response of the set-up was limited to a few microseconds, so that the static field had to be kept above a few tenths of Tesla. By contrast, T_2 slowly increases when decreasing the applied field in $Zn_{0.9}Mn_{0.1}Se$ [72] or $Cd_{1-x}Mn_xTe$ [75].

In this chapter, I present a new experimental technique of fast magnetic pulses, which enables investigation of the Mn^{2+} spin dynamics in zero magnetic field with nanosecond resolution. The pulses of magnetic field are generated by a miniature magnetic coil placed directly on a sample surface.

4.1 Concept of the experiment

In the experiment, the magnetization of the magnetic system in the quantum well was investigated under pulsed magnetic field by optical methods: photoluminescence, reflection and transmission. The basic idea is to use a giant Zeeman splitting [4] of the excitons confined in the quantum well as a measure of the magnetization of investigated system. The principle of applied procedure is shown in Figure 4.1.

Figure 4.1(a) shows representative photoluminescence spectra of a diluted magnetic semiconductor quantum well without (grey) and with (red and blue) applied magnetic field, in two different circular polarizations. A single line visible in the spectra is related to optical recombination of a charged exciton photocreated in the quantum well. The splitting of this line in magnetic field is due to the giant Zeeman splitting of the exciton. If the field is applied in Faraday configuration (parallel to the excitation and collected beam) and perpendicularly to the quantum well plane, then the two split lines have opposite circular polarization. To obtain signal proportional to the splitting, and therefore proportional to the magnetization of the system under investigation, one can measure the intensity of the photoluminescence at specific wavelength on the slope of observed line, as shown in Figure 4.1(a) by vertical line. As long as the splitting is much smaller than the width of the photoluminescence line, the obtained signal is linearly dependent on the position of the line and thus on the magnetization. By applying magnetic pulses in such configuration one obtains temporal profiles of the photoluminescence shown in Figure 4.1(b). The difference between the profiles measured in opposite circular polarization is proportional to the magnetization (see Figure 4.1(c)). The most interesting part of this signal is visible a few hundreds of nanoseconds after switching the field off, when the magnetization relaxation in zero external magnetic field is observed (Figure 4.1(d)). This tran-

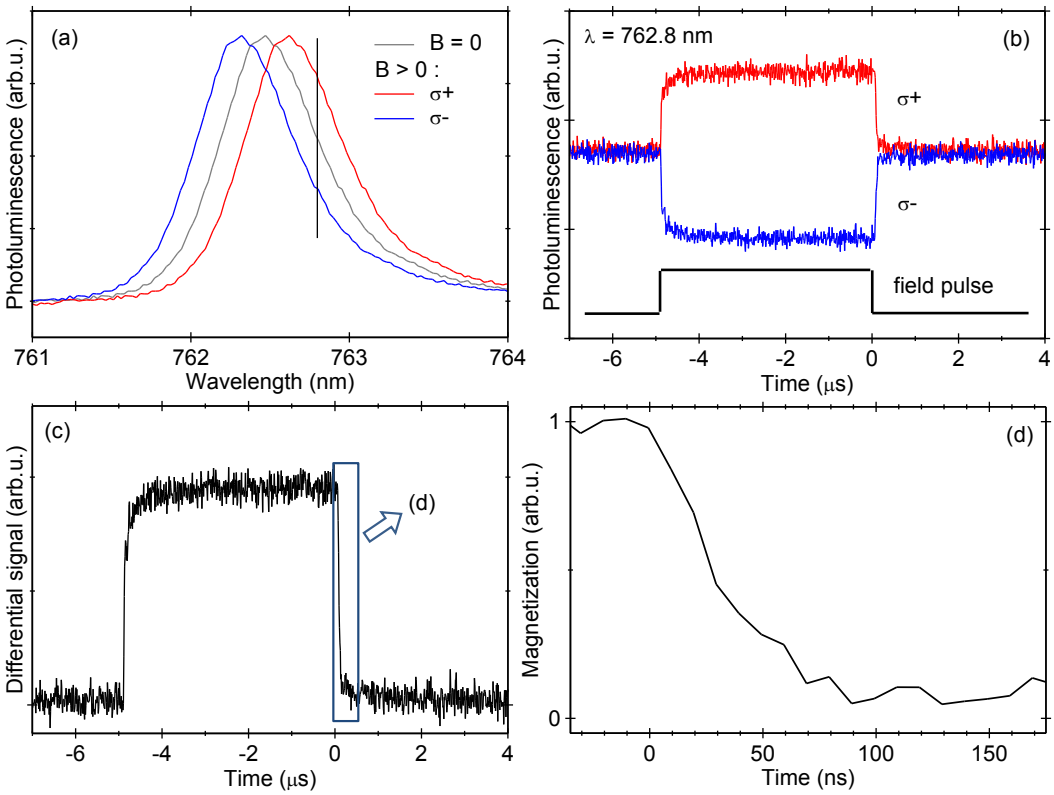

Figure 4.1: The idea of the optical measurement of the magnetization dynamics of a diluted magnetic semiconductor quantum well after a pulse of magnetic field. A detailed description in text.

sient is significantly longer then the decay of applied pulse of magnetic field. In our experiment, instead of measuring two temporal profiles of photoluminescence with different circular polarization, we record two profiles with the same polarization, but with two different directions of the current in the coil (and therefore two different directions of pulsed magnetic field). Such approach assures better stability and repeatability of the measurements. It also eliminates the influence of the electric field produced by the micro-coil and its wiring (see section 4.4)

This scenario of the measurement, however, is not limited to the zero field case. Exactly the same procedure can be performed after applying additional constant magnetic field produced for example with external superconductive magnet. The only difference is that in such case the measured signal does not reflect the total

Zeeman splitting, but only its changes caused by the magnetic pulses produced with the micro-coil.

It is important to note that the exciton lifetime in investigated quantum wells is of order of 100 ps [91]. This is much shorter than the characteristic magnetization relaxation time under investigation. Therefore one can assume that the excitonic Zeeman shift change immediately (in the time scale of the magnetization relaxation) and follows the change of the quantum well magnetization. In other words the observed spectral lines move simultaneously with changes of the magnetization without any delay.

4.2 Micro-coils

The major problem in producing rapidly alternating, controllable magnetic fields is the inductance of the coils used to produce the field. The inductance, in the approximation of long solenoid is given by:

$$L = \frac{\mu_0 \pi r^2 n^2}{l} \tag{4.1}$$

where μ_0 is magnetic permeability of vacuum, r is radius of the coil, n is the number of turns and l is the coil length. Therefore the easiest way to reduce the inductance is reducing the radius of the coil and the number of turns. The latter solution, however, also reduces the magnetic field, linearly dependent on n. The former one has a major disadvantage as well. Since the sample beneath the coil is investigated by optical methods, the size of the coil aperture is crucial for the strength of the optical signal. Therefore the coil parameters have to assure the compromise between the coil inductance, the strength of magnetic field and the strength of the optical signal. Satisfying values of these three parameters were obtained with a coil with 28 turns and 400 μm internal diameter, made of 25 μm thick copper wire. Measured inductance of such coil was equal to about 0.4 μH which in connection with 50 Ω transmission line allows obtaining pulse rise and fall time equal to 7 ns.

A current equal to 1 A in the coil produces at the surface of the sample

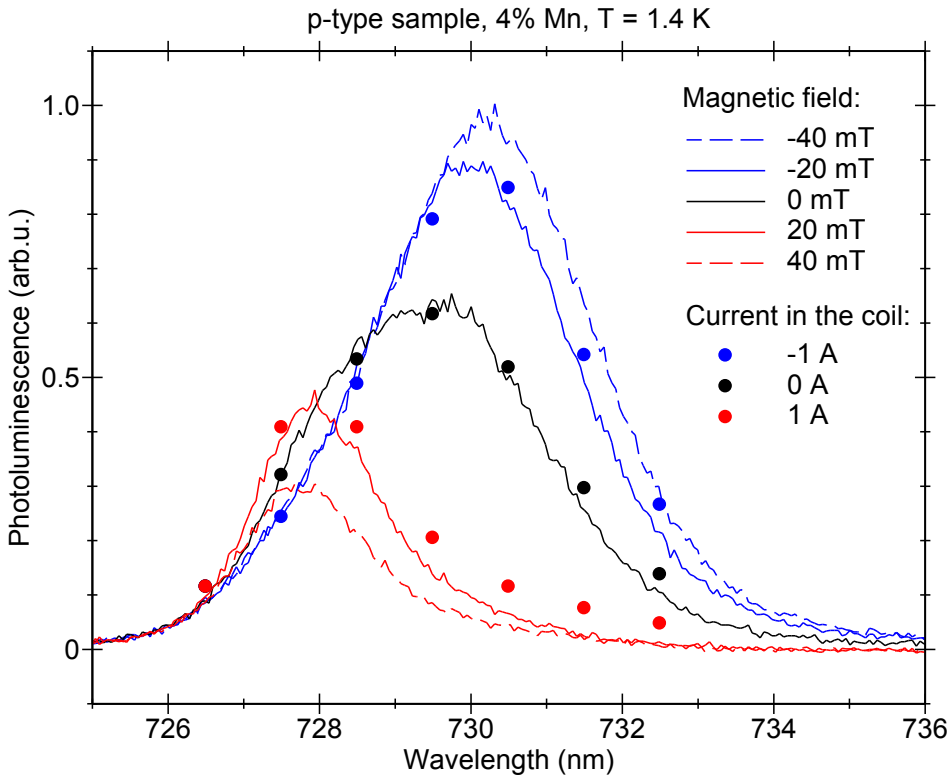

Figure 4.2: Result of calibration of the magnetic field produced by micro-coil performed using a ferromagnetic sample with manganese content equal to 4%. Solid lines represent photoluminescence spectra of the ferromagnetic quantum well taken in magnetic field produced with a superconductive magnet. Symbols represent photoluminescence intensity measured during a long magnetic pulse produced with the micro-coil. The only fitting parameter is normalization factor.

magnetic field of about 20 mT. This value was calibrated by comparing the photoluminescence spectrum of a sample with a $Cd_{1-x}Mn_xTe$ quantum well with relatively high Mn content ($x = 4\%$) in a magnetic field generated by the coil and by the external superconductive magnet. The result of this comparison is shown in Figure 4.2. Solid lines represent photoluminescence spectra of the quantum well taken in magnetic field produced with a superconductive magnet. Symbols represent photoluminescence intensity at specific wavelengths measured during a long magnetic pulse produced with the miniature coil.

In further sections, I will refer to the miniature coils as micro-coils.

4.3 Power supplying

Because of the small number of turns of the micro-coils a large value of the current is needed to produce a magnetic field which is useful from the point of view of the experiment (a few tens of militesla). Moreover, a rapid changes in the current value are needed in the experiment. Therefore the current needs to be provided to the coil by a transmission line to assure a high bandwidth of the connection between the coil and the power supply. In order to reduce the voltage needed to supply the coil the transmission line should have the lowest impedance possible. Due to technical limitations in mounting such line inside the cryostat we have decided to use widely commercially available 50 Ω coaxial cable. Therefore the power supply had to produce pulses of the amplitude in the range 100-200 V in order to supply the coil with the current of a few Amperes. Because of the lack of commercial pulse generators capable of producing in a convenient way such pulses with rising and falling time below 10 ns we decided to build such generator on our own. The main switching element is a high-voltage, high-current MOSFET transistor with extremely low gate capacity. The transistor is switched on and off by a high-current MOSFET driver assuring rising and falling time around 2 ns in connection with 50 Ω transmission line.

The micro-coil was connected as a part of the transmission line (see Figure 4.3) which was terminated with a suitable resistor outside the cryostat. The terminating resistor is made of 80 1 kΩ, 5 W metal film resistors to assure required power handling and proper impedance in a wide frequency range (metal film resistors in the range 0.1-1 kΩ have usually low impedance and capacitance, thus they are appropriate for high frequency circuits). Using an oscilloscope connected to the terminating resistor we were able to record temporal profiles of the current in the coil which gives its magnetic field.

4.4 Electric field of the micro-coil

Due to relatively high voltage used to feed the micro-coil and presence of grounded metal plane below the sample (see Figure 4.3), the coil produces not only magnetic field, but also the electric one. This can be observed in the luminescence

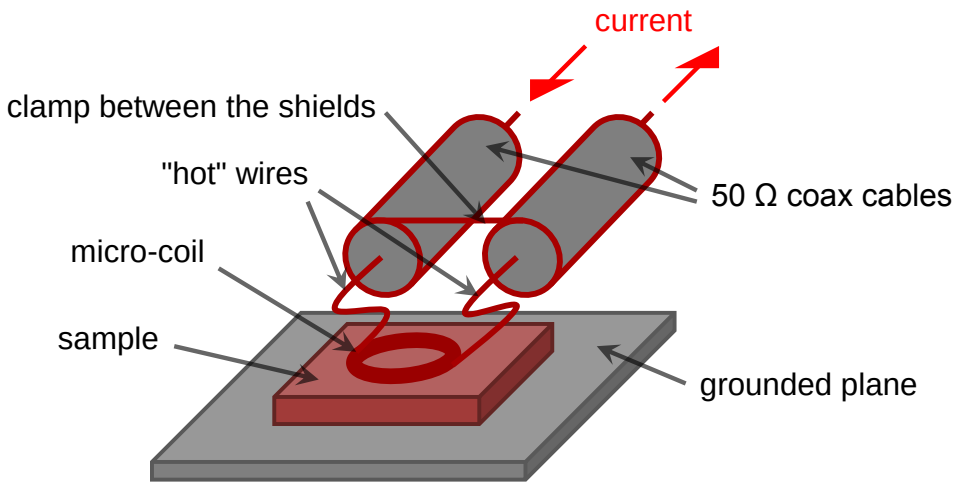

Figure 4.3: A schematic drawing presenting the connection of the micro-coil placed on the surface of the sample to the coaxial transmission line.

signal when the carrier gas in the quantum well is depleted so that both neutral and charged excitons (X and X^+, respectively) lines are visible in the spectrum of the sample (see section 2.2). In such a case, small external electric field induces relatively large changes in the carrier gas density. As a result, the relative intensities of the X and X^+ lines changes. This is visible in Figure 4.4. When the hole gas density is high, only the X^+ line is visible. The difference of the luminescence temporal profiles measured on the slope of the line with different directions of the current in the coil is proportional to the Zeeman splitting. The sum of these two profiles is flat, indicating that no changes in the line intensity occur. This was also verified by performing the same measurement on the other slope of the line. When the hole gas is depleted and both X and X^+ lines are visible, the difference of the two signals is qualitatively the same as in the previous case. However, the sum of the signals shows large variation, indicating changes in the lines intensities. When the magnetic field is switched on, the X line first rapidly diminishes. Then a slow recovery of the line intensity occurs. When the magnetic pulse finishes, an opposite situation is observed - the X line intensity first rapidly increases, and then slowly decreases to the previous value. The changes of the

X^+ line intensity are exactly opposite. It increases when the X line diminishes and *vice versa*, which was verified on both slopes of both lines.

We interpret this phenomenon as the influence of the electric field created by the high voltage between the coil placed above the sample and the grounded plane below. When the magnetic field is on, the rapid change of the electric field injects additional carriers into the quantum well. Then, the carrier diffusion between the barriers and the quantum well brings back the steady state, which is perturbed again by switching the magnetic field off. This interpretation can be easily verified by performing similar experiment with a different micro-coil. For example, a coil with the same dimensions but smaller number of turns will produce smaller magnetic field, while the electric field (dependent only on the voltage and geometry of the setup) will remain the same. Therefore we performed such experiment with a coil with only one turn, instead of 28. The comparison of results obtained with the two coils is shown in Figure 4.5. As opposed to the case presented in Figure 4.4, two consecutive current pulses (positive and negative) were used instead of one. The Zeeman splitting observed with the coil with one turn is smaller by a factor of 30 when compared with the one measured with the previous coil. At the same time the changes of the excitonic line intensities are the same within the experimental accuracy. This proves that these changes are caused by the electric field. It also shows that the procedure of measurement described in section 4.1 makes the experiment sensitive only on the magnetic field and independent of the electric one.

4.5 Optical excitaction and detection

4.5.1 Illumination of the sample

In order to collect the optical signal only from the part of the sample placed in the magnetic field the sample was illuminated through the aperture of the coil (see Figure 4.6). In the case of photoluminescence measurements on the quantum wells, the excitation was done below the energy gap of the barrier material with a 675 nm laser beam. In case of transmission experiment, a halogen lamp with suitable low-pass filter was used. During the reflectance measurements the sample

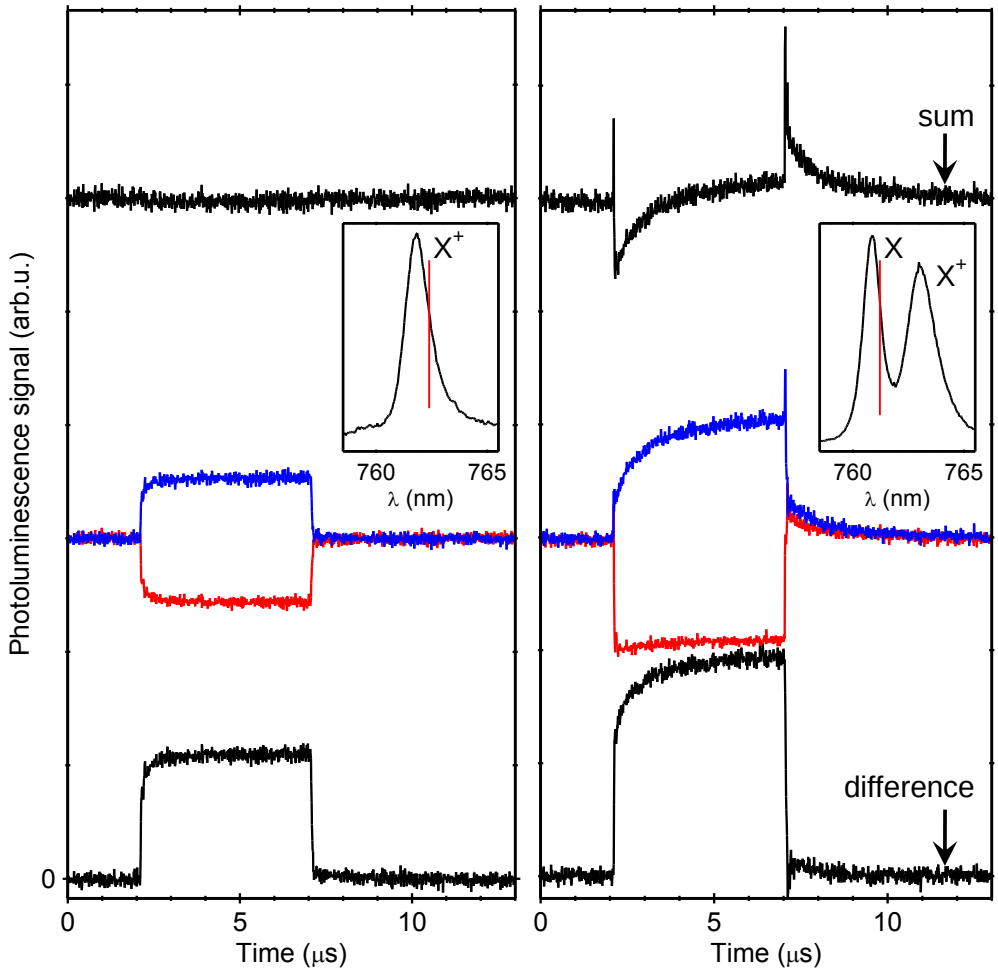

Figure 4.4: Photoluminescence intensity temporal profiles during the magnetic pulse (red and blue) measured on the slope of photoluminescence lines (marked with red lines in insets) of a $Cd_{1-x}Mn_xTe$ quantum well with 0.8% of Mn. Black lines represent difference and sum of the profiles measured with a different directions of the current in the micro-coil. Measurements were performed without (left panel) and with (right panel) additional illumination, which causes lower hole gas density and presence of neutral exciton line (X) in the photoluminescence spectrum.

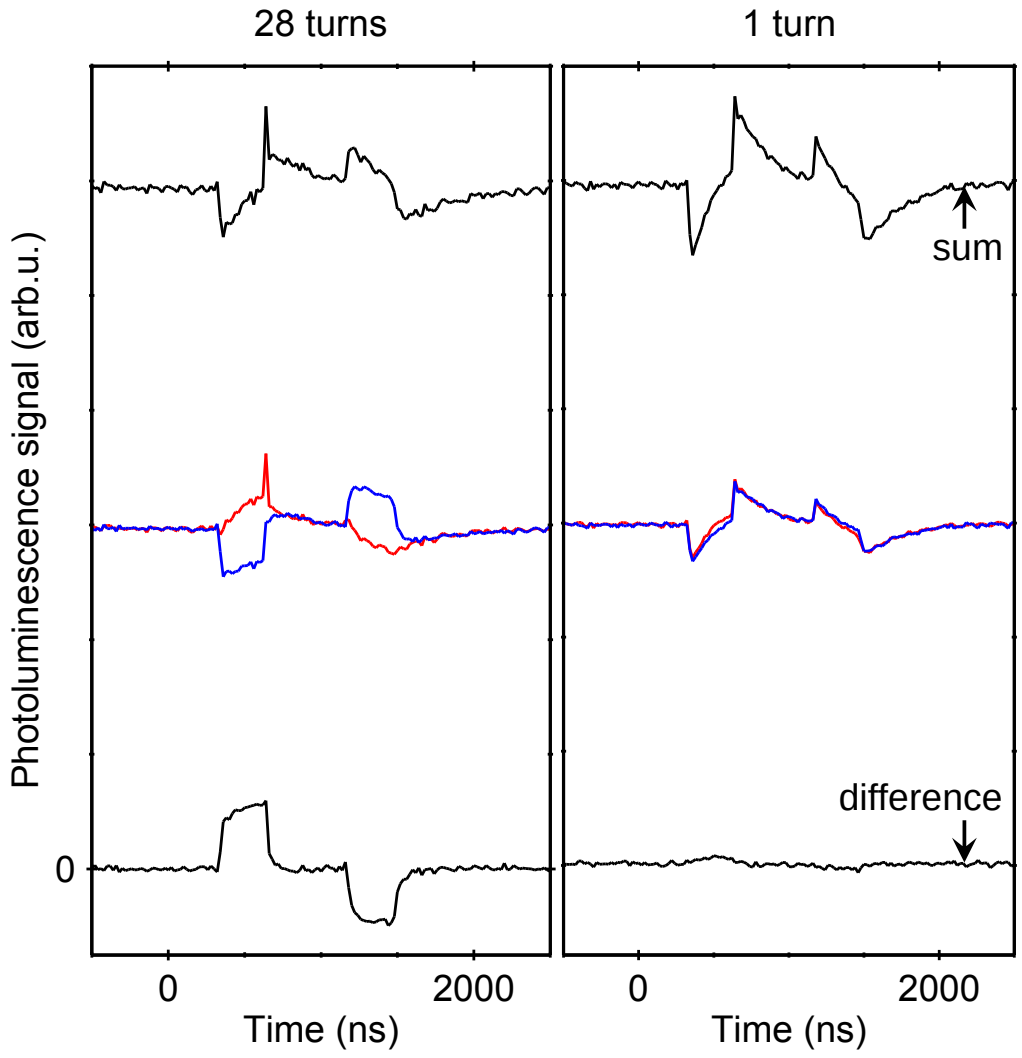

Figure 4.5: Comparison of the results of the two experiments performed with micro-coil with different number of turns: 28 (left panel) and 1 (right panel). The effect of the magnetic field (visible in the differential signal) is much smaller in the case of the latter coil, while the effect of the electric field (observed in the sum of the temporal profiles) is the same within the experimental accuracy.

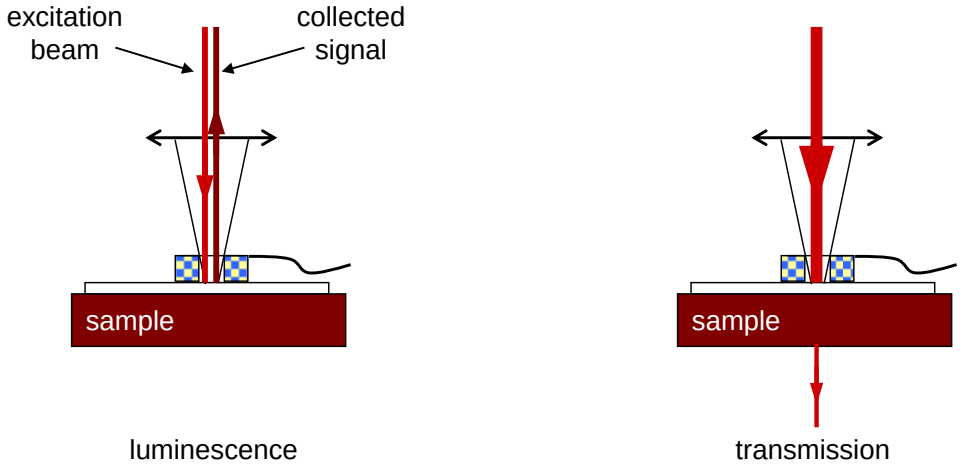

Figure 4.6: Illumination method of the sample in the case of photoluminescence and transmission measurements.

was illuminated using a tuneable continues wave or pulsed Al_2O_3:Ti laser beam.

4.5.2 Detection of the optical signal

4.5.2.1 Photon counting setup

In case of photoluminescence measurements, we used continuous wave (CW) excitation. The excitation power has to be kept as low as possible, to avoid heating of the sample. This makes the photoluminescence signal very low. At the same time the temporal resolution of the detection signal has to be better than rising and falling time of the current in the micro-coil (equal to about 7 ns). Therefore the best solution for detecting the optical signal was a time-resolved photon counting system. Photons emitted by the sample were detected by an avalanche photodiode (Perkin Elmer SPCM-AQR-13) installed on one of the exits of a monochromator. The second exit was equipped with a CCD camera enabling recording of the spectrum of the sample. In some cases two separate monochromators were used. Such a setup enabled simultaneous recording of the sample spectrum and temporal profiles of the photoluminescence at selected wavelength. A schematic diagram of the experimental setup in this configuration is presented

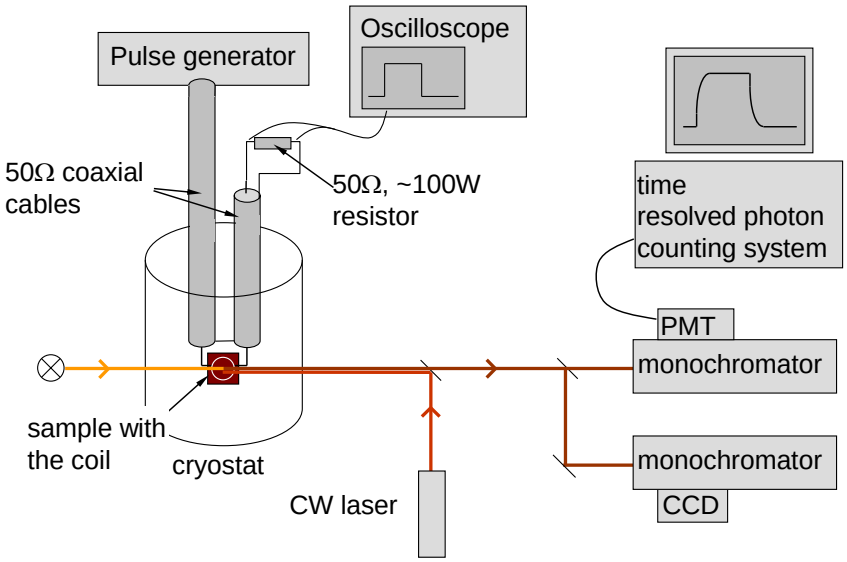

Figure 4.7: A schematic diagram of the experimental setup in the configuration using single photon counting technique.

in Figure 4.7.

The avalanche photodiode was connected to a time-resolved single photon counter (PicoQuant TimeHarp 200). The device precisely measures the time interval between electric pulses on two input channels. However, the full-scale time range of the measurement is equal to about 4 μs, which usually is not enough. Therefore the counter was used in Time-Tagged Time-Resolved (TTTR) mode in which the time interval between the two pulses is recorded along with a global clock of the device with resolution of 100 ns. In this mode the avalanche photodiode was connected to one channel of the photon counter, while the second channel was synchronized directly with the internal global clock of the device. At the same time the pulse generator used to supply the micro-coil was synchronized with the same global clock and generated a pulse every n-th period of this clock (with $n > 100$ and $n < 10000$). Every time the pulse was generated the generator sent a signal to the additional, low temporal resolution input of the photon counter. Such connections allowed recording of the global time of arrival of every detected photon with temporal resolution better than 1 ns and a global

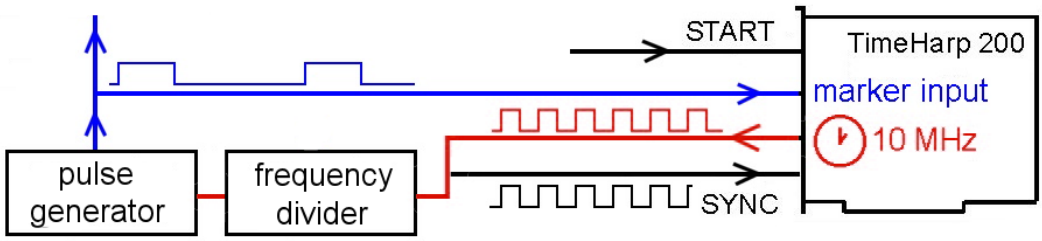

Figure 4.8: A schematic diagram of connections between the photon counter and the pulse generator using the internal global clock of the counter and enabling synchronization between pulsed magnetic field and detection setup.

time of every pulse of magnetic field. Therefore it was possible to reproduce the averaged temporal profile of the photoluminescence intensity at given wavelength before, during and after the magnetic pulse. The schematic diagram of connections between the counter and the pulse generator is shown in Figure 4.8.

4.5.2.2 Optical bridge

In case of the reflectance and transmission measurements, the optical signal is much stronger in comparison with the photoluminescence measurements. Therefore it was possible to use an optical bridge setup for detection of the signal. Such system is less sensitive, yet more precise than the setup with avalanche photodiode described in section 4.5.2.1. The optical bridge is made of two photodiodes, each detecting a different linearly polarized component of incoming light. This is done by splitting the light into two oppositely polarized beams by a Wollaston polariser. A quarter-wave plate placed before the polarizer enables independent detection of two circularly polarized components of incoming light. Then the signal from the two photodiodes is amplified by a differential amplifier which enables a very precise measurement of the difference between the intensities of the two components with opposite polarizations.

The spectral resolution of such a setup is achieved by using a tuneable laser beam as a source of reflected or transmitted light. The response time of the optical bridge is highly limited, however measurements with the temporal resolution are also possible due to proper illumination setup, making the pulsed

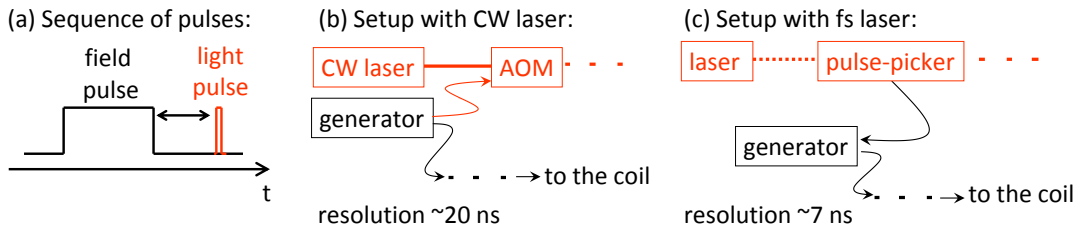

Figure 4.9: (a) A schematic diagram of the light and magnetic field pulses sequence in the setup comprising an optical bridge. (b) A schematic diagram of connections between the pulse generator and acousto-optic modulator (AOM) in the setup with a CW laser. (c) A schematic diagram of connections between the pulse generator and the pulse picker in the setup with a femtosecond laser.

excitation possible (see Figure 4.9(a)). This is done by either use of pulsed laser or continuous wave laser. In the latter case the laser beam was modulated with an acousto-optic modulator. A schematic diagram of the experimental setup in the latter configuration is shown in Figure 4.10, and the diagram of connections between the pulse generator and the acousto-optic modulator is presented in Figure 4.9(b). This setup allowed measurements with temporal resolution of about 20 ns, limited only by the response time of the acousto-optic modulator.

In cases when a better resolution was needed, the pulsed laser which produced pulses of about 40 fs was used. To reduce the spectral width of the illuminating light we used an additional simple monochromating setup. To reduce the repetition rate of the laser (equal to 78 MHz) and therefore extend the available range of the characteristic timescales of the processes under investigation, a pulse-picker was used in the laser beam. It decreased the laser repetition rate by a factor in the range 100-10000. A diagram of connections between the pulse generator and the pulse picker is presented in Figure 4.9(c).

Synchronization between the laser pulses and the magnetic pulses was realized in two slightly different ways, both relying on the pulsed generator used to supply the micro-coil. In the case when the acousto-optic modulator was used, two channels of the generator were used to drive both the micro-coil and the modulator, enabling independent control over the pulses width and the delay between them. In the case with a pulsed laser used as a light source, the laser worked also as a

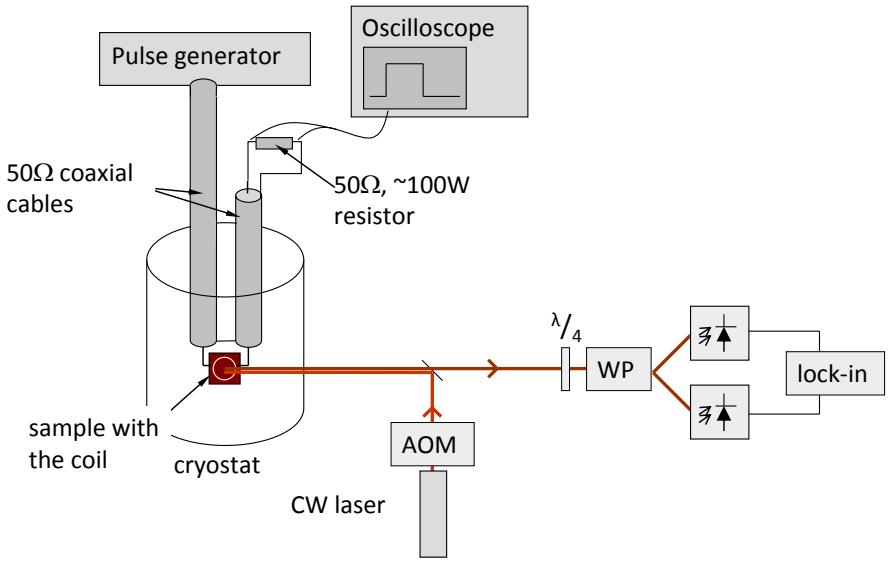

Figure 4.10: A schematic diagram of the experimental setup in the configuration using the optical bridge.

global clock of the setup. The pulsed generator was synchronized to this clock and governed only magnetic pulses.

In both cases the optical bridge worked in continuous mode. The repetition rate of the pulsed light source was much higher than the response frequency of the bridge. Therefore, collected signal was related only to the specific short period during or after the magnetic pulse. The whole measurement was performed as a series of measurements with a specific delay between the light pulse and magnetic pulse. The best temporal resolution available in such experiment was better than 10 ns.

In order to reduce observed noise and increase the dynamic range of the collected signal a heterodyne detection was used. The optical signal was modulated with frequency of 1 kHz by gating the magnetic pulses. The signal from the optical bridge was detected with a lock-in amplifier, synchronized with the modulation of the magnetic pulses. Such a setup allowed collection of the temporal profiles of the optical signal with at least two orders of magnitude better than the setup described in section 4.5.2.1 in the same acquisition time.

4.6 Data analysis

The magnetization temporal profile $M(t)$ collected with the experimental setups described above is given by a convolution of the temporal profile of the magnetic field (we assume that it is proportional to the current in the micro-coil $I(t)$ recorded with the oscilloscope), and the response function of the sample $f(t)$:

$$M(t) = \int_0^\infty I(t-\tau) f(\tau) \mathrm{d}\tau \tag{4.2}$$

In principle, to obtain the $f(t)$ function, it is sufficient to calculate the deconvolution of $M(t)$ and $I(t)$. This can be done by calculating Fourier transform of these two profiles, dividing the results and then calculating the inverse Fourier transform. However, due to relatively high noise present in the collected signal, a deconvolution algorithm did not give satisfactory results. Instead, different decay functions $f(t)$ were tested by convoluting them with $I(t)$ and fitting the result to the $M(t)$. It was found that in all cases a multi-exponential decays:

$$f(t) = \sum_{i=1}^{k} A_i e^{-\frac{t}{\tau_i}} \tag{4.3}$$

gave a very good agreement with the experimental data with k not greater than 3. Figure 4.11 shows a typical temporal profile of the magnetization of a $Cd_{1-x}Mn_xTe$ quantum well with 0.8% of Mn (points), measured after the magnetic pulse produced by the micro-coil, along with the profile of the current in the coil (blue dashed line). The convolution of the current profile with two different exponential decays (red lines) clearly shows that in this case the bi-exponential decay reproduces the experimental data with very good accuracy. At $t \approx$160 ns and $t \approx$320 ns characteristic kinks in profiles of the current and the magnetization (marked with black arrows) are clearly visible. These kinks are the consequence of the fact that due to relatively large inductance, the micro-coil does not exactly match the impedance of the transmission line. As a result, part of high-frequency

components of the current pulse bounces back to the pulse generator. The output of our home-made generator does not match the impedance of the transmission line either, therefore the current kink bounces back towards the micro-coil. This process repeats several times, therefore several kinks are visible in the experimental data. The repetition rate of these kinks is determined by the length of the transmission line between the pulse generator and the micro-coil.

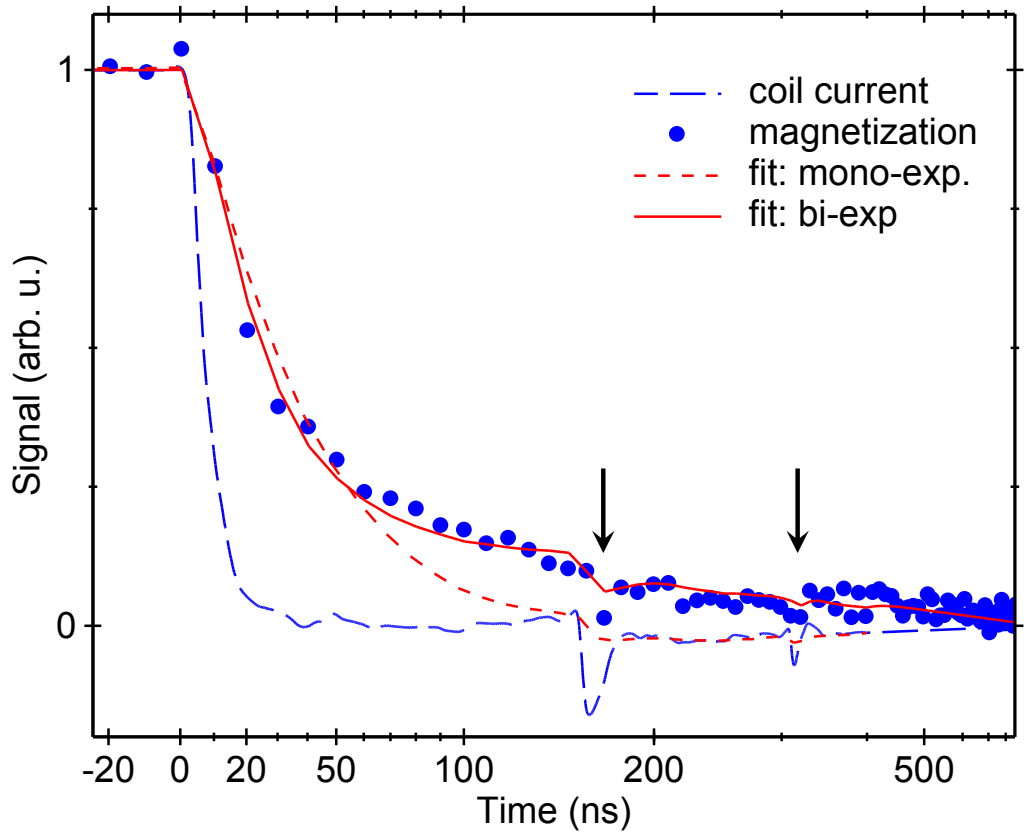

Figure 4.11: A typical temporal profile of the magnetization of a $Cd_{1-x}Mn_xTe$ quantum well with 0.8% of Mn (points), measured after the magnetic pulse produced by the micro-coil. The profile of the current in the micro-coil (blue dashed line) is shown along with its convolution with different response functions of the sample: mono-exponential and bi-exponential decays. Characteristic kinks in profiles of the current and magnetization (black arrows) are described in text.

Note, that if the current profile was a step function:

$$I(t) = \begin{cases} 1 \text{ for } t \leqslant 0 \\ 0 \text{ for } t > 0 \end{cases} \tag{4.4}$$

then after the convolution with function 4.3 we obtain:

$$M(t) = \sum_{i=1}^{k} B_i e^{-\frac{t}{\tau_i}} \tag{4.5}$$

where $B_i = A_i\tau_i$. Therefore, in next sections, whenever we deal with more than one exponential component of the decay function, for convenience by a relative amplitude A_i^{rel} of a specific component i, I will understand the expression:

$$A_i^{rel} = A_i\tau_i \tag{4.6}$$

Chapter 5

Spin orientation

In this chapter, I present the experiment of optical manipulation of a single Mn^{2+} ion embedded in the CdTe quantum dot. The experiment exploits the interaction between the magnetic ion and excitons confined in the dot. The dynamics of this interaction is studied in section 5.1 by means of correlation spectroscopy (the first such measurements of single Mn-doped quantum dots were performed by L. Besombes and co-workers [92]). In order to manipulate the Mn^{2+} spin, polarized excitons are injected to the dot with the magnetic ion using the spin-conserving exciton transfer between neighbouring dots (sections 5.2.1 and 5.2.2). The dynamics of the orientation process is also investigated (section 5.2.4).

5.1 Influence of exciton state on Mn^{2+} spin

As described in section 1.3.2, the optical readout of the spin state of a single Mn^{2+} ion embedded in the CdTe quantum dot is possible by recording the energy and polarization of photons emitted by the dot. This gives opportunity to investigate the Mn^{2+} spin dynamics in a dot under illumination by a laser beam. Photon correlation technique, described in section 3.2 is particularly useful in this purpose.

A measurement of auto-correlation of a selected component of the excitonic sextuplet gives the information about the time in which the spin state of the ion remains unchanged. On the other hand the study of cross-correlation of photons

from two different components allows us to measure the time of a transition between two particular spin states. The selection of investigated spin states is made either by choosing opposite circular polarizations and the same energy of detected photons or the same polarizations and different energies.

In order to better understand the results of correlation experiments performed on single Mn-doped dots let us first focus on the case of a non-magnetic quantum dot. Typical results of auto-correlation and cross-correlation of photons emitted by such a dot are presented in Figure 5.1. The curves represent normalized number of such events that both detectors detected a photon, plotted *vs.* the time delay between these two photons.

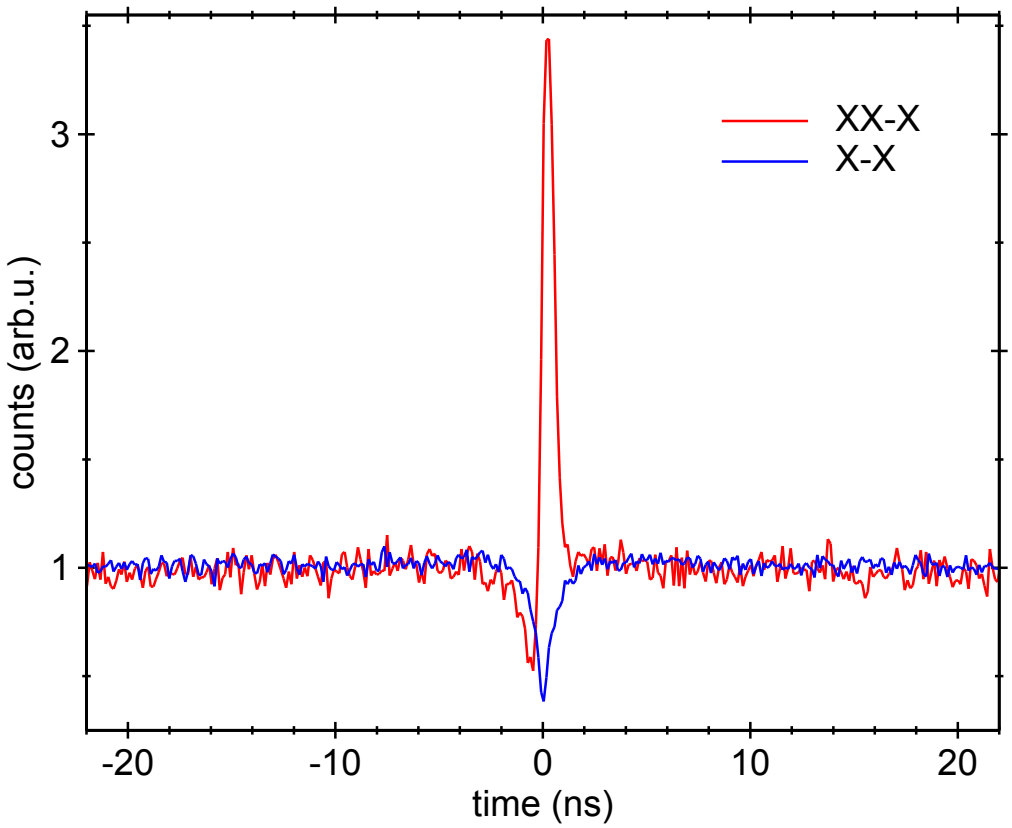

Figure 5.1: Typical results of photon correlation measurements of non-magnetic quantum dot. The blue curve corresponds to the auto-correlation measurement performed on the neutral exciton (X) line, the red one represents cross-correlation measurement between neutral exciton and biexciton (XX) lines.

Narrow features visible around the delay equal to 0 are related to dynamics of excitons confined in the quantum dot. In case of auto-correlation, both detectors detect photons related to the optical recombination of a neutral exciton. Since the quantum dot is a single photon source [93, 94] it is unlikely to detect two such photons with zero delay (τ) between them, *i.e.* two photons emitted exactly at the same time. Therefore in the auto-correlation measurement a sharp anti-bunching dip is clearly visible at τ=0. The width of the dip is given by an exciton lifetime in the quantum dot for weak excitation regime and becomes narrower with increasing excitation power [95, 96]. In an ideal experiment the depth of the dip would be equal to 100%, *e.i.* the number of the detected pairs of photons at τ=0 would be equal to 0. The depth of the dip is, however, limited due to temporal resolution of the experimental setup, the dark counts of the detectors used and some background luminescence usually present along with the quantum dot luminescence.

In case of cross-correlation of photons related to the transition of neutral exciton and biexciton, observed signal shows an asymmetric feature at the time delay equal to 0. Such an asymmetric shape is a fingerprint of a biexciton-exciton cascade [97]. It indicates a higher probability of emission of a photon related to the neutral exciton recombination right after the photon related to the biexciton one and low probability of emission of such photons in the opposite sequence.

Basically the same results can be obtained on a single Mn-doped quantum dot, when the detectors are insensitive to the Mn^{2+} spin state. This might be achieved by intentional reduction of the spectral resolution of the spectrometers by changing the gratings and opening widely the entrance slits. The result of such experiment along with the observed excitonic spectrum is shown in Figure 5.2. The features observed at $\tau = 0$ has the same width as those visible in Figure 5.1.

When the resolution of the detection system is high enough to resolve lines related to different Mn^{2+} spin states, the results of the correlation measurements are qualitatively different. Figure 5.3 shows typical results of the auto-correlation measurement performed on neutral exciton components related to the Mn^{2+} spin states with spin projection equal to $-5/2$ and $-3/2$ in comparison to the result of the cross-correlation between these two components. In the case of auto-correlation, a strong bunching with a narrow, sub-nanosecond antibunching dip is

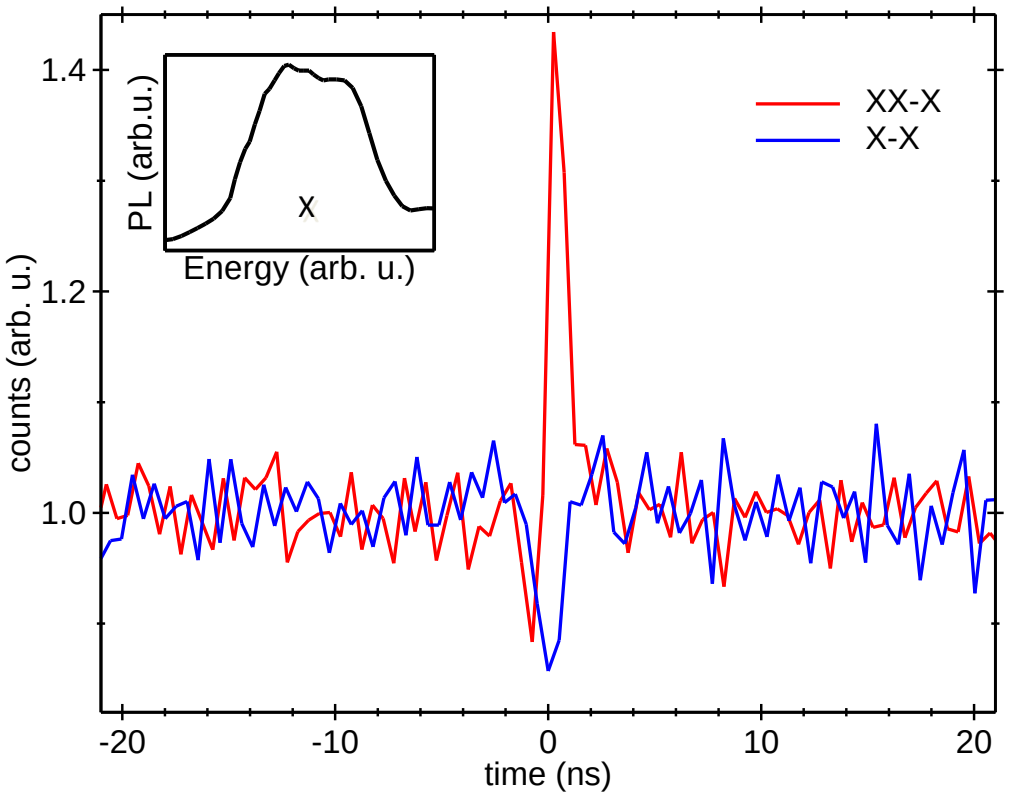

Figure 5.2: Typical results of photon correlation measurements insensitive on the Mn^{2+} spin state. The blue curve corresponds to the auto-correlation measurement performed on the neutral exciton (X) line, the red one represents cross-correlation measurement between neutral exciton and biexciton (XX) lines. Inset: excitonic spectrum recorded with intentionally reduced resolution of the detection setup.

clearly visible. The origin of the dip is the same as in the case of auto-correlation measurement on a non-magnetic quantum dot. It denotes the single-photon emitter character of the dot.

The dynamics of the Mn^{2+} ion's spin is revealed by the wide bunching, which has characteristic time equal to a few nanoseconds. Its presence is a consequence of the fact, that if the two photons are emitted within a small delay, then the probability that the Mn^{2+} spin state is conserved during this delay is high. Contrary to that, if the delay is large, the Mn^{2+} spin states during emission of the two photons are independent as long as the Mn^{2+} spin fluctuates randomly. Therefore the

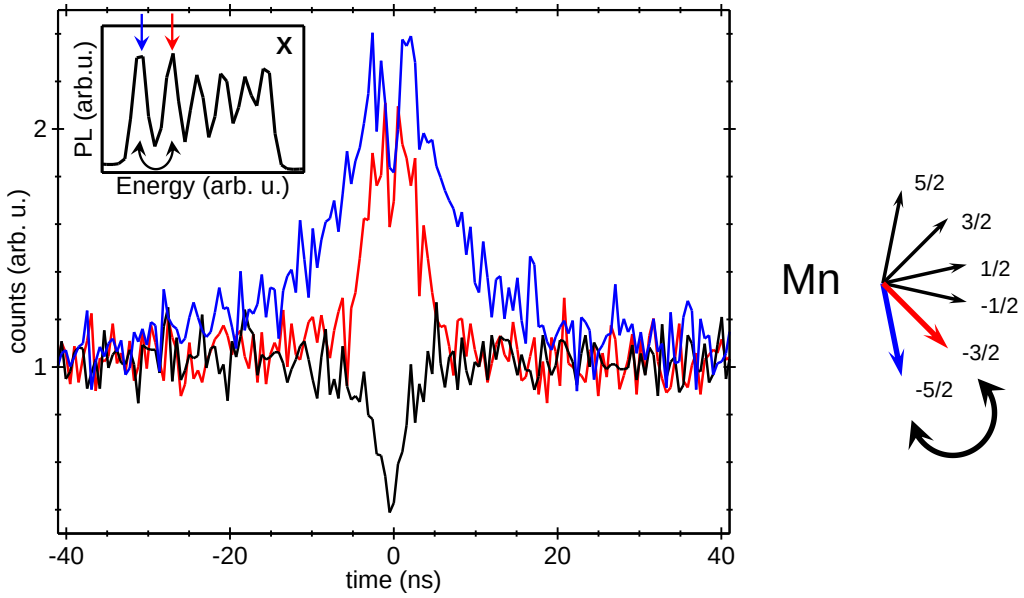

Figure 5.3: Typical results of photon correlation measurements between different components of a single-Mn doped quantum dot excitonic spectrum. Inset: neutral exciton photoluminescence spectrum.

width of the bunching visible in the auto-correlation measurement corresponds to the time in which the spin state of the ion remains unchanged.

What is attracting the attention in the results presented in Figure 5.3 is the fact that this characteristic time depends on the Mn spin state which is under investigation. It is significantly shorter in case of measurement performed on the line corresponding to the state with spin projection equal to $-3/2$, when compared to the one with the spin projection equal to $-5/2$. This might be explained if we assume that the most likely random transitions of the Mn^{2+} spin are those which involve adjacent spin states. In that case there is only one transition which drives the Mn^{2+} ion out of the $\pm 5/2$ states, while two such transitions exist in case of any other state. Assuming that all these transitions are random and equally probable one could expect that the Mn^{2+} ion will remain in the $-5/2$ state twice longer than in the $-3/2$ state. This is consistent with the experimental results within the experimental accuracy.

In case of cross-correlation of two excitonic lines, we observe strong antibunch-

ing which consist of two components with different time scale. A representative result of such experiment, involving adjacent lines related to the $-5/2$ and $-3/2$ lines is shown in Figure 5.3. As previously, the narrow, sub-nanosecond dip is related to dynamics of excitons confined in the quantum dot. The slower, nanosecond antibunching is related to the dynamics of the Mn spin. The time scale of this antibunching is related to the time scale of the wide bunching visible in auto-correlation experiments, as both these features origin from the same spin-flip transitions of the Mn^{2+} ion.

A different type of a correlation experiment revealing both the excitonic and the Mn^{2+} ion spin dynamics is a measurement involving lines related to the same state of the Mn^{2+} ion, but to different excitonic states. An example result of such measurement, involving neutral excitonic and biexcitonic lines is shown in Figure 5.4.

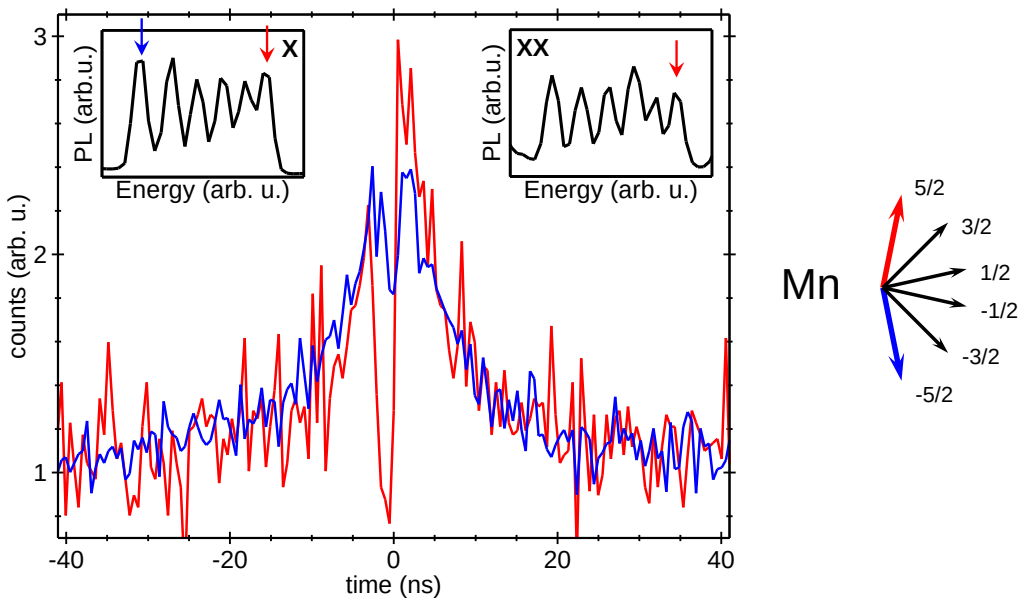

Figure 5.4: Result of cross-correlation measurement of the photons related to the same Mn^{2+} ion spin state with spin projection equal to $+5/2$, but different excitonic states (neutral exciton (X) and biexciton (XX)), compared with the result of the auto-correlation measurement of the photons related to the neutral exciton. Insets: excitonic and biexcitonic photoluminescence spectra

The observed signal is a product of a narrow asymmetric shape with the broad bunching related to the dynamics of the Mn^{2+} ion. The narrow feature denotes the neutral biexciton-exciton cascade. Its width is the same as the width of the cascade-related asymmetric features visible in Figures 5.1 and 5.2. The broad bunching is related to the dynamics of the Mn^{2+} ion. The width of the bunching is exactly the same as in the previously described measurement of auto-correlation of one of the excitonic lines, which can be easily seen in Figure 5.4.

All features related to the dynamics of the Mn^{2+} ion can be well described by a simple model of spin transitions of the Mn^{2+} ion. In the proposed model the transitions are assumed to be possible only between adjacent states and the transition probability p per unit time is equal for each pair of states (see Figure 5.5). A similar model was proposed in Ref. [92]. The rate equations for the occupation q_m of the Mn^{2+} spin states are following:

$$dq_m/dt = \begin{cases} p\left(q_{m-1} + q_{m+1}\right) - 2pq_m \text{ for } |m| \leqslant 3/2 \\ pq_{m+1} - pq_m \text{ for } m = -5/2 \\ pq_{m-1} - pq_m \text{ for } m = 5/2 \end{cases} \tag{5.1}$$

Result of fitting such a model to the experimental data is shown in Figure 5.6. It is clearly visible that the model reproduces all major features observed in the experiment. Note that the only fitting parameter is the transition probability p. In the best fit, the transition time, $\tau = \frac{1}{p}$, is equal to 5 ns for the data shown in Figure 5.6.

In order to better understand the mechanism of the spin transitions of the Mn^{2+} ion we performed a series of the auto-correlation measurements with different excitation power. Results of these measurements are shown in Figure 5.7. Using the same model as described above, we determined the dependence of the parameter p on the excitation power. Figure 5.8 shows the experimental results compared with the model curves. It is clearly seen that the characteristic time of the wide bunching strongly (super linearly) depends on the excitation power - by increasing the power by a factor of 2 we decreased the bunching width by a factor of 3.6, from 5 ns at 50 μW excitation to 1.4 ns at 100 μW. These characteristic times are longer than the mean time between exciton injection into the quantum

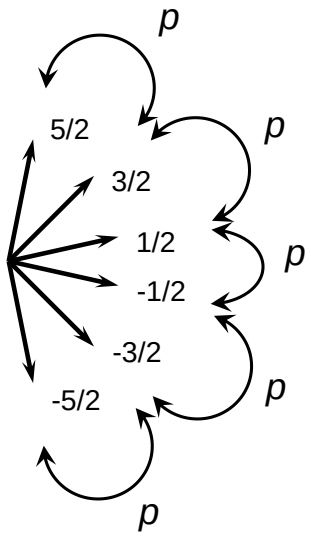

Figure 5.5: A schematic diagram of the Mn^{2+} ion spin transitions calculated with the model described in text.

dot (proportional to the excitation power), ranging roughly from 2 ns to 1 ns for excitation power equal 50 μW and 100 μW, respectively[1]. This result suggests that the random spin-flips of the Mn^{2+} ion are mainly caused by the interaction with randomly polarized, photogenerated carriers, which are trapped and recombine in the quantum dot. The exploitation of this fact by using spin-polarized excitons to polarize the single magnetic ion in the quantum dot is described in section 5.2. The super linear dependence of the p on the excitation power might be caused by the influence of biexcitons. Their creation probability is known to depend almost quadratically on the quantum dot excitation intensity [34].

5.2 Spin orientation by polarized photons

Results presented in section 5.1 suggest that the main driving force of the random spin-flip transitions of the Mn^{2+} ion is the interaction with randomly polarized

[1]The mean time between exciton injection into the QD is estimated by using X and XX intensity power dependence and the exciton lifetime. This method is described in more detail in section 5.2.3 and in Ref. [98].

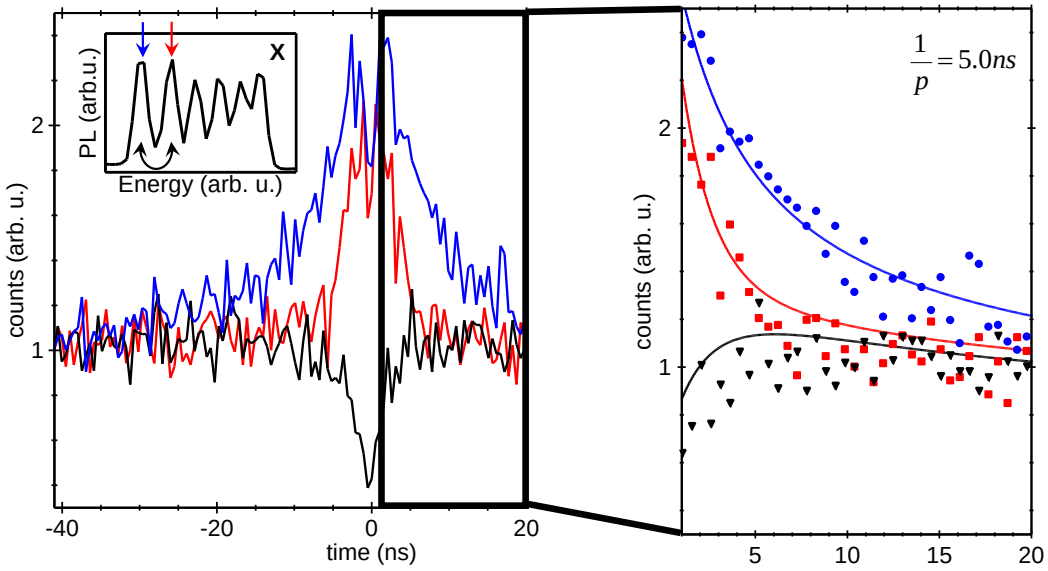

Figure 5.6: Comparison of the results of the auto- and cross-correlation measurements (points on the right panel) with the model described in text using the time constant of the Mn^{2+} spin flips as a fitting parameter.

carriers trapped in the quantum dot. This brought the idea of inducing the polarization of the Mn^{2+} ion by injecting spin polarized excitons into the dot. In this section, I describe in detail how such an experiment was performed.

5.2.1 Coupled quantum dots

In order to create spin polarized excitons one has to excite them with circularly polarized light. Moreover, it is necessary to create them resonantly inside the quantum dot. Otherwise, if they are created in the barrier material, their spin polarisation is significantly reduced or even completely lost during the relaxation process. The resonant excitation not only solves this problem, but also significantly increases the quantum dot excitation efficiency.

There is, however, a major experimental difficulty in using this type of excitation. If the excited state is the ground exciton state in the quantum dot it very difficult to observe the photoluminescence from this dot, as it occurs in the

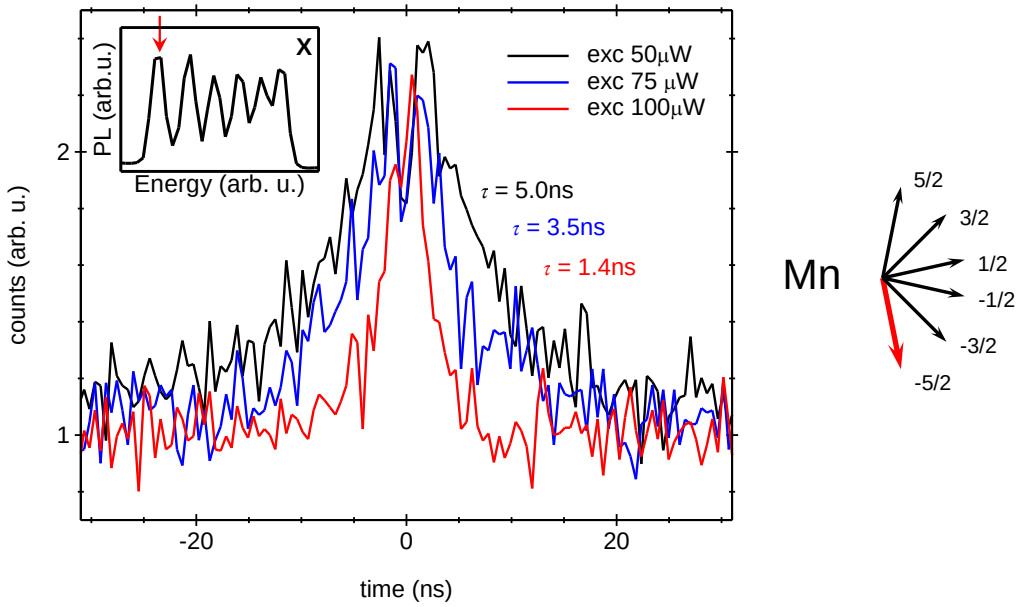

Figure 5.7: Result of auto-correlation measurements of the σ^+-polarized photons related to the Mn^{2+} ion spin state with spin projection equal to $-5/2$, performed for different values of excitation power.

same or very close energy as the excitation. One of the solutions of this problem proposed by Besombes *et al.* is excitation resonant with a higher excitonic level in the dot [45]. In this work a different method is proposed: the resonant excitation of the ground excitonic level in a non-magnetic quantum dot and use of the tunnelling of the exciton to the neighbouring dot containing a single Mn^{2+} ion. To realize this excitation scenario, among the identified quantum dots with single Mn^{2+} ions we have selected those exhibiting a sharp resonance in photoluminescence excitation (PLE) spectra, as shown in Figure 5.9. As it was shown on similar samples with and without Manganese [46, 99], such resonances are fingerprints of pairs of coupled quantum dots and of transfer of excitons between them. Following arguments support the inter-dot energy transfer: (i) resonances are very sharp (width equal to tens of μeV); (ii) they appear at energy much larger than energy of observed emission (more than 0.2 eV), with no correlation between the two energies; (iii) all the observed charge states of the emitting quantum dots share the same resonance energy; (iv) optical in-plane anisotropy

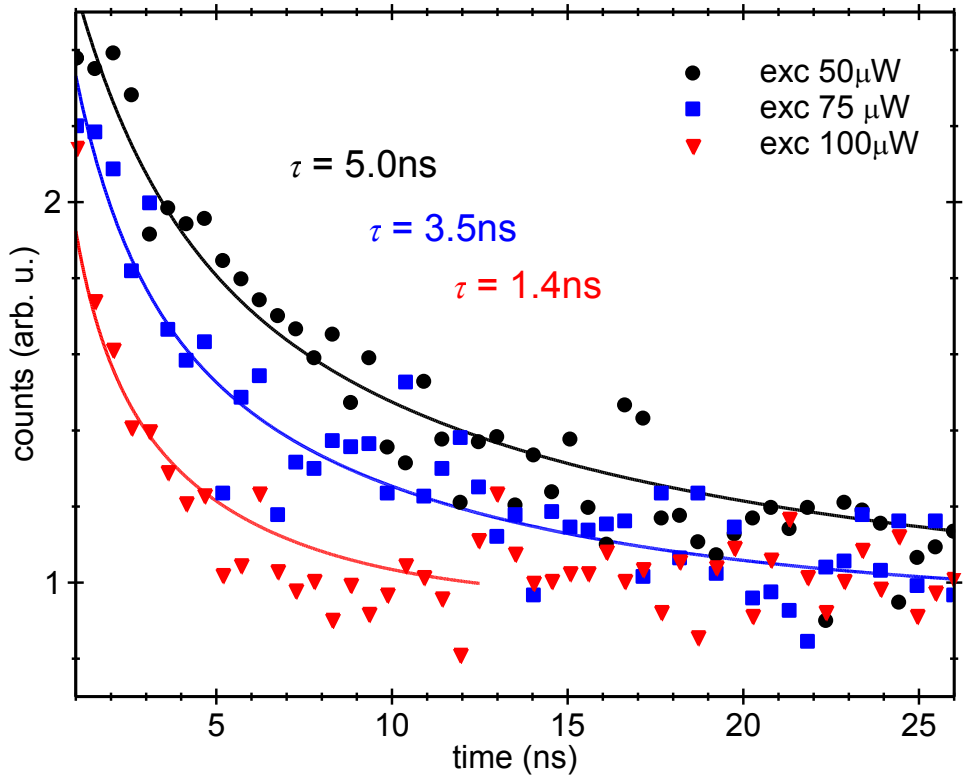

Figure 5.8: Experimental data (points) shown in Figure 5.7 compared with model described in text (the time constant of the Mn^{2+} spin flips (τ) used as a fit parameter.

(characteristic for the neutral exciton) is different and uncorrelated in absorption and in emission; (v) the Zeeman splitting as well as diamagnetic shift (in high magnetic field) for both absorption and emission are typical for neutral excitons observed in photoluminescence of quantum dots without magnetic ions (see Figure 5.10); (vi) while the PL exciton lines exhibit characteristic sixfold splitting due to the interaction with single Mn^{2+} ions, the absorption line is usually not split by this interaction (see Figure 5.9).

Basing on these findings we conclude that the resonance is related to absorption in a quantum dot with no Manganese. The photocreated exciton is then transferred to a larger dot containing a single Mn^{2+} ion. As shown in Ref. [99] the transfer time is of order of 10 ps. Note that finding such pair of quantum

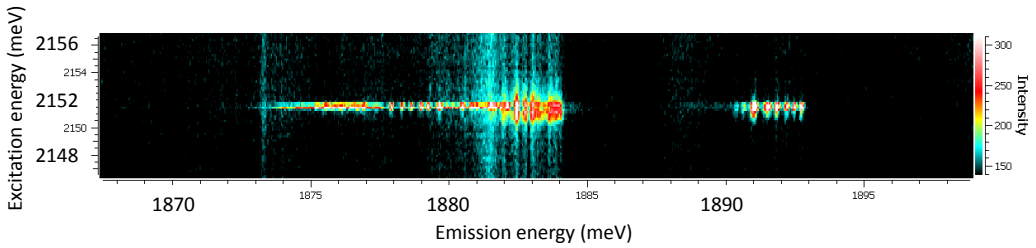

Figure 5.9: Photoluminescence excitation map (density plot of PL intensity versus excitation/emission photon energy) close to the resonance.

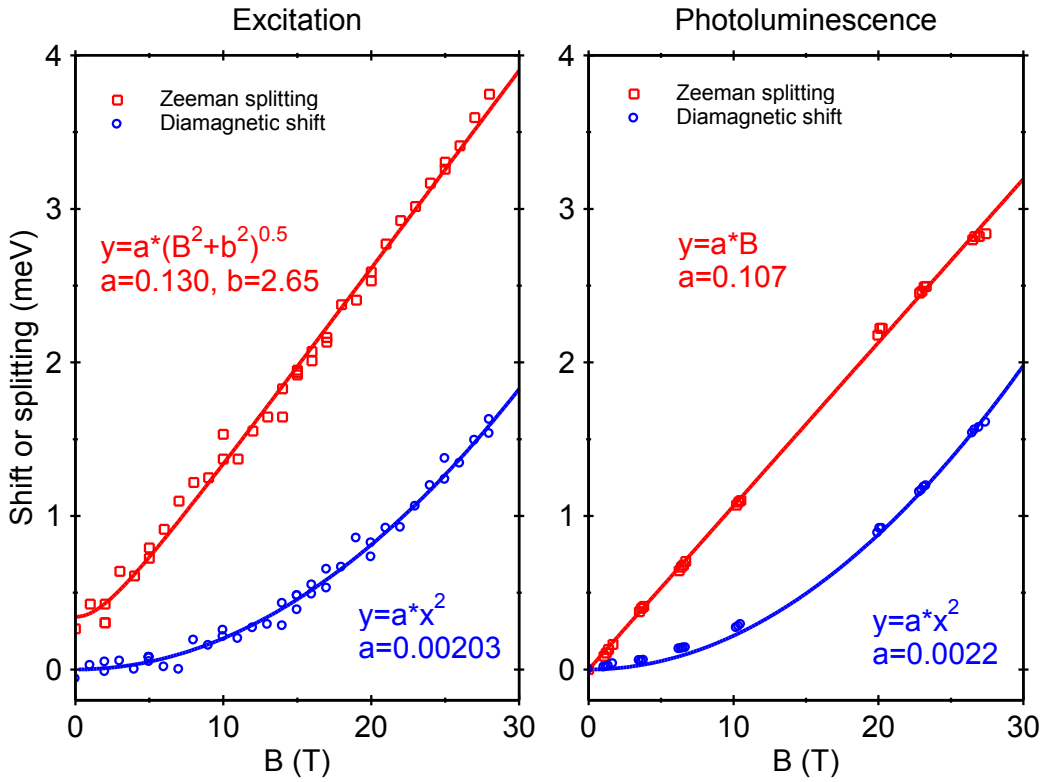

Figure 5.10: Comparison of the Zeeman splitting and diamagnetic shift of the ground excitonic level in the absorbing (left) and emitting (right) quantum dot.

dots is possible even despite quite low dot density (equal to about 5×10^9 cm^{-2}) since in our samples quantum dots tend to form groups of closely-spaced dots

[47]. A more detailed discussion of the interdot transfer mechanism can be found in Refs. [37, 99].

5.2.2 Spin-conserving exciton transfer

As it was shown in Ref. [46] and Ref. [99], during the transfer between two coupled quantum dots the spin of the exciton is conserved. The experimental proof for this fact in case of singly Mn-doped quantum dot is a higher intensity integrated over the 6 exciton lines in the photoluminescence spectra measured in the same circular polarizations of excitation and detection (co-polarized) then the integrated intensity of the excitonic lines measured in different polarizations (cross-polarized). The lower intensity equals about 65% of the higher one which gives a lower bound for the polarization transfer efficiency. The transfer efficiency depends on the details of the parameters of the coupled quantum dots (such as in-plane anisotropy and excitation transfer rate). In our case it is almost independent on magnetic field up to 28 T. It decreases for higher excitation power due to the increased probability of biexciton formation. The biexciton ground state is a spin the spin singlet state, thus it cannot carry any spin memory. Therefore the presence of biexcitons leads to a suppression of the spin polarization transfer.

5.2.3 Mn^{2+} spin orientation

The exciton polarization transfer is used as a tool for optical writing of information on the Mn^{2+} spin. Carriers created by a defined circular polarization of light act on the Mn^{2+} ion and orient its spin. The details of the mechanism of this process are, however, not known. There are several hypotheses which are proposed, including dark exciton recombination [100] (see chapter 6), simultaneous spin-flip of the Mn^{2+} ion and the hole localized on the quantum dot and relaxation of the Mn^{2+} spin in the effective magnetic field of the exciton. The leading orientation mechanism has not been determined so far. This issue requires further studies.

The Mn^{2+} spin orientation appears as a non-uniform distribution of intensities between the 6 exciton photoluminescence lines, which reflects a non-equal probability of finding the Mn^{2+} ion in different spin states. The orientation is much

more efficient in presence of a magnetic field of about 1 T, due to suppression of fast spin relaxation channels [101] (see section 7.2.1). Figure 5.11 shows an typical excitonic spectra taken under circular excitation at B=1 T compared to the one taken under linear excitation without magnetic field. It is clearly seen that the polarization of excitation beam affects not only the distribution of intensities between the 6 excitonic lines, but also the overall intensity integrated over these 6 lines. As mentioned in section 5.2.2, this proves that the polarization of exciton is indeed conserved with reasonable probability during the transfer between two coupled quantum dots.

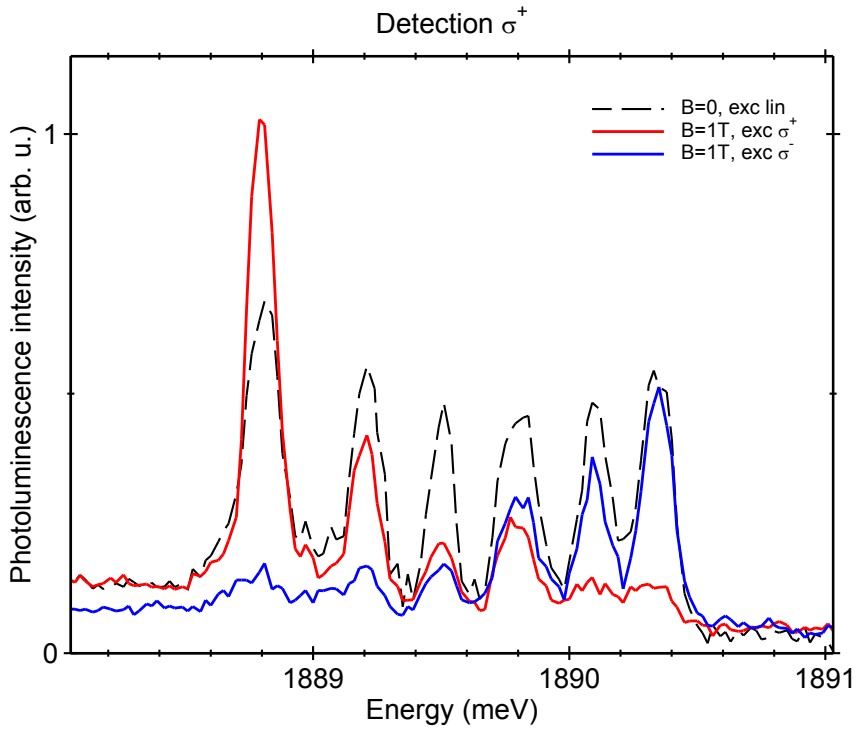

Figure 5.11: Typical excitonic spectra taken under circular excitation at 1T compared to the one taken under linear excitation without magnetic field. The measurements were performed with σ^+ polarized detection.

As a quantitative measure of the spin orientation we use the mean spin value of the Mn^{2+} ion determined from the centre of mass of the PL sextet (weighted by intensity). A typical variation of this value versus excitation power is shown in

Figure 5.12. For B=0 it shows a maximum at about 0.1 mW/μm^2 and decreases for higher and lower power. The decrease at the high power corresponds to the increased probability of the biexciton formation and - as a consequence - a decrease of the efficiency of the Mn^{2+} spin alignment. The decrease at low excitation power is due to the competition between the Mn^{2+} spin relaxation, and the spin orientation by the photo-created excitons. The relaxation becomes dominant when the average time delay between capture of two excitons is longer than the relaxation time. This condition provides an estimate of the relaxation time, being in our case of the order of a few nanoseconds. This value compares reasonably with the relaxation time determined for very diluted $Cd_{1-x}Mn_xTe$ quantum wells in the absence of magnetic field (see section 7.2.1). The fast relaxation was caused mainly by the hyperfine interaction with nuclear spin.

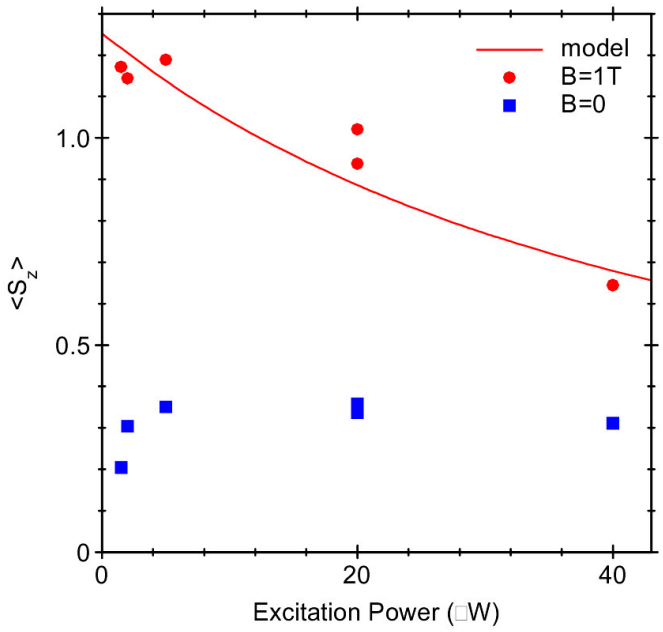

Figure 5.12: The mean spin of the Mn^{2+} ion as a function of excitation power for B=0 and B=1 T compared with model described in text (solid line).

The situation is different for B=1 T. Similarly to the zero-field case, the mean spin value of the Mn ion shows a decrease at high power, resulting from an increase of the probability of biexciton formation. However, no decrease is observed at

low power, down to its lowest values, due to suppression of fast spin relaxation channels (see section 7.2.1 and Ref. [101]). Such dependence of the Mn^{2+} mean spin on the excitation power can be described by a simple optical orientation model. It is based on the assumption that any Mn^{2+} state, characterized by its quantum number m, can be transferred to a state with m different by 1 with a fixed probability p_0 during the presence of a suitably polarized exciton in the quantum dot. Moreover, it takes into account the influence of biexcitons, assuming that each of them contributes with equal probability $p_0/2$ to the Mn^{2+} up- and down spin flips. This gives following rate equation for the probability of the occupation (q_m) of each Mn^{2+} spin state (with a suitable cut-off for $|m| = 5/2$):

$$\begin{aligned} dq_m/dt = \; & q_{m-1}p_0\left(\varphi_{X_{-1}} + \tfrac{\varphi_{XX}}{2}\right) + q_{m+1}p_0\left(\varphi_{X_{+1}} + \tfrac{\varphi_{XX}}{2}\right) \\ & -q_m p_0\left(\varphi_{X_{-1}} + \varphi_{X_{-1}} + \varphi_{XX}\right)) \end{aligned} \tag{5.2}$$

where $\varphi_{X_{\pm 1}}$ are frequencies of arriving of excitons into the quantum dot and φ_{XX} is the biexciton creation frequency. Within these assumptions of the model, the steady state of Mn^{2+} spin does not depend on absolute exciton transfer rate or p_0 value, but only on the relative numbers of biexcitons and spin-up and spin-down excitons arriving in the emitting dot. To determine the biexciton/exciton ratio of arrival rates in the quantum dot, we use a rate equation model of exciton dynamics introduced by Regelman *et al.* [98]. We select a basis containing up to three excitons in the dot. Using thus obtained biexciton/exciton arrival rate ratio, the power dependence of Mn^{2+} spin orientation was calculated, with the exciton spin transfer efficiency as a free parameter. As shown in Figure 5.12 an excellent agreement with the experimental data was obtained with spin-up to spin-down probability ratio of 0.62. This value agrees well with the lower limit of the polarization transfer determined experimentally from the net polarization of the exciton line at low excitation power (see section 5.2.2).

5.2.4 Dynamics of the Mn^{2+} spin orientation

Dynamics of the Mn^{2+} spin orientation was studied by the use of the spin-conserving exciton transfer between quantum dots. The dynamics in magnetic

field was analyzed in a time-resolved experiment in which the intensity and polarization of excitation were modulated. The excitation sequence was following: first, the Mn^{2+} spin was oriented using a σ^+ - polarized excitation. Then the light was switched off for a controlled delay and subsequently the light with σ^- polarization was switched on to accomplish the read-out of the spin state and then to reorient the Mn^{2+} spin. After a period long enough to allow the Mn^{2+} spin reaching a steady state the polarization of excitation was switched back to σ^+. Such a pattern reveals different properties of the spin reorientation processes, both in the absence and in the presence of illuminating light. The Mn^{2+} state was investigated by measuring the photoluminescence intensity of a selected component of the exciton sextuplet in a given circular polarization. Its evolution reflects the orientation of the Mn^{2+} spin combined with the exciton optical orientation. The measurements were repeated for both circular polarizations of detection.

Here I will consider a relatively simple case when the dark period was short enough to neglect all Mn^{2+} spin relaxation processes in the dark. An analysis of the situation involving long dark period is presented in section 7.1.

A representative result of measurement taken under excitation following abovementioned pattern is presented in Figure 5.13(a). It shows a temporal profile of the photoluminescence intensity of the lowest-energy component of the exciton sextuplet (as marked on the inset in Fig. 5.13(a)) observed in σ^+ polarization. The excitation power was low enough to neglect the formation of any excitonic states in the quantum dot except the neutral exciton ground state. It is easy to distinguish four phases of the profile. The first flat region is related to excitation with σ^+ polarization, the same as the detection polarization. Second phase with no photoluminescence corresponds to the period when the excitation is off. When subsequently a σ^- polarized excitation is turned on, the photoluminescence intensity first rises rapidly. This is due to the fact that during the short dark period the Mn^{2+} spin state is conserved (see section 7.1). The maximum value of the signal after turning the excitation on is determined only by the efficiency of the exciton polarization transfer and is equal to about 65% of the previous value.

After the initial rapid increase, the photoluminescence intensity slowly decreases with a characteristic time of tens of nanoseconds (part A of the profile presented in Figure 5.13(a)). This decrease is related to the reorientation of the

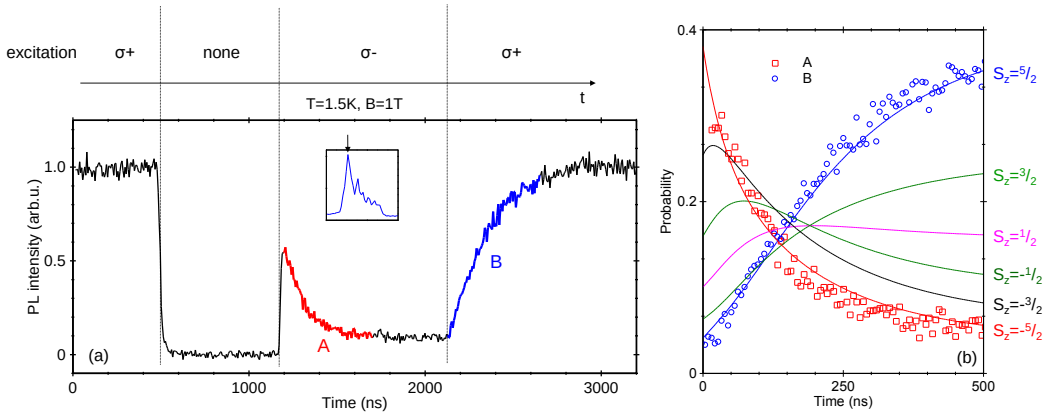

Figure 5.13: (a) The temporal profile of the intensity of one of the six excitonic lines (marked in the inset) under the excitation pattern shown in the upper part of the figure and described in the text. (b) Calculated temporal profiles of occupation of six Mn^{2+} spin states with indicated spin projection after the rapid change of excitation polarization from σ^+ to σ^- (solid lines) compared with the temporal profiles of occupation of the extreme state measured in the experiment (symbols).

Mn^{2+} spin by circularly polarized light. This process accelerates with increasing excitation power, as shown in Figure 5.14. Its characteristic time is approximately inversely proportional to the excitation power. This property suggests that the simple model, introduced in section 5.2.3 to describe the steady-state Mn^{2+} spin orientation, can also be used to interpret its dynamics. In contrast to the steady-state case, now the rate at which excitons arrive in the emitting quantum dot, as well as the spin-flip probability p_0, becomes important. We determine the former from the biexciton-exciton intensity ratio, using our rate equation model. The latter enters the model calculation as a free parameter. The result of such a calculation, presented in Figure 5.14(b), describes well the experimental values, assuming p_0=0.05. It is also important to note that in our case the photocreated excitons are well defined and no free photocreated carriers are expected to contribute to the spin relaxation. We excite resonantly excitons in the neighbouring quantum dot with an excitation power sufficiently low to make any non-resonant processes negligible. Therefore, in contrast to Ref. [92], we do not consider the spin exchange with individual carriers surrounding the quantum dot.

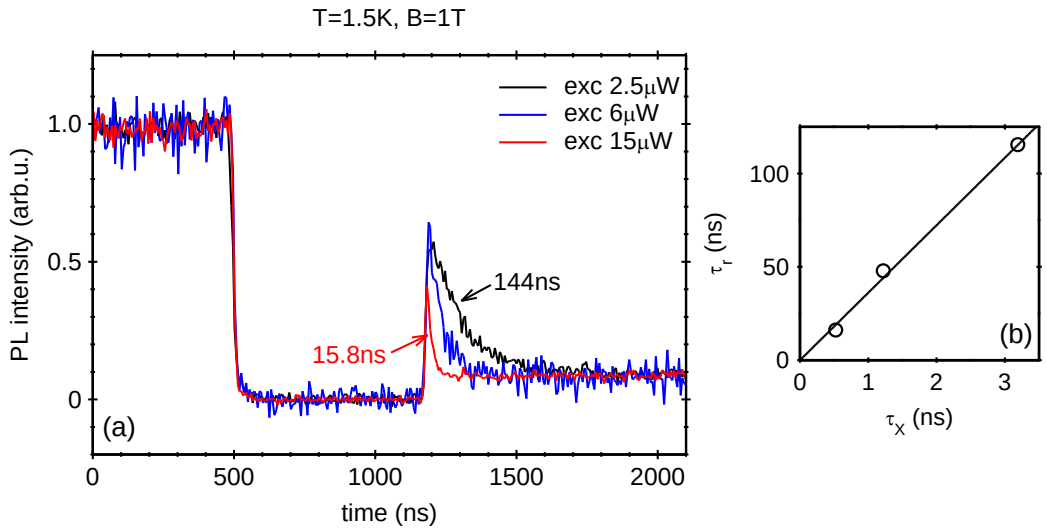

Figure 5.14: (a) Temporal profile of the photoluminescence intensity at one of the six components of the exciton spectrum during the excitation sequence described in text for B=1 T and indicated values of excitation power. (b) The Mn^{2+} reorientation time upon illumination in σ^- polarization (τ_r) *vs.* averaged time delay between capture of two excitons (τ_r).

The last part of the temporal profile presented in Figure 5.13(a) (part B) starts when the polarization of excitation is switched back to σ^+. The observed signal slowly increases due to reorientation of the Mn^{2+} spin back to the initial state. It is clearly seen that the decrease of the signal observed under σ^- excitation (A) is much faster than the increase observed after switching the excitation to σ^+ (B). It can be explained by a rate equation model introduced in the section 5.2.3. Using this model we are able to calculate the expected evolution of probability of finding the Mn^{2+} ion in each of six spin states after a rapid change of the excitation polarization to the opposite one. This evolution is shown in Figure 5.13(b) (six solid lines, each corresponding to a specific spin state of the Mn^{2+} ion). It is clearly seen that the probability of occupation of the state, which was initially the least occupied, is much slower than the decrease calculated for state which was the most occupied at t=0. This is due to the fact that before the occupation of the former state is built, the Mn^{2+} spin has to pass many possible projections

onto the quantization axis, as transition are allowed only between adjacent states. The comparison with increase and decrease of the occupation probabilities of the extreme state measured in the experiment (symbols in Figure 5.13(b) shows that this model describes measured evolution with very good accuracy.

Chapter 6

Dark excitons

An important, but nevertheless, little investigated recombination channel of the excited state in the quantum dot is related to the dark exciton states *i.e.* states with total angular momentum equal to 2 [102]. Random transitions between dark and bright excitonic states lead to exciton decoherence [103] and a significant modification of the recombination dynamics which can result in the delayed emission of photons [104, 105]. Despite their importance, dark exciton states are difficult to probe. The radiative recombination of dark excitons is forbidden so that they usually cannot be studied directly using spectroscopic techniques. Their properties can be accessed indirectly by a detailed analysis of the dynamics in time-resolved profiles of the bright exciton photoluminescence [104, 105, 106]. The other possibility is to measure the weak optical transitions under conditions in which the dark exciton recombination is partially allowed. This has been achieved either by the use of the in-plane magnetic field which mixes the heavy-light hole states [107, 108] or by placing the quantum dot in a micro-pillar which enhances the coupling of the exciton with light [109].

In this chapter, I present an investigation of dark exciton optical transitions which are allowed due to the simultaneous spin flip of coupled single magnetic impurity. An important conclusion from this experiment is that these transitions are one of the mechanisms of the optical orientation of the single Mn^{2+} spin in the quantum dot.

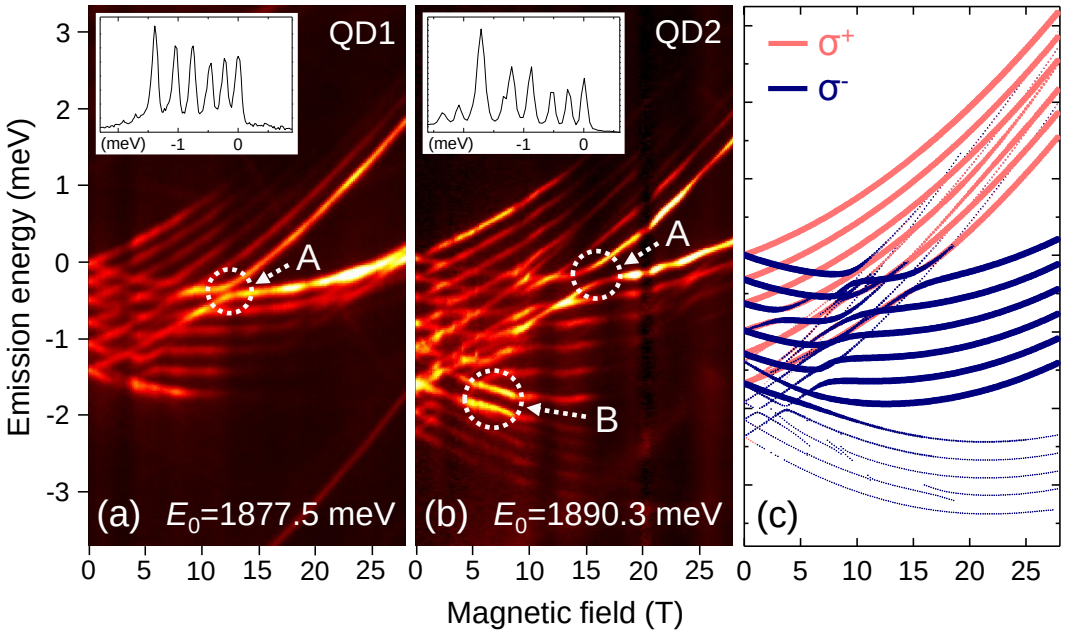

Figure 6.1: (a-b) Colour-scale plots of the photoluminescence spectra of two single Mn-doped quantum dots as a function of magnetic field. Two dots (QD1 and QD2) differ by in-plane anisotropy. The vertical scale of each panel is shifted by E_0. Insets: PL spectra at $B = 0$. (c) Simulation of the optical transitions in the QD2 with the model described in text. The line thickness corresponds to the oscillator strength of the transitions.

6.1 Optical recombination of dark excitons

The ability to control the state of the Mn^{2+} ion presented in section 5.2.3 enables easy featuring of selected spectroscopic lines from the Mn-doped quantum dot excitonic spectrum. This, along with the use of high magnetic field, which allows separation of lines related to specific spin states of the exciton (by controlling the Zeeman splitting), facilitates convenient observation of the transitions related to the dark excitonic states.

Figure 6.1(a-b) shows the evolution of exciton photoluminescence spectra with magnetic field, measured without polarization resolution for the two selected quantum dots. To elucidate the most characteristic features of this evolution we initially focus on Figure 6.1(a) showing the quantum dot with the smaller in-plane

anisotropy. In the magnetic field, the exciton sextuplet splits into two distinct Zeeman branches corresponding to σ^+ and σ^- circular polarizations for the upper and lower branch respectively. The lowest component of each branch corresponds to the Mn^{2+} spin antiparallel to the exciton spin [49]. The resonant excitation with σ^- polarization, combined with the magnetic field which significantly slows down the Mn^{2+} spin relaxation [101], prevents the Mn^{2+} spin from thermalizing [46]. Therefore all six lines are visible in both branches up to magnetic fields $\sim$15 T.

At a magnetic field of around 12 T, an anticrossing of the outermost lines of both branches is clearly visible ("A" in Figure 6.1(a)). These two lines correspond to the same $-5/2$ state of the Mn^{2+} spin, but two opposite spin states of X. At this field, the excitonic Zeeman splitting exactly compensates the X-Mn exchange interaction. The splitting (anticrossing) of these two lines is then simply due to the in-plane anisotropy of the quantum dot, acting via the anisotropic component of the electron-hole (e-h) exchange interaction, as observed for excitonic lines in the absence of magnetic field for non-magnetic quantum dot [110]. As we have checked, the two split lines show linear polarization (presumably along the symmetry axes of the anisotropic dot), in contrast to the remaining sextuplet lines which are polarized circularly. The anisotropic exchange splitting, determined from the anticrossing, is equal to 60μeV for QD1 in Fig 6.1(a), and 230μeV for QD2 in Fig 6.1(b).

Our optical method to align the Mn^{2+} spin against the action of the external magnetic field [46] (see section 5.2.3) becomes less efficient at magnetic fields above $\sim$ 15 T. This is due to the accelerated spin-lattice relaxation of the Mn^{2+} spin at high magnetic field. Details of the dependence of relaxation rate on the magnetic field are discussed in section 7.1.2.2. As a result, the Mn^{2+} spin orientation thermalizes and the excitonic lines related to the less populated spin states vanish.

Strikingly, the quantum dot with the larger anisotropic exchange splitting value (Figure 6.1(b)) has an additional, albeit weaker, lower branch consisting of only five lines. To understand the origin of this branch one should notice that optical transitions are possible in two situations: (a) The projection of total angular momentum of the exciton on the quantization axis is equal to ± 1 (bright

exciton). In this case the transition is dipole allowed and the Mn^{2+} spin projection is conserved during the X recombination. Branches with six lines are related to this kind of recombination. (b) The projection of total angular momentum of the exciton is equal to ± 2 (dark exciton, X_d). Then, in the first approximation the optical transition is dipole forbidden. However, the valence band mixing and the exchange interaction with the Mn^{2+} ion result in a mixing of the electron and hole spin states. As a result, the X_d states have an admixture of the X states with the Mn^{2+} spin projection different by 1. Thus, the X_d recombination is possible when accompanied by the simultaneous spin-flip of the Mn^{2+} ion. As there are only 5 possible transitions between the 6 Mn^{2+} spin states, the photoluminescence lines related to X_d present a fivefold spitting. The upper energy branch of X_d is not clearly visible in our experiment because it overlaps with much stronger X transitions.

The quantum states of the exciton and Mn^{2+} spin can be described in the basis given by three quantum numbers: $|S_z, \sigma_z, j_z\rangle$ indicating the Mn^{2+}, electron and hole angular momentum projections onto the quantization axis parallel to the magnetic field. Using the available information for the g-factors of the carriers and the Mn^{2+} ion [111], we attribute the X_d low energy branch to the recombination of $|S_z, +1/2, +3/2\rangle$ states. Therefore, to satisfy the selection rules for X_d dipolar recombination the projection of the Mn^{2+} spin must be increased by 1. This implies that each possible X_d recombination is related to a spin-flip of the Mn^{2+} ion towards the state polarized opposite to the thermalized state. There are three different admixtures of the X_d states which make this process possible (see Figure 6.2). The first one is the state with the opposite spin projection of the electron ($|S_z + 1, -1/2, +3/2\rangle$). It is mixed with the X_d state due to the *e*-Mn exchange interaction. The second admixture, caused by the *h*-Mn exchange interaction, consists of a light hole with a spin projection different by 1 from the heavy hole of the X_d ($|S_z + 1, +1/2, +1/2\rangle$). The last admixed state, $|S_z + 1, +1/2, -3/2\rangle$, consists of a heavy hole with a spin projection different by 3 from the spin projection of the original state. This admixture is induced by two interactions acting together: the heavy-light hole mixing, which mixes hole states with spin projection different by 2, and by the *h*-Mn exchange interaction. A direct experimental evidence for the presence of valence band mixing is provided

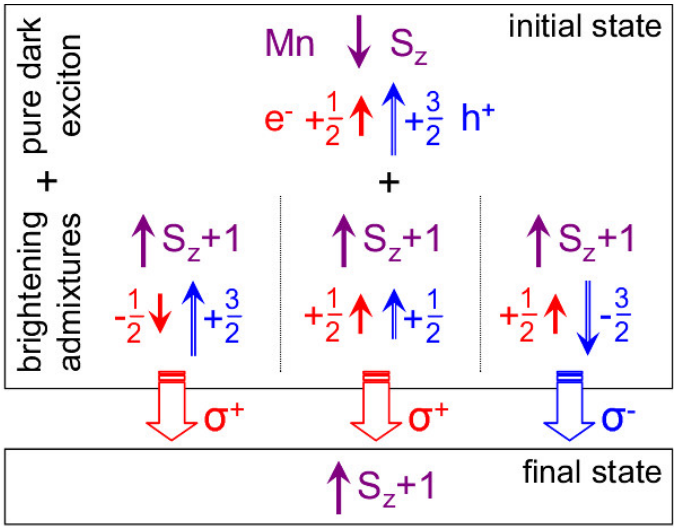

Figure 6.2: A schematic diagram of X admixtures in the X_d states and possible channels of optical transitions related to the X_d recombination.

by the anticrossing of the highest energy line of X_d and the lowest energy line of X at a magnetic field ~ 7 T (labelled "B" in Figure 6.1(b)). These lines correspond to $|+1.5, +1/2, +3/2\rangle$ and $|+2.5, +1/2, -3/2\rangle$ states, respectively.

The radiative recombination related to the first two of these admixtures results in the emission of a photon with σ^+ polarization. The amplitudes of these admixtures depend only on the e-Mn and h-Mn exchange constants, *i.e.* on the overlap of the Mn^{2+} ion and the carrier wave functions. In contrast, the recombination related to the third admixture produces a σ^- polarized photon. The amplitude of this admixture depends not only on the X-Mn exchange interaction, but also on the valence band mixing, which, similarly to the anisotropic exchange splitting, results from the in-plane anisotropy of the quantum dot [86, 108, 112, 113]. The role of this anisotropy in determining the polarization of the X_d lines is clearly visible in our experiment. Figure 6.3 shows spectra of the two quantum dots shown in Figure 6.1 for similar excitation conditions and magnetic field near the anticrossing of the lines related to $|-2.5, -1/2, +3/2\rangle$ and $|-2.5, +1/2, -3/2\rangle$ states ("A" in Figure 6.1(a-b)). In the X_d region the σ^- polarized lines are much more pronounced with respect to the σ^+ polarized ones for a highly anisotropic QD2.

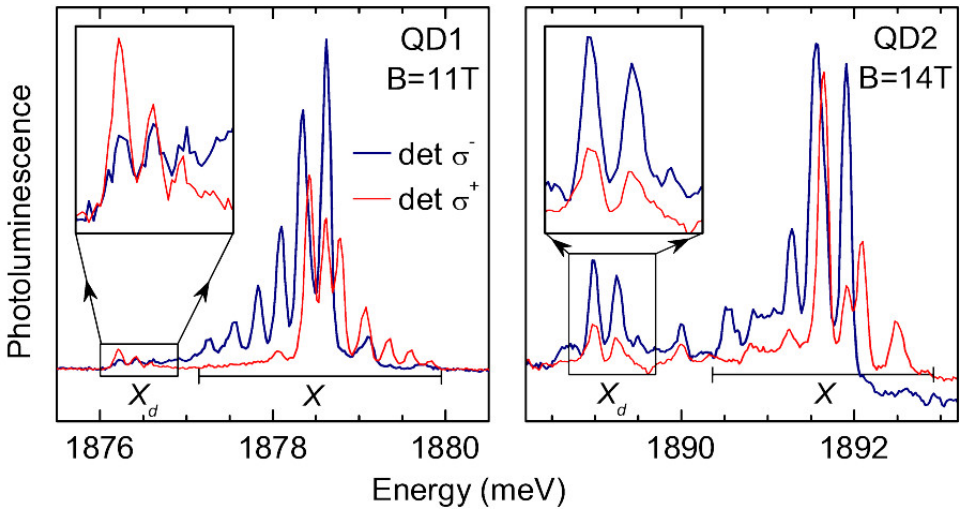

Figure 6.3: Spectra of the two quantum dots shown in Fig. 6.1 taken under excitation with σ^- polarized light and with polarization resolved (σ^+ or σ^-) detection for magnetic fields near the anticrossing of lines corresponding to $|-2.5,-1/2,+3/2\rangle$ and $|-2.5,+1/2,-3/2\rangle$ states ("A" in Fig 6.1(a-b)).

As a quantitative measure of the X_d oscillator strength for both circular polarizations we use the X_d/X intensity ratio. Since this ratio depends on the excitation power [35], one should use identical excitation conditions to be able to compare its value for different quantum dots. Experimentally, this is achieved by choosing the same XX/X intensity ratio equal in our case to 1/3. The XX intensity increases roughly quadratically with the excitation power, while the X intensity follows linear power dependence [34, 114]. Thus, this ratio gives a measure of the excitation efficiency.

A strong increase of the X_d/X intensity ratio in σ^+ polarization with increasing X-Mn exchange constant (calculated from the splitting of excitonic sextuplet) is clearly visible in Figure 6.4(a). It confirms the origin of the first two recombination channels described above. However, the X_d oscillator strength for σ^- polarization depends both on the X-Mn exchange interaction and the quantum dot anisotropy. To elucidate the role of the anisotropy, we can use the circular polarization of the X_d. Figure 6.4(b) shows that it evolves towards σ^- as the anisotropic exchange splitting increases. Therefore, we conclude that a high in-

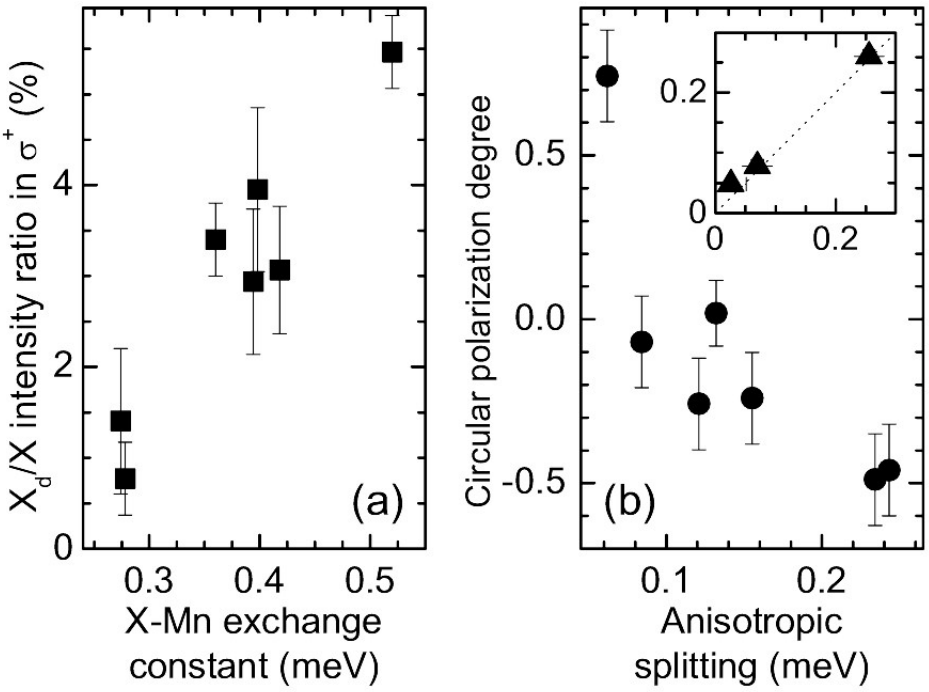

Figure 6.4: (a) X_d/X intensity ratio in σ^+ polarization *vs.* X-Mn exchange constant. (b) Degree of circular polarization of X_d spectrum *vs.* anisotropic exchange splitting of the quantum dot. A value of -1 denotes pure σ^- polarization, while a value of $+1$ refers to pure σ^+ polarization. Inset: The width of splitting between the $|+1.5, +1/2, +3/2\rangle$ and $|+2.5, +1/2, -3/2\rangle$ lines ("B" in Fig. 6.1(b)) calculated from the model *vs.* splitting between these lines determined directly from the PL for those quantum dots for which it was possible.

plane anisotropy of the quantum dot leads to a strong mixing of light and heavy holes, which combined with the presence of the Mn^{2+} ion is the reason for the strong σ^- polarization and high intensity of the X_d spectrum. It is important to note that for non-magnetic quantum dots showing similar anisotropy [108] the optical transitions of X_d are not observed, except in the presence of a strong in-plane magnetic field.

A quantitative description of key features of the data in Fig. 6.1(a-b) is provided by a simple model with the initial state of the quantum dot after excitation event given by the following Hamiltonian ([107, 108, 115, 116, 117, 118]),

$$\begin{aligned}\mathcal{H} &= g_{Mn}\mu_B \overrightarrow{B}.\overrightarrow{S} + g_e\mu_B \overrightarrow{B}.\overrightarrow{\sigma} + g_h\mu_B \overrightarrow{B}.\overrightarrow{j} - I_e \overrightarrow{S}.\overrightarrow{\sigma} \\ &\quad - I_h \overrightarrow{S}.\overrightarrow{j} + \sum_{i=x,y,z} \left(a_i j_i \sigma_i + b_i j_i^3 \sigma_i\right) - \gamma j_z^2 + \beta\left(j_x^2 - j_y^2\right) \qquad (6.1)\end{aligned}$$

where S, σ and j are the Mn^{2+}, electron and hole spin operators, respectively, the first three terms represent the Zeeman energy of the Mn^{2+} ion, the electron and the hole, I_e and I_h are the e-Mn and h-Mn exchange interaction constants, a_i and b_i are e-h spin-spin coupling constants, 2γ is the heavy-light hole splitting and β represents the strength of the heavy-light hole mixing. The first term is also the Hamiltonian of the final state of the system after the exciton recombination. We also introduced an additional, phenomenological term related to the excitonic diamagnetic shift to facilitate a comparison of the model and experimental data.

The energies of the optical transitions versus magnetic field, calculated using this Hamiltonian for the two circular polarizations, are plotted in Figure 6.1(c)[1]. The calculations clearly reproduce the key features of the experimental data in Figure 6.1(a-b), such as for example the X-Mn exchange splitting and the anisotropic exchange splitting. All parameters in the Hamiltonian (except for γ assumed to be 15 meV [86]) can be extracted by fitting to the experimental data. In particular, the heavy-light hole mixing can be estimated using the degree of circular polarization of X_d lines. Such an approach permits an estimation of the β parameter even for those quantum dots, for which the anticrossing between the $|+1.5,+1/2,+3/2\rangle$ and $|+2.5,+1/2,-3/2\rangle$ lines ("B" in Figure 6.1(b)) is not clearly visible. As shown in the inset of Figure 6.4(b) the obtained value of this anticrossing remains in very good agreement with the value estimated directly from the photoluminescence data. This confirms the proposed mechanism of X_d brightening.

[1]Parameters used for calculation can be found in Appendix A

6.2 Mn^{2+} spin orientation by dark exciton recombination

As shown in section 6.1, multiple events of injection and recombination of σ^- polarized excitons in a single Mn-doped quantum dot induce the spin polarization of the Mn^{2+} ion towards the states with positive spin projection. Since under σ^- polarized excitation the lower energy X_d branch is always visible for anisotropic quantum dots and each recombination of such X_d involves an increase of the Mn^{2+} spin projection by 1, these recombinations can play the role of an effective Mn^{2+} spin orientation mechanism. In our experiment the X_d/X intensity ratio for a highly anisotropic quantum dot was as high as 10%. This is comparable to the probability of a spin-flip of the Mn^{2+} ion per one recombination of the X which was estimated to be ∼5% in section 5.2.4. While this orientation mechanism should be present for both circular polarizations of excitation, only the case of σ^- is fully seen. Under σ^+ polarized excitation, which decreases the Mn^{2+} spin projection [46], the high energy branch of X_d should be populated and the low energy branch should be virtually invisible. The latter is, indeed, confirmed in our experiment. However, it is not possible to observe directly the high energy X_d branch, since it occurs in the same energy region as the much stronger X lines.

Chapter 7

Spin relaxation

As described in chapter 1 many features of the spin dynamics, particularly of the spin relaxation of a system of magnetic ions in a semiconductor crystal are well understood. There are still, however, several aspects that remain little investigated. In this chapter, I will present results of new experiments concerning two important fields.

In section 7.1, I describe the investigation of the spin relaxation of a single magnetic spin caused by spin-lattice interaction in low and high magnetic field. Although this kind of interaction have been studied intensively in $Cd_{1-x}Mn_xTe$ material, all of these studies were performed on quantum wells or bulk material, where the magnetic system under investigation consist of a large number of magnetic ions. The ability to grow CdTe quantum dots with single Mn^{2+} ion, along with the ability to optically control the spin state of this ion, described in section 5.2, gave the unique possibility to analyze the spin-lattice relaxation of the magnetic ion unperturbed by the spin-spin interaction.

Section 7.2 presents results of the new experiment on spin relaxation performed on diluted magnetic quantum wells and quantum dots with number of magnetic ions much larger than one. The unique in these measurements are the conditions of the experiment. The new experimental technique described in chapter 4 for the first time allowed detailed investigation of the spin dynamics in zero magnetic field with temporal resolution down to a few nanoseconds.

7.1 Single isolated spin

A disadvantage of using systems containing a large ensemble of magnetic ions for investigation of the spin-lattice relaxation is that in such system there is always not negligible interaction between neighbouring ions. Due to this fact one should always consider the spin-spin interaction as leading to one of the relaxation channels. This makes the picture more complicated and obstructs analysis of the SLR.

Among many advantages of the single quantum dot with single magnetic ion, the great distance to any other magnetic atom is particularly useful in investigation of the spin-lattice relaxation. The mean distance between quantum dots in the sample used in the experiment is of order of 100 nm (see section 2.3). The magnetic ions are present only in the quantum dots material and are embedded in roughly 1% of the dots, which give the mean distance between the ions of order of 1 μm. This distance, orders of magnitude bigger than in the DMS bulk material or quantum well system, lets us consider the magnetic ion in the quantum dot as truly isolated spin. Thus the only mechanism which can lead to its relaxation is the spin-lattice relaxation.

In this section, I present detailed studies of the spin-lattice relaxation of the single Mn^{2+} ion performed in low and high magnetic field. The spin-lattice relaxation time was determined in two independent experiments. Section 7.1.1 describes the first one, in which we measured the efficiency of the optical orientation of the Mn^{2+} ion [46] as function of excitation power and magnetic field. This approach is relatively simple and fast, however needs additional assumptions and gives results with limited accuracy. In the second, time-resolved experiment, described in section 7.1.2, we measured directly the Mn^{2+} spin relaxation time. This gives much more precise results. It is, however, more complicated and time consuming.

7.1.1 Efficiency of the optical orientation of the magnetic ion

The steady state of the Mn^{2+} spin in the quantum dot upon circularly polarized excitation is determined by two processes: the optical orientation of the Mn^{2+} spin by spin-polarized excitons injected into the quantum dot and thermalization of the magnetic ion in external magnetic field caused by spin-lattice relaxation. Given that the excitation is σ^- polarized, these two processes are competitive: interaction with polarized excitons rotates the spin of the Mn^{2+} ion towards states with positive spin projection (see section 5.2), while for the thermalized system the most occupied state is the one with the spin projection equal to $-5/2$. This competition results in different spin polarization of the Mn^{2+} ion, depending on the ratio between rates of the two processes. This ratio can be easily changed by changing the excitation power, *i.e.* changing the exciton injection rate into the quantum dot. Knowing this rate for a given excitation power and the corresponding steady state of the Mn^{2+} ion one can determine the SLR rate.

One of the simplest quantitative measures of the optical spin orientation efficiency is determination of the mean spin projection value of the Mn^{2+} ion ($\langle S_z \rangle$). As described in section 1.3.2, the relative intensities of the six components of the excitonic spectrum of the singly-Mn doped quantum dot gives the occupation of the six spin states of the Mn^{2+} ion. Therefore the value of the $\langle S_z \rangle$ can be easily determined from the excitonic spectrum of the dot by using following formula:

$$\langle S_z \rangle = \frac{\sum_{i=-5/2}^{5/2} i I_i}{\sum_{i=-5/2}^{5/2} I_i} \tag{7.1}$$

where I_i is the integrated intensity of excitonic line corresponding to the Mn^{2+} state with spin projection equal to i. Representative spectra taken under excitation with different power, together with the value of $\langle S_z \rangle$, are shown in Figure 7.1. The spectra are normalized so that the intensities integrated over the 6 exciton lines are the same.

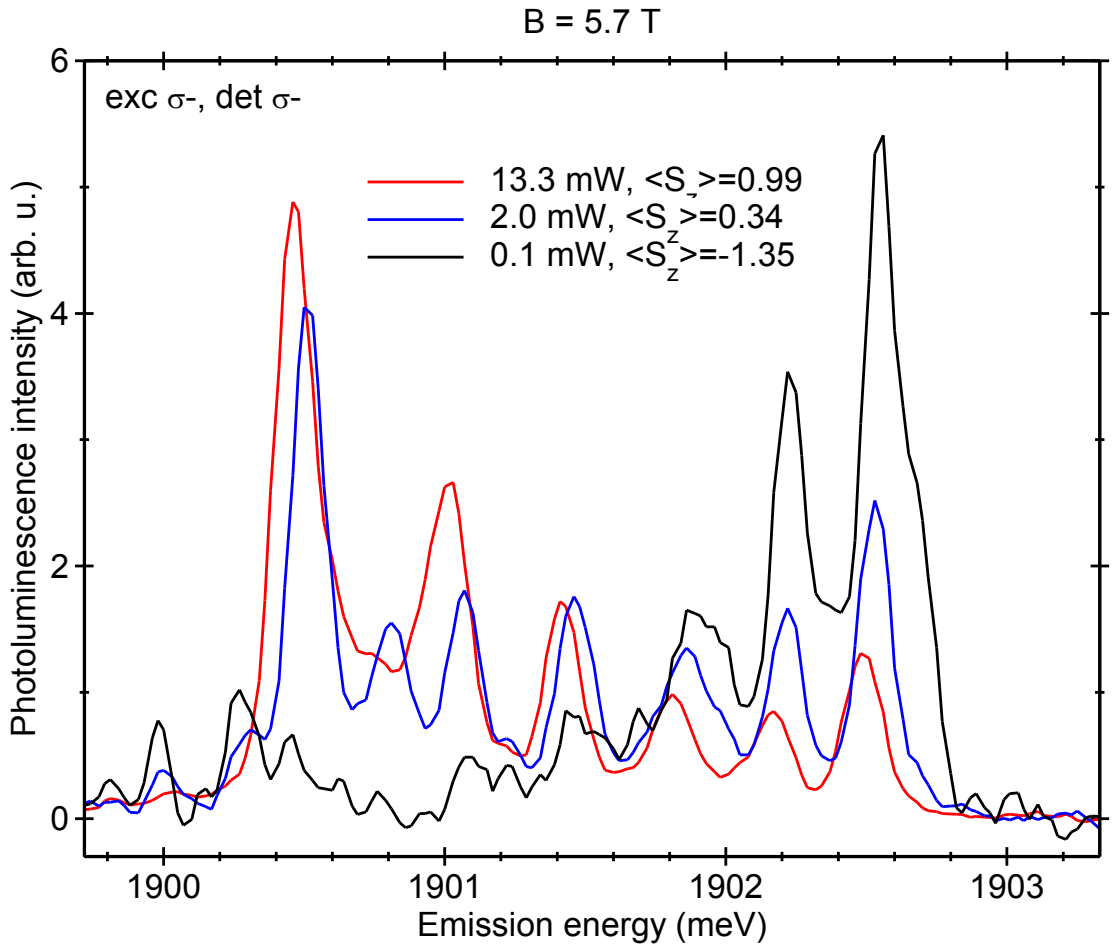

Figure 7.1: Photoluminescence spectra of a single-Mn doped quantum dot under circularly polarized excitation for indicated values of excitation power. The spectra are normalized so that the intensity integrated over the 6 exciton lines is the same. Note that for the intermediate power a weak additional line (second left) related to the dark exciton recombination (see section 6.1) is also visible.

The photoluminescence measurements *vs.* excitation power were performed in different magnetic field in the range of 0.5 - 11 T. Figure 7.2 shows the value of the $\langle S_z \rangle$ as a function of excitation power measured in Faraday configuration for different values of magnetic field under σ^- polarized excitation. Similarly as in the section 5.2.4 we have ensured that the excitation power is a good measure of the excitation efficiency of the quantum dot by checking the XX/X intensity ratio.

As the excitation power approaches zero, the distribution of the occupation of the Mn^{2+} six spin states approaches the one given by the Boltzmann distribution for a given temperature and magnetic field. Thus the $\langle S_z \rangle$ converges to specific negative value, different for different values of magnetic field. For the limit of high excitation power, when the exciton injection rate into the quantum dot is higher than the spin-lattice relaxation rate, the occupation distribution between the Mn^{2+} spin states is governed mainly by the ratio between the probability of arrival of the σ^- and σ^+ polarized excitons. As described in section 5.2.3 the σ^- polarized excitation orients the Mn^{2+} ion against the magnetic field. Therefore the $\langle S_z \rangle$ approaches a positive value, independent on the magnetic field. The maximum excitation power used in this experiment was low enough to neglect the influence of creating higher excitonic states (*e.g.* biexcitons) on the Mn^{2+} spin orientation (see section 5.2.3).

The simplest observation enabling the estimation of the spin-lattice relaxation rate is following: when the optical orientation exactly compensates the thermalization, *i.e.* the spin orientation rate is exactly equal to the relaxation rate, then the Mn^{2+} ion is completely depolarized (the $\langle S_z \rangle$ is equal to 0). Thus the spin orientation rate can be estimated using the exciton injection rate to the quantum dot and probability of the Mn^{2+} spin flip per one exciton measured in the experiment described in section 5.2.4. This approach, however, is useful for a limited range of the values of the SLR rate. When the relaxation is too slow one should use extremely low excitation power to reach above-mentioned condition, too low to be able to collect the quantum dot photoluminescence spectrum with acceptable signal quality in a reasonable time. On the other hand, when the SLR rate is too high it is impossible to inject the excitons into the quantum dot with sufficient rate because of the finite exciton lifetime. If the mean time between the excitons injection is shorter than the excitonic lifetime, then the biexcitons are created, which leads to suppression of the optical orientation of the Mn^{2+} ion (see section 5.2.2). Therefore, to extend the range of the SLR rates we introduce a rate equation model describing transitions between the Mn^{2+} spin states caused by the processes under consideration. Then we extract the SLR rate from the dependence of the $\langle S_z \rangle$ on the excitation power even for such conditions for which complete depolarization of the Mn^{2+} ion ($\langle S_z \rangle = 0$) is impossible to obtain.

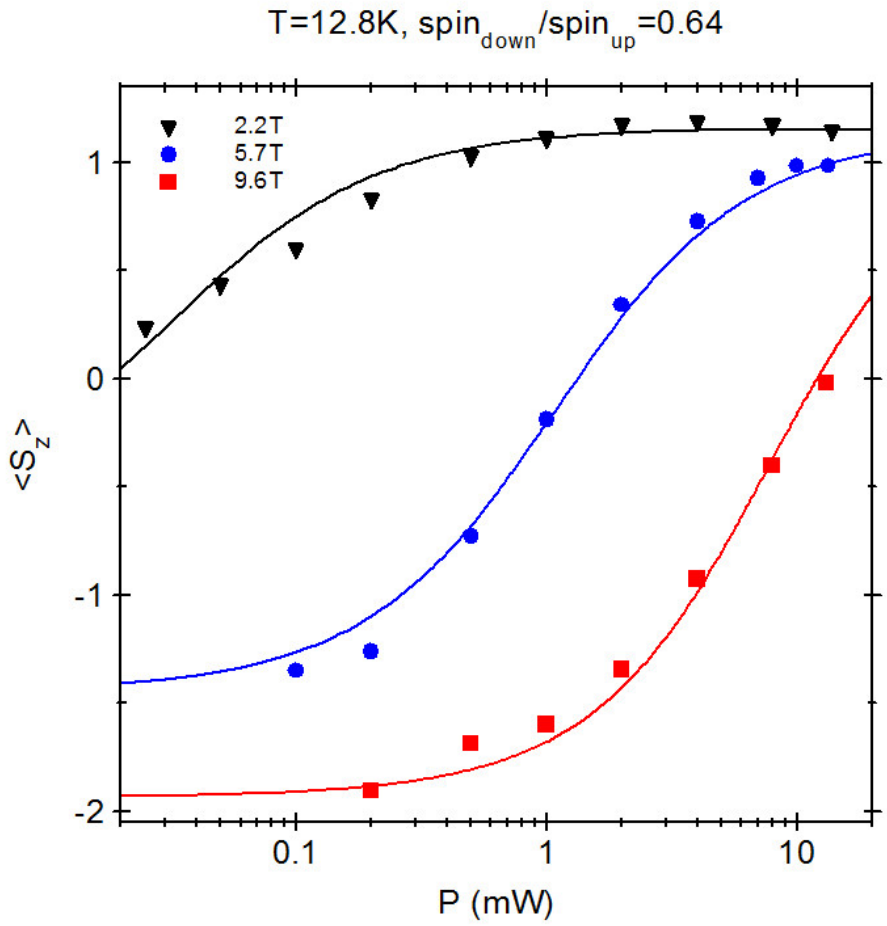

Figure 7.2: The mean value of the spin projection $\langle S_z \rangle$ of the single Mn^{2+} ion in the quantum dot measured *vs.* excitation power for indicated values of magnetic field (symbols) compared with the model described in text (solid lines).

The model introduced here takes into account two types of transitions of the Mn^{2+} spin. The first one is caused by the spin-lattice relaxation. The probability of transfer of any Mn^{2+} state, characterized by its quantum number m, to a state with m different by 1, is reciprocally proportional to the relaxation time τ_{SLR} and dependent on the Boltzmann factor $P = e^{\frac{g_{Mn}\mu_B B}{k_B T}}$. The rate equation for the occupation q_m of each Mn spin state is following:

$$dq_m/dt = \; p_{SLR}\,(q_{m-1}P + q_{m+1}P^{-1} - q_m(P + P^{-1})) \tag{7.2}$$

(with a suitable cut-off for $|m| = 5/2$), where $p_{SLR} = \frac{1}{\tau_{SLR}}$. The solution of such system of equations is the Boltzmann distribution of occupation of the Mn^{2+} states. As a consequence, the value of the $\langle S_z \rangle$ is given by the Brillouin function (formula 1.2).

The second type of transitions was already discussed in section 5.2.3. The transitions occur with a fixed probability p_0 during the presence of a suitably polarized exciton in the quantum dot. By combining equations 5.2 and 7.2 one obtains:

$$\begin{aligned} dq_m/dt = \; & q_{m-1}(p_0\varphi_{X_{-1}} + p_{SLR}P) + q_{m+1}(p_0\varphi_{X_{+1}} + p_{SLR}P^{-1}) \\ & -q_m(p_0\varphi_{X_{-1}} + p_0\varphi_{X_{-1}} + p_{SLR}(P + P^{-1})) \end{aligned} \tag{7.3}$$

where $\varphi_{X_{\pm 1}}$ are frequencies of arriving of excitons into the quantum dot. Terms from equation 5.2 related to biexciton formation have been skipped because - as mentioned above - the influence of higher excitonic states can be neglected due to low excitation power. By numerically solving this system of equations it is possible to calculate the q_m and consequently the $\langle S_z \rangle$. Thus it is possible to fit this quantity to the experimental data using following variables as free parameters: T which gives the limit of the $\langle S_z \rangle$ for an excitation power approaching zero and a given magnetic field; the $\varphi_{X_{+1}}/\varphi_{X_{-1}}$ ratio which determines the maximum value of the $\langle S_z \rangle$ for the high excitation power limit; τ_{SLR} which determines the zero-cross point on the dependence of the $\langle S_z \rangle$ on the excitation power. Additionally one needs two quantities which were already measured in previously described experiments: the overall frequency of exciton injection into the quantum dot ($\varphi_{X_{+1}}+\varphi_{X_{-1}}$) and the probability p_0. As described in section 5.2.4, the former one can be determined using the XX/X intensity ratio and the excitonic lifetime in the quantum dot. The latter one was measured in the experiment presented in section 5.2.4 and is typically equal to 5%.

As can be seen on Figure 7.2 such model fits to the experiment with very good agreement. It is important to note that for different values of magnetic field only the value of the τ_{SLR} is different, while the temperature T and the $\varphi_{X_{+1}}/\varphi_{X_{-1}}$ are common. T is equal to about 13 K which stays in agreement within experimental accuracy with the value estimated using calibrated resistor

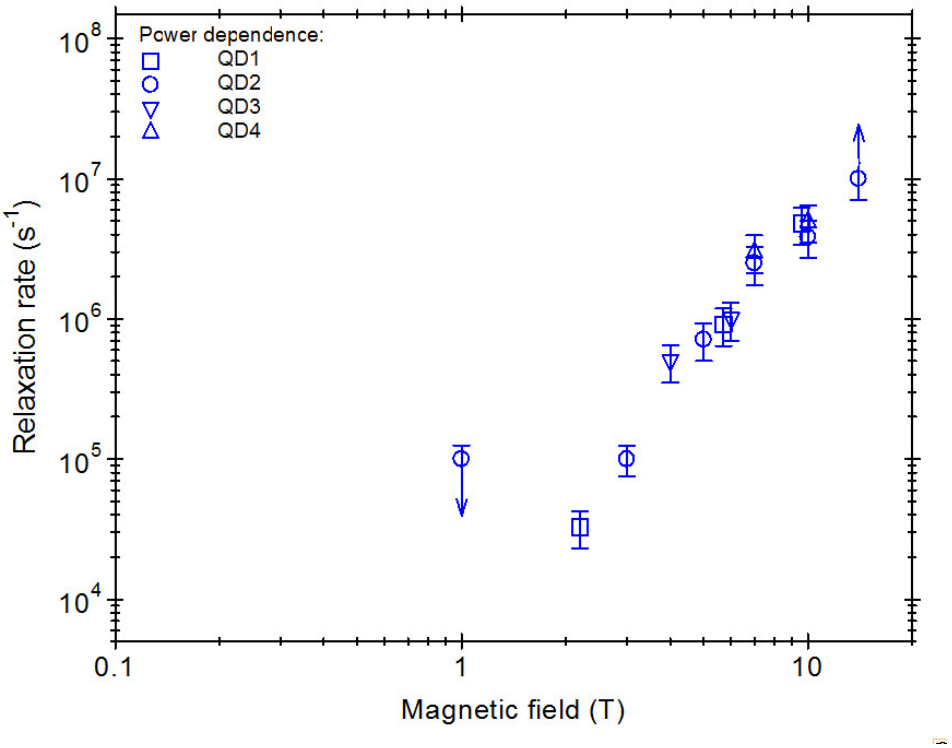

Figure 7.3: Spin-lattice relaxation rate of a single Mn^{2+} ion in the quantum dot as a function of magnetic field, measured for several dots.

placed close to the sample. The value of $\varphi_{X_{+1}}/\varphi_{X_{-1}}$ is 0.64, very close to the value obtained in different experiment (0.65 - see section 5.2.2).

Figure 7.3 shows the dependence of the spin-lattice relaxation rate on the magnetic field determined using the method described above. The relaxation rate of the single Mn^{2+} ion in the QD for low magnetic field (around 1 T) is of order of $10^4 - 10^5$ s^{-1}. It is strongly increasing with the magnetic field and reaches more than 10^7 s^{-1} at 11 T. It is, however, necessary to note that these extreme values for lowest and highest magnetic field are only lower and upper bound, respectively, due to limitations of this experimental technique.

7.1.2 Direct time-resolved measurement

7.1.2.1 Low magnetic field

In the second, time-resolved experiment we measured directly the Mn^{2+} spin relaxation time. We used the same mechanism as previously - the spin-conserving exciton transfer between two neighbouring quantum dots - to orient the magnetic ion (see section 5.2.3). The idea of the experiment is presented in Figure 7.4.

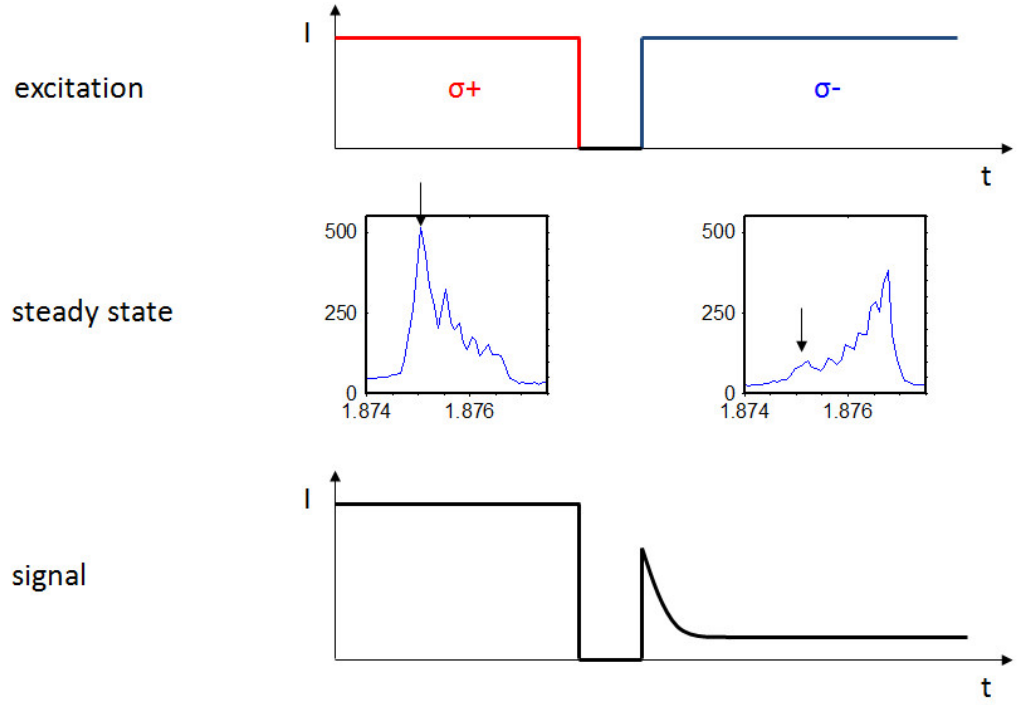

Figure 7.4: The idea of the direct measurement of the spin relaxation time of a single Mn^{2+} ion in the quantum dot for low magnetic field

First, the sample is illuminated with σ^- polarized light to orient the Mn^{2+} ion towards the states with positive spin projection. Once the ion reaches the steady state we switch the excitation off for a controlled period. Then we turn the excitation on again in opposite circular polarization to probe the Mn^{2+} spin. The Mn^{2+} state is read by measuring the photoluminescence intensity of a selected component of the exciton sextuplet (related to the Mn^{2+} state with spin

projection equal to +5/2) in a given circular polarization. Its evolution reflects the orientation of the Mn^{2+} spin combined with the exciton optical orientation. During the first part of the excitation cycle (σ^- polarized excitation) we observe strong signal, indicating high occupation of the +5/2 state of the Mn^{2+} ion. When the excitation is switched off, the photoluminescence signal vanishes and remains zero as long as the excitation is off. When subsequently a σ^+ polarized excitation is turned on, the photoluminescence intensity first rises rapidly to an initial value determined by the Mn^{2+} spin state and the efficiency of the exciton polarization transfer. If the Mn^{2+} orientation is conserved, this value is given only by the exciton polarization transfer and should be equal to about 65% of the previous value. Any loss of the Mn^{2+} spin orientation would decrease this value. After the initial rapid increase, the photoluminescence intensity slowly decreases. This decrease is related to the reorientation of the Mn^{2+} spin by circularly polarized light.

Figure 7.5 shows an example of the temporal profile of the photoluminescence signal measured in σ^- polarization at B=1 T for relatively short dark period. It is clearly visible that the Mn^{2+} spin state immediately after the dark period is very close to that aligned by the light. The initial value of the photoluminescence intensity is presented versus delay in Figure 7.6. Its decrease allows us to roughly estimate the Mn^{2+} spin relaxation time in darkness to be about 0.4 ms.

7.1.2.2 High magnetic field

The method for investigating the spin-lattice relaxation time described in section 7.1.2.1 needs to be modified when used in magnetic field stronger than about 1 T. This is due to the Zeeman splitting of the excitonic ground level in the absorbing quantum dot. The splitting makes the change of circular polarization of the resonant excitation impossible without changing the excitation energy. Therefore we simplified the excitation scheme by skipping the polarization modulation and using only the intensity switching. The idea of such experiment is explained in Figure 7.7. First we illuminate the sample with σ^- polarized light, which causes polarization of the Mn^{2+} ion against the magnetic field. Then the excitation is switched off for a controlled delay and switched on again in the same circular po-

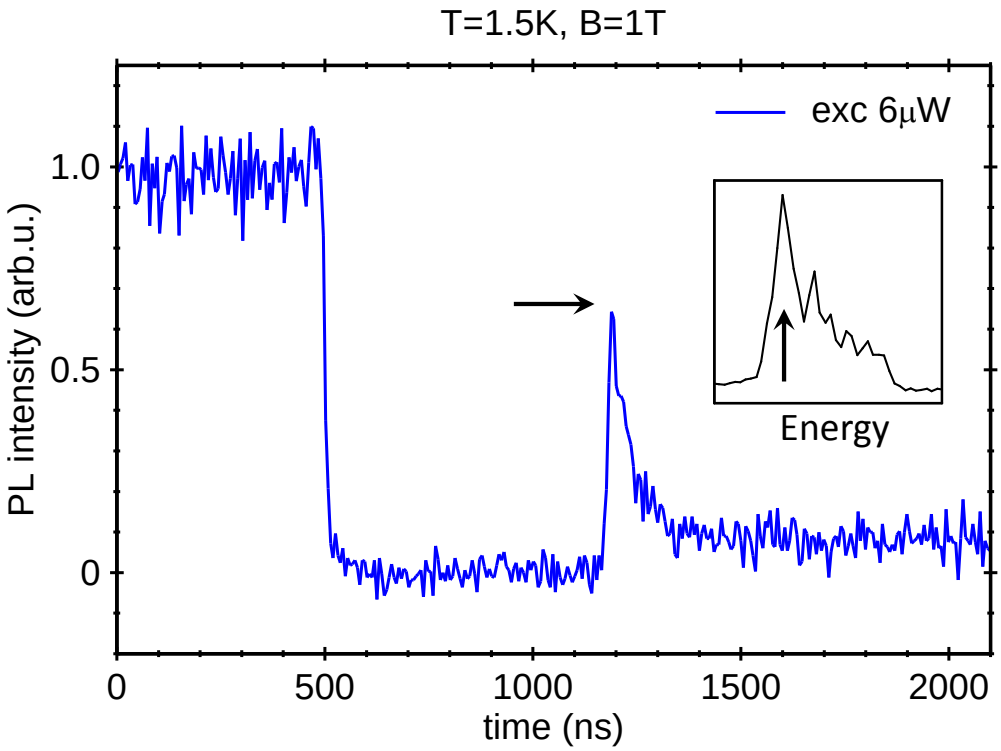

Figure 7.5: Temporal profile of the photoluminescence intensity at one of the six components of the exciton spectrum (indicated in inset) during the excitation sequence described in text for B=1 T with excitation power equal to 6 μW. The horizontal arrow indicates the ratio between photoluminescence intensity measured in co-polarization and cross-polarization setup.

larization. Similarly to the low magnetic field case, the Mn^{2+} state is monitored by measuring the intensity of a selected component of the exciton photoluminescence spectrum. It is the component related to the most occupied Mn^{2+} state under σ^- polarized excitation. If the Mn^{2+} orientation remains unchanged during the dark period, the observed intensity immediately rises to the same value as it was before, after switching the excitation on. If, however, there is non-negligible Mn^{2+} spin relaxation, the intensity of the observed component rises to a lower value. Subsequently, a relatively slow increase of the intensity is observed. It is related to the Mn^{2+} spin orientation by polarized carriers. If this increase is slow enough it is possible to determine the initial intensity with a good precision.

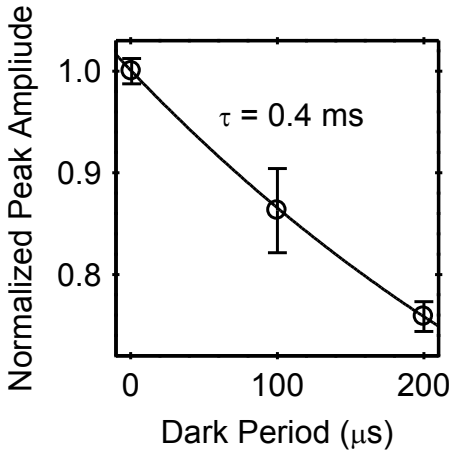

Figure 7.6: Initial photoluminescence intensity after turning the excitation on in σ^- polarization versus length of dark period.

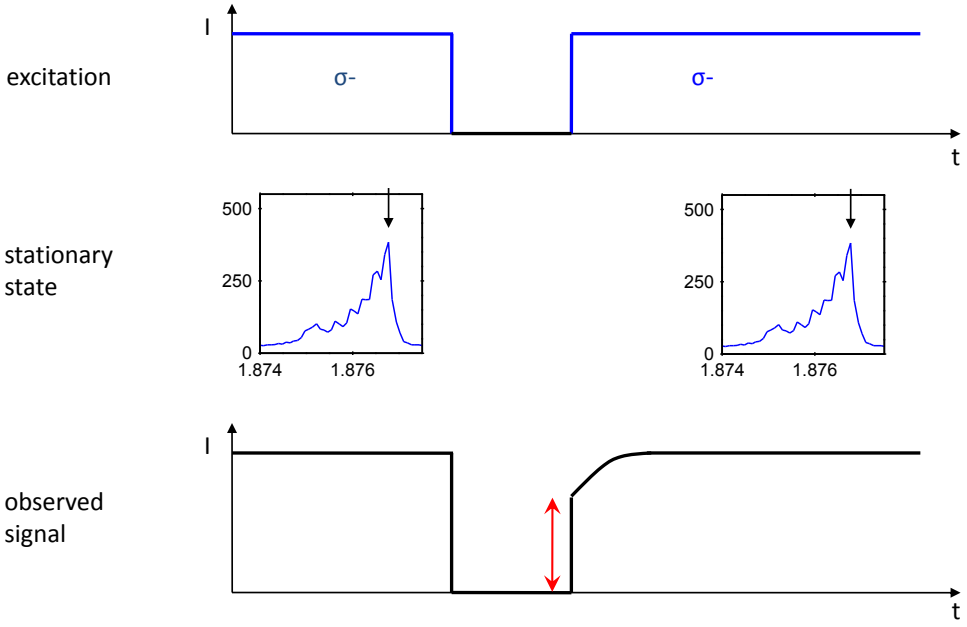

Figure 7.7: The idea of the direct measurement of the spin relaxation time of a single Mn^{2+} ion in the quantum dot for high magnetic field

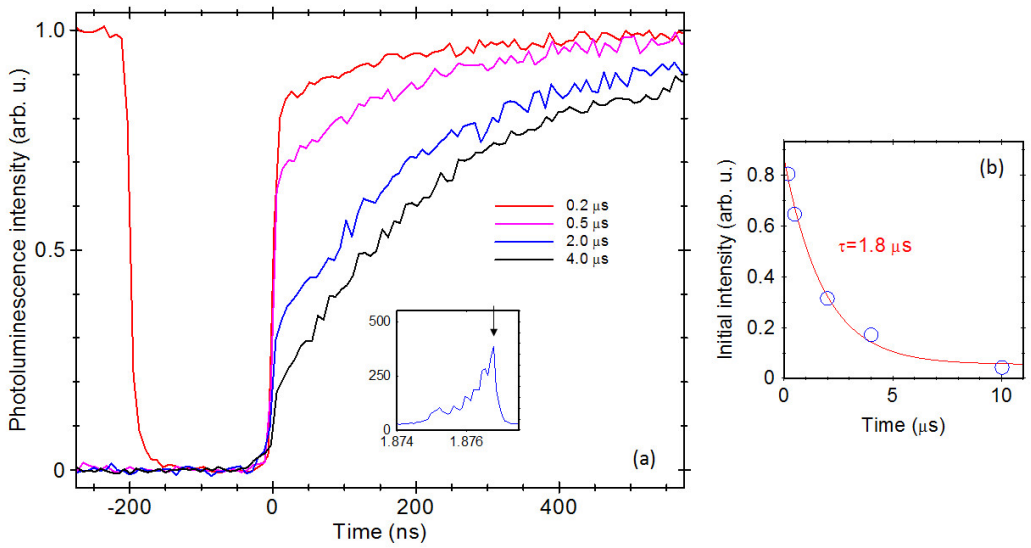

Figure 7.8: Temporal profile of the photoluminescence intensity of one of the six components of the exciton spectrum (indicated in inset) during the excitation sequence described in text for B=5.7 T and indicated values of the length of the dark period.

By varying the length of the dark period in the range of 20 ns-500 μs, we were able to measure the broad spectrum of relaxation times and, consequently, its dependence on the magnetic field in a wide range of fields.

Figure 7.8a shows example temporal profiles of the intensity of the observed photoluminescence line at magnetic field equal to 5.7 T for various length of the dark period. As demonstrated in Figure 7.8b the initial intensity after switching the excitation on decreases exponentially with the length of the dark period. This allows easy calculation of the spin-lattice relaxation time.

Such experiment was repeated for various values of magnetic field in the range of 0.5 - 11 T. Figure 7.9 shows the dependence of the spin-lattice relaxation rate on the magnetic field determined using the method described in this section together with data measured in the indirect method described in section 7.1.1 and in the former experiments on bulk diluted $Cd_{1-x}Mn_xTe$ material [71]. It is clearly visible that two presented methods for the quantum dots, the direct and the indirect one, gave results which agree within experimental accuracy.

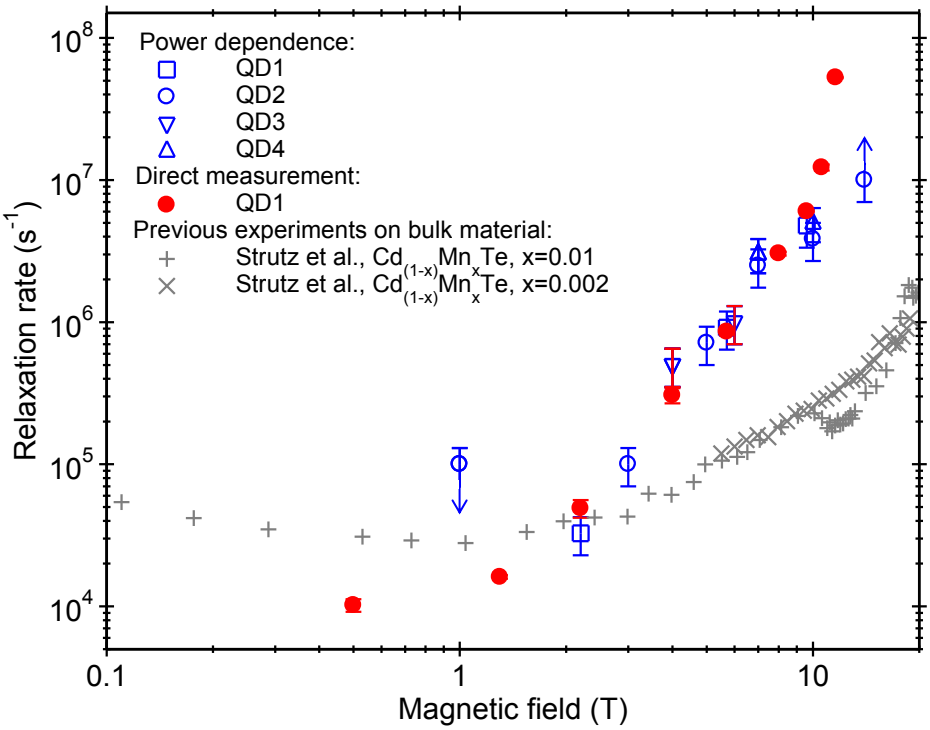

Figure 7.9: Spin-lattice relaxation rate of a single Mn^{2+} ion in the quantum dot as a function of magnetic field, measured for several dots (colour points) using two different methods described in text in comparison with the relaxation rate measured in diluted $Cd_{1-x}Mn_xTe$ bulk material (black points).

However, the direct method allows us to measure the spin relaxation time with greater accuracy. Moreover, the wider range of available time-scales enables the investigation of the spin relaxation in a wider range of magnetic field.

The relaxation rate of the single Mn^{2+} ion in the quantum dot for low magnetic field (around 1 T) is of order of 10^4 s^{-1}, slightly lower than in bulk material at 4.2 K. It is, however, increasing rapidly with the magnetic field and reaches almost 10^8 s^{-1} at 11 T. This is over two orders of magnitude higher than the value measured for bulk $Cd_{1-x}Mn_xTe$.

The vast difference of the spin-lattice relaxation rate measured in present experiments and the previous one [71] may be partially explained by the different temperature: the quantum dots with single Mn^{2+} ions were investigated at about

13 K, while the experiment with the bulk material was performed at 4.2 K. At the same time it is well known that the spin-lattice relaxation strongly increases with the temperature [63, 67]. However, the difference at low field cannot be explained this way. This, however, does not explain the fact that for low magnetic field the relaxation rate in quantum dots is actually slightly lower than in bulk $Cd_{1-x}Mn_xTe$. Possible origins of this difference include strain fields, usually high in structures containing quantum dots. Confirmation of this hypothesis requires further studies and is beyond the scope of this work.

7.2 System of coupled spins

As mentioned in chapter 1, a great majority of previous studies of spin dynamics of a large system of Mn^{2+} ions in $Cd_{1-x}Mn_xTe$ material was performed in the presence of a magnetic field. Under such conditions, the relaxation of the transverse component of magnetization is an adiabatic process, which was ascribed to anisotropic spin-spin interactions [119]. It is fast, and accelerates with the Mn content. The relaxation of the longitudinal component involves a transfer of the Zeeman energy to the lattice (spin-lattice relaxation). For isolated Mn^{2+} ions, this is a slow process, due to the absence of spin-orbit coupling within the orbital singlet which forms the ground state. In DMSs, the spin-lattice relaxation rate increases with the Mn content, as a result of a fast transfer via the Mn spins towards "killer centres", in particular Mn clusters [66, 67] which statistically exist within the random Mn distribution. For compositions where both have been measured, the spin-spin time is faster than the spin-lattice relaxation time, by 2 to 3 orders of magnitude [120] (see Fig. 7.11). The general picture that emerges, is that fast processes are expected in a DMS with relatively high Mn content, while strongly diluted or isolated Mn^{2+} spins should exhibit long relaxation times. More recently, the role of free carriers has been stressed: they form an efficient channel to transfer the Mn Zeeman energy to the lattice [73].

Since the most promising possible applications of DMS involve information storage and processing in spintronics, a better knowledge of the magnetization or spin dynamics is needed, particularly in the absence of an applied magnetic field. In Ref. [70], the magnetization of a bulk $Cd_{1-x}Mn_xTe$ sample, in the presence

of a static field, was changed by the collinear AC field of a coil, and monitored by Faraday rotation. The spin-lattice relaxation time was clearly identified and exhibits a dramatic decrease at low field. In principle, this method can be used down to zero field but the frequency response of the set-up was limited to a few microseconds, so that the static field had to be kept above a few tenths of Tesla. By contrast, T_2 slowly increases when decreasing the applied field in $Zn_{0.9}Mn_{0.1}Se$ [72] or $Cd_{1-x}Mn_xTe$ [75].

In this section, I describe the magnetization dynamics in $Cd_{1-x}Mn_xTe$ quantum wells and quantum dots with similar, low Mn content. In case of quantum dots, the nominal density of Mn^{2+} in the CdTe material results in an average number of magnetic ions in each dot equal to a few tens. A new experimental technique of short magnetic pulses created by a small coil is used. As described in chapter 4 this technique allows investigation of the Mn spin relaxation down to zero magnetic field and with a temporal resolution of a few nanoseconds.

7.2.1 Diluted magnetic quantum wells

The magnetization relaxation of quantum wells with Mn content in the range 0.2% - 1.5% was measured using the technique described in chapter 4. Figure 7.10 shows an example of the temporal evolution of the magnetization as extracted from the photoluminescence signal observed for sample with 0.8% of Mn after the pulse of magnetic field and without applied external static field. The time t=0 on the plot denotes the moment when the pulse is finished. The shape of the current pulse (dotted line), as recorded by an oscilloscope measuring the voltage across a 50 Ω resistor terminating the current line, was convoluted with different possible decay functions and compared to the experimental signal (points) (see section 4.6). We found that a bi-exponential decay was sufficient to describe the magnetization relaxation in the absence of magnetic field with very good accuracy. The characteristic time of the fast component of this decay was of order of 10 ns, and it is measurably longer than the experimental resolution (≈7 ns). The long component is relatively weak and its characteristic time is equal to a few hundreds of nanoseconds. Figure 7.11 presents a comparison of the fast decay rate (blue symbols) with the spin-lattice relaxation rate measured previously in magnetic

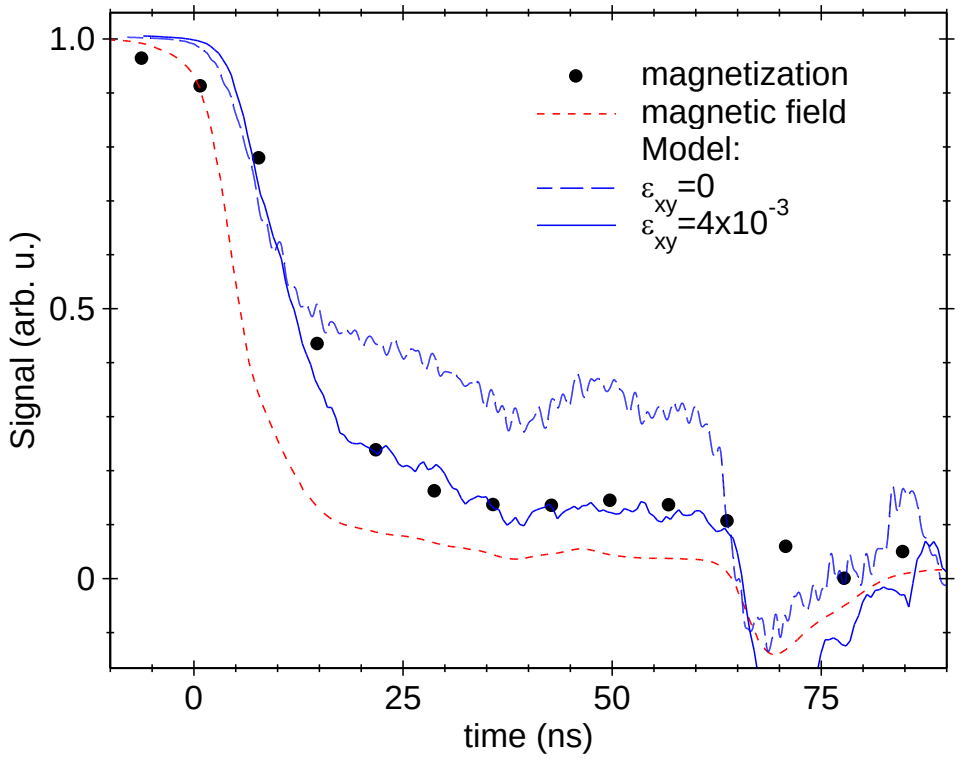

Figure 7.10: Magnetization dynamics of a $Cd_{1-x}Mn_xTe$ quantum well with 0.8% of Mn at B = 0 after the pulse of magnetic field (symbols), coil current (dotted line), and the result of calculations (solid and dashed lines) described in the text.

field in materials with comparable Mn content [70, 71]. The rate observed in the absence of magnetic field is higher than the values obtained in magnetic field by about three orders of magnitude. It shows almost no dependence on the Mn content, as expected for isolated Mn ions.

The fast zero-field decay may be caused by many different interactions: the hyperfine interaction with the nuclear spin of the Mn^{2+} ion, the superhyperfine interaction with the nuclear spin of neighbour Cd atoms, dipolar interaction with nuclear or electronic spins of other Mn^{2+} ions, the single ion anisotropy due to the cubic crystal field and strain in the epitaxial structure, fluctuations in the interaction with carriers, *etc.*

It is well known, from EPR spectroscopy of Mn diluted in CdTe bulk material [63] and CdTe- and ZnTe-MnTe super lattices [121, 122], that the Mn^{2+} electronic

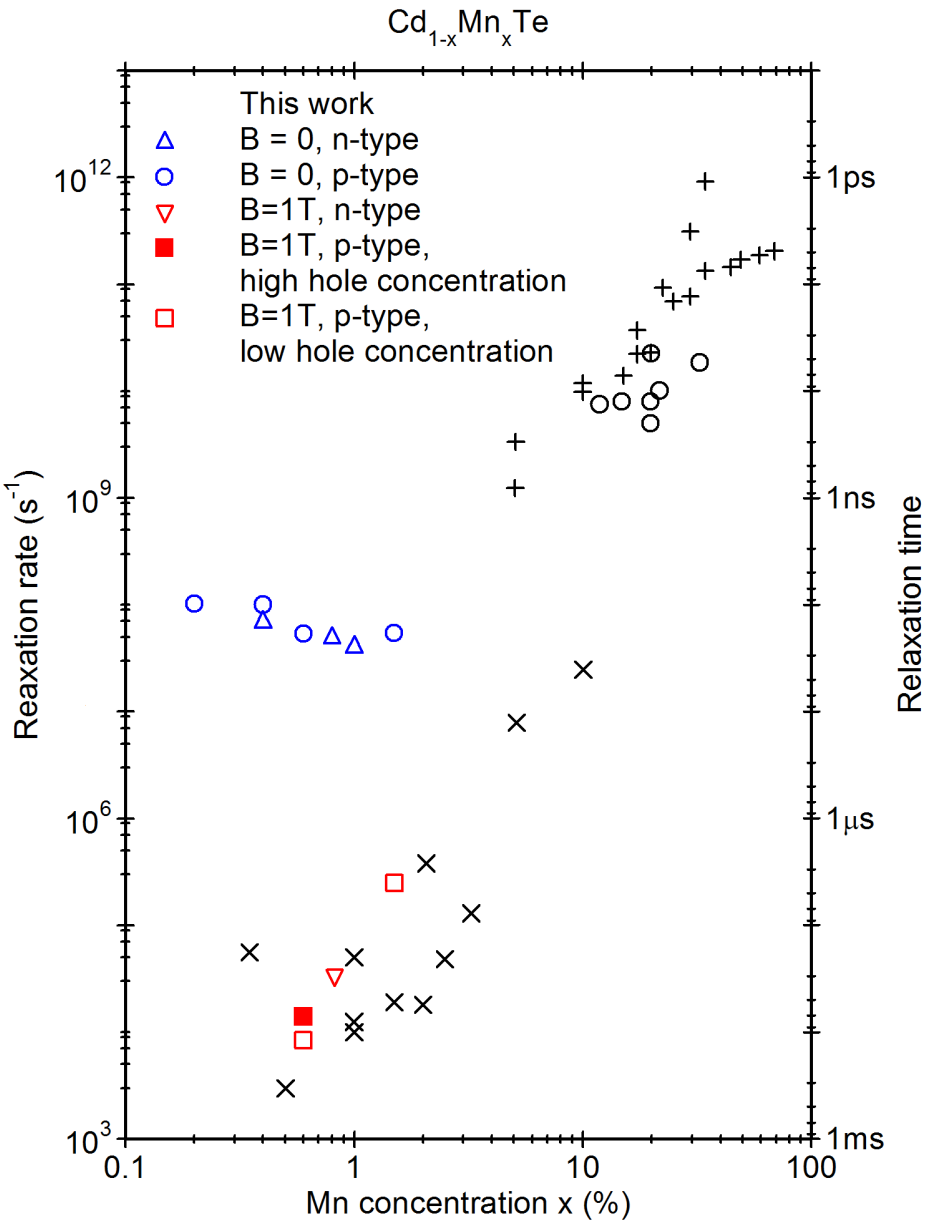

Figure 7.11: Spin-spin relaxation rate at 5 K (+), spin-lattice relaxation rate at 1.5-4.7 K (×) (adapted from [120]), and present data at 1.5 K: fast and slow magnetization decay at 0 and 1 T, respectively (open symbols - carrier densities in the 10^{10} cm^{-2} range; closed symbol - carrier density equal to 1.5×10^{11} cm^{-2}).

spin $\overrightarrow{S}$ interacts strongly with its nuclear spin $\overrightarrow{I}$ (both 5/2), with a sizable crystal field, and with strain. The Hamiltonian taking into account these interactions is following [122, 123]:

$$\begin{aligned}\mathcal{H} &= g_{Mn}\mu_B \overrightarrow{B}.\overrightarrow{S} + A\overrightarrow{I}.\overrightarrow{S} + D[S_z^2 - \frac{S(S+1)}{3}] \\ &+ \frac{a}{6}[S_x^4 + S_y^4 + S_z^4 - \frac{S(S+1)(3S^2+3S-1)}{5}]\end{aligned} \tag{7.4}$$

with $A = 680$ neV for the hyperfine coupling, $a = 320$ neV for the cubic crystal field. The dominant strain component in epitaxial layers grown pseudomorphically on substrates with 4% and 12% Zn is biaxial, with $\varepsilon_{xx} = \varepsilon_{yy} = -(c_{11}/2c_{12})\varepsilon_{zz} = -2.3 \times 10^{-3}$ and -7×10^{-3}, respectively. Its effect is described by the DS_z^2 term, with values of D deduced from Ref. [122] using following formula [124]:

$$D = -\frac{3}{2}G_{11}\left(1 + \frac{2C_{12}}{C_{11}}\right)\frac{a_{xy} - a_0}{a_0} \tag{7.5}$$

where G_{11} is the spin-lattice coefficient describing the energy shift of spin levels per unit strain [125], C_{11} and C_{12} are the elastic constants, a_{xy} is the in-plane lattice constant of the quantum well and a_0 is the lattice constant of unstrained CdTe.

The eigenvalues of the Hamiltonian were calculated for various values of magnetic field in the range 0-100 mT[1]. The resulting energy diagram is shown in Figure 7.12. In the field stronger than about 50 mT the Zeeman splitting of the Mn^{2+} ion becomes the strongest among the interactions included in the Hamiltonian 7.4. As a result the energy levels split into 6 branches, each related to a specific Mn^{2+} spin projection onto the direction of the magnetic field. Each branch show sixfold splitting caused by the hyperfine interaction. For lower field the situation is more complicated. As it is shown in Figure 7.12b, a number of strong anticrossings appear at magnetic field in the range of about 5 to 20 mT. If the change of magnetic field was immediate, then it would cause only the change

[1]Parameters used for calculation can be found in Appendix A

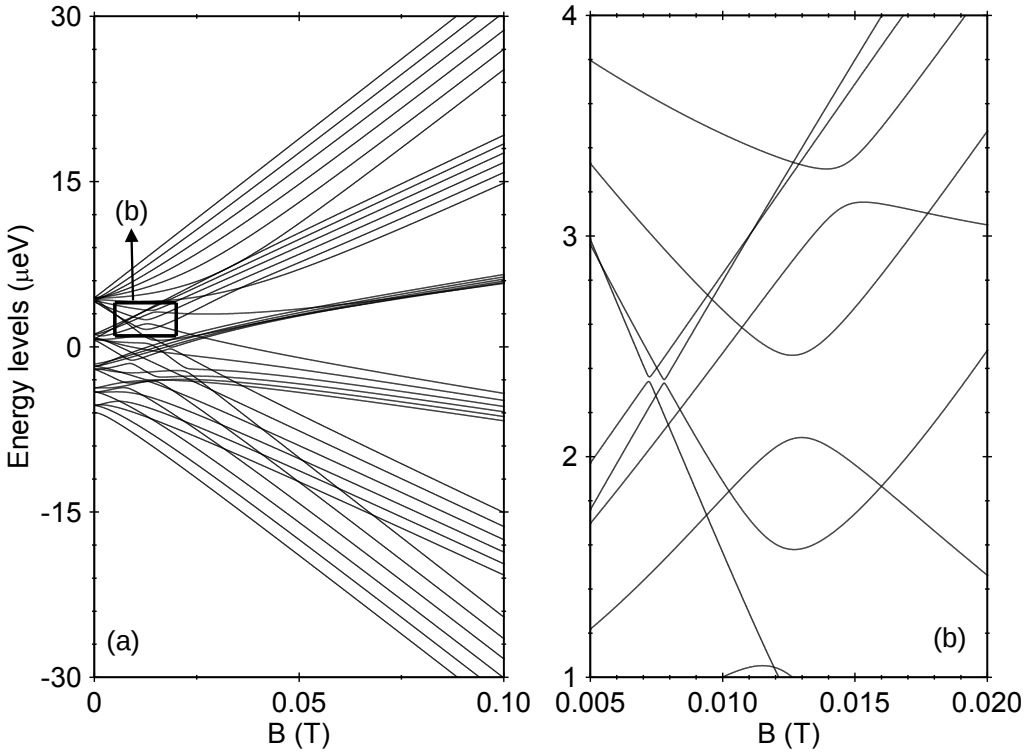

Figure 7.12: Energy levels of a Mn^{2+} ion in a CdTe crystal taking into account the hyperfine coupling, cubic crystal field and mismatch strain.

in the Zeeman energy of all the levels. However, if we sweep down the magnetic field with finite speed, than at the end of the pulse we will obtain also the change of the occupation of these levels. The evolution of the magnetization can be viewed as a series of transitions between different states caused by the coherent oscillations, which occur every time the coupling between these states becomes significant (*i.e.* close to the anticrossing on the energy diagram).

The magnetization evolution can be calculated numerically using the density matrix formalism. The spin state of ensemble of magnetic moments is represented by the matrix ρ. Its initial value ρ_0 is given by a thermalized system:

$$\rho_0 = \sum_j p_j |\Psi_j\rangle\langle\Psi_j| \tag{7.6}$$

where $|\Psi_j\rangle$ is a pure jth eigenstate of the Hamiltonian 7.4 at t=0 and p_j is the probability (given by the Boltzmann distribution) that a single ion is in the Ψ_j state. The evolution of the system is given by the von Neumann equation:

$$i\hbar\frac{\partial\rho}{\partial t} = [\mathcal{H}, \rho] \tag{7.7}$$

where the brackets denote a commutator. If $\mathcal{H}$ was a time-independent Hamiltonian, the solution would be:

$$\rho(t) = e^{-i\mathcal{H}t/\hbar}\rho_0 e^{i\mathcal{H}t/\hbar} \tag{7.8}$$

Since the Hamiltonian evolves (as the magnetic field change), we consider small time intervals δt and assume that during each interval $\mathcal{H}$ is constant. In order to model a realistic case, the temporal profile of the magnetic field used in the calculation is taken from the experiment.

As shown by the dashed line in Figure 7.10, such calculation of the magnetization evolution using Hamiltonian 7.4 with no additional effect of the environment, well describes the first fast drop in the experimental data. However, as it is clearly visible in Figure 7.10, there is still some persistent magnetization, which remains after this first fast drop of the calculated curve. This is easy to understand, as the hyperfine coupling has non-zero matrix elements only between states with $\Delta S_z = \pm 1$. Therefore several levels show no anticrossing, and the spin states remain eigenstates when varying the magnetic field.

In order to reproduce the experimental data, which do not show strong remaining magnetization, we introduce additional mechanisms which mix states with different values of S_z. Within the single Mn^{2+} system, this is simulated when considering strain components which are anisotropic within the quantum

well plane. For instance, the effect of a strain $\varepsilon_{xy} = 4 \times 10^{-3}$, calculated using Ref. [125, 126], is shown in Fig. 7.10 as a solid line. It shows a good agreement with the experimental data. Such a strain in a quantum well could be caused by local fluctuations or dislocations, but its estimated value is surprisingly large: x-ray diffraction data gives a 4 times smaller estimate for similar structures [127]. This suggests that mechanisms related to the environment of the Mn^{2+} impurity should be considered.

Note also that even for the best fit, the calculated evolution leaves a small but non-zero persistent magnetization. The experimental data in Figures 7.10 and 7.13 ($B = 0$) shows indeed such a long-time component, which decays with characteristic times equal to about 500 ns in case of the sample with 0.8% of Mn. This decay time slightly varies from sample to sample, but always remains in the sub-μs range.

A dramatic change in the magnetization relaxation was observed after applying a static magnetic field, additional to the pulsed one created with the coil. The example results are shown in Fig. 7.13. The slow component becomes dominant at about B=0.3 T while its characteristic time slightly increases. At field as high as 1.0 T the fast components are not visible at all and the decay can be described with monoexponential curve with characteristic time in the range of tens of microseconds. The values of this characteristic time are in good agreement with previous data of spin-lattice relaxation in $Cd_{1-x}Mn_xTe$ [70, 71]. Furthermore the well known increase of relaxation rate with Mn content is clearly seen (see Figure 7.11).

This result can be understood along the lines developed by Scalbert *et al.* [70]. The magnetization relaxation in zero magnetic field does not require any transfer of energy[1], however upon applying magnetic field all fast adiabatic processes are suppressed and a spin-lattice relaxation becomes dominant.

In order to verify the role of the intrinsic background carriers in the quantum well in the relaxation process we performed measurements on samples with different density of the hole gas. We found that in significant magnetic field the

[1]For that reason the magnetization decay in the absence of magnetic field should be called "coherent evolution", rather than "relaxation". However, for simplicity in this work we refer to all magnetization decay processes as "relaxation".

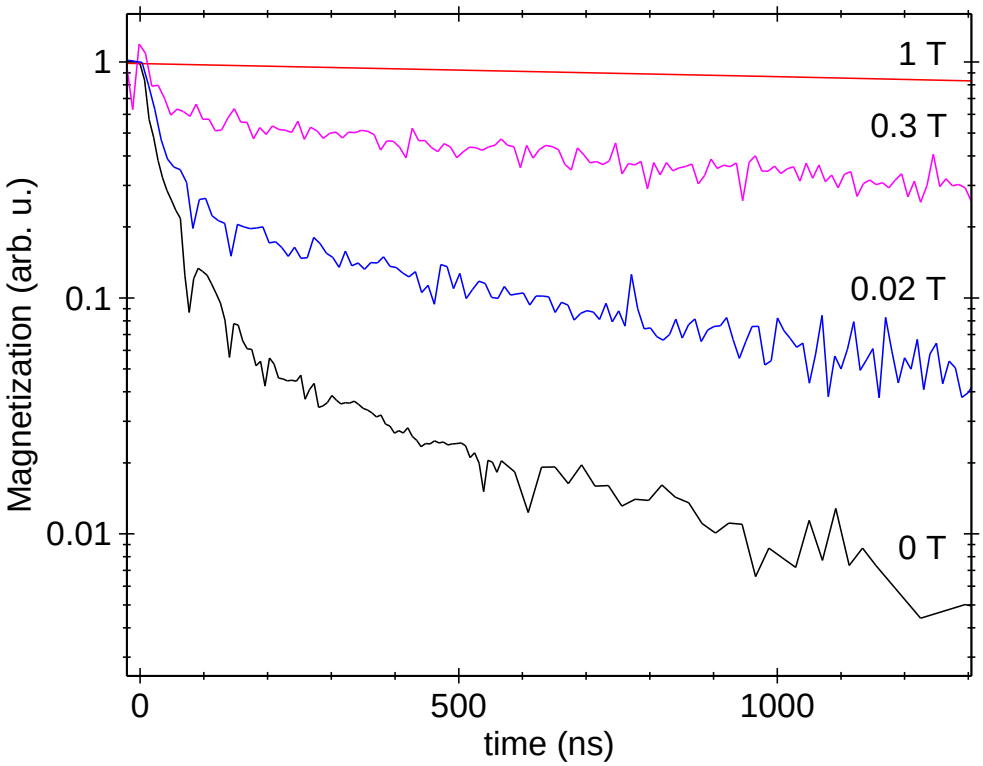

Figure 7.13: Magnetization dynamics of a $Cd_{1-x}Mn_xTe$ quantum well with 0.8% of Mn at different values of magnetic field.

hole gas can play role of an additional relaxation channel. This is easily seen in Figure 7.14, where the decay is faster for a larger hole density (which can be controlled by additional illumination - see section 2.2), in agreement with Ref. [69].

An opposite influence of hole gas on the magnetization dynamics is observed in zero magnetic field. Figure 7.15 shows the comparison between magnetization relaxation measured for n-type and p-type samples with the same Mn content. In the case of the p-type sample the slow component of the relaxation is much more pronounced. We ascribe this effect to the anisotropy introduced by hole gas. As mentioned in section 1.1.1, these are heavy holes with projections $\pm 3/2$ of their moment along the growth direction. Due to the strong exchange coupling between holes and Mn^{2+} spins, the $\pm 5/2$ doublet of the Mn^{2+} spin (with the proper orientation of the holes) forms the ground state, while the $\pm 3/2$ and $\pm 1/2$ ones are at higher energy. A polarized hole gas of density in the 10^{11} cm^{-2} range

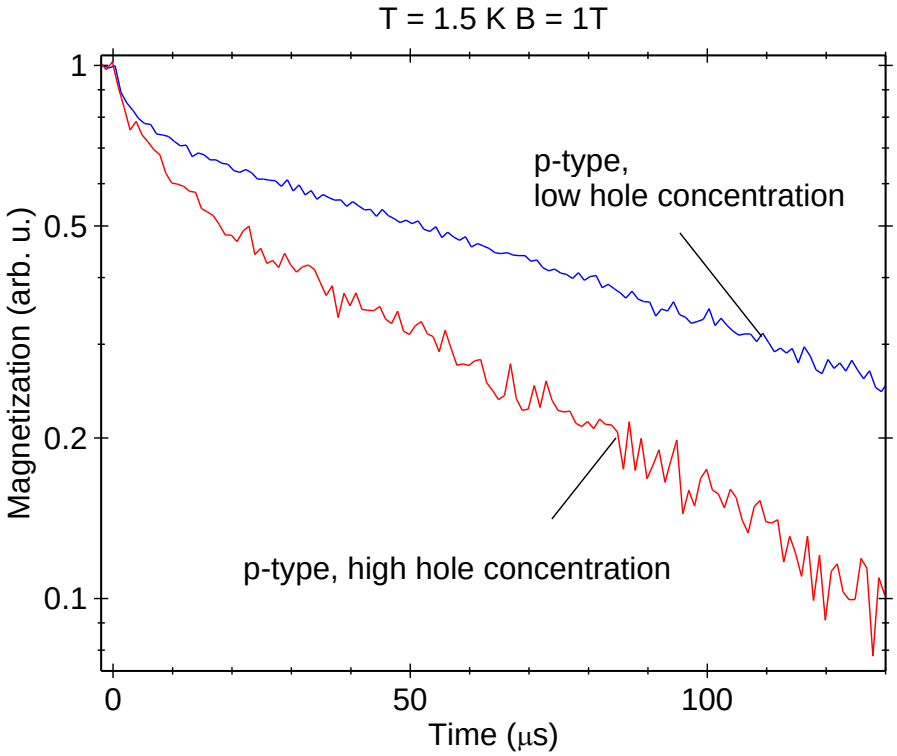

Figure 7.14: Magnetization dynamics of a p-type $Cd_{1-x}Mn_xTe$ quantum well with 0.8% of Mn and different hole gas concentration at B = 1 T. The high concentration is equal to 1.5×10^{11} cm^{-2}, the low one is of order of 10^{10} cm^{-2}.

induces an exchange field of the order of 0.1 T, *i.e.*, a splitting of 10 μeV between the $\pm 5/2$ and $\pm 3/2$ doublets. This results in an effective anisotropy similar to that occurring in molecular magnets, where it gives rise to a slow dynamics of the magnetization [128]. The extreme case of this slowing down is appearance of the ferromagnetic phase in the $Cd_{1-x}Mn_xTe$ quantum wells with high Mn content and carrier concentration [6, 129, 130, 131, 132]. In a ferromagnetic $Cd_{1-x}Mn_xTe$ quantum well, this coupling results also in a softening of the Mn resonance when approaching the critical temperature [131, 133].

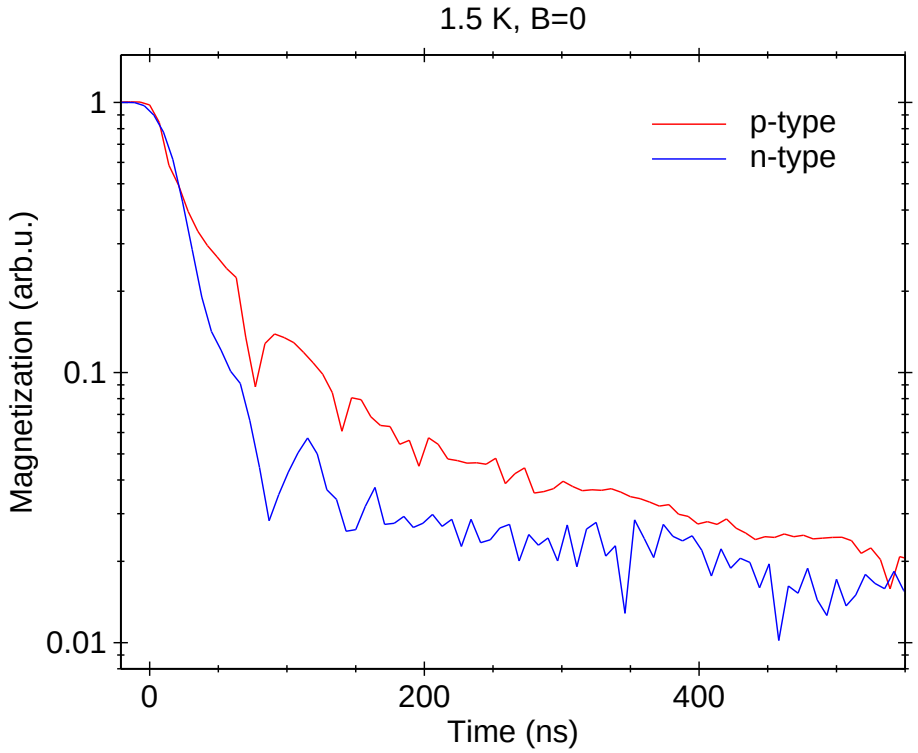

Figure 7.15: Magnetization dynamics of a n-type and p-type $Cd_{1-x}Mn_xTe$ quantum wells with 0.8% of Mn at B = 0.

7.2.2 Mn doped quantum dots

As shown in the previous section, one of the reasons of the fast spin relaxation in zero magnetic field in quantum wells is the perturbation of the Mn^{2+} ion's ground state by local strain of the crystal. This contribution is known to be usually much larger in quantum dots than in quantum wells. Therefore, one may expect that in the case of quantum dots much larger magnetic fields would be required to suppress the fast relaxation channel. On the other hand, the experiment described in section 7.1 has shown, that the spin-lattice relaxation of single Mn^{2+} ion embedded in a quantum dot is extremely slow in low magnetic field, down to 0.5 T. Thus the field necessary to suppress the fast relaxation should be lower than this value.

In order to compare the results of experiments on quantum dots and quantum

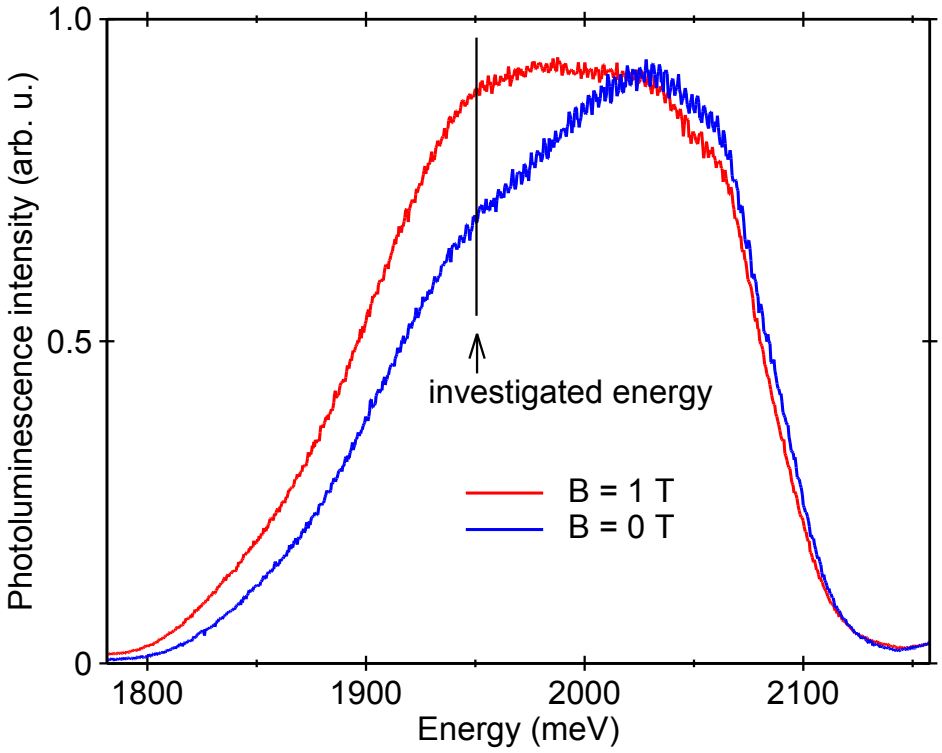

Figure 7.16: Typical photoluminescence spectra of an ensemble of $Cd_{1-x}Mn_xTe$ quantum dots with 1% of Mn, with and without applied magnetic field. The spectra were recorded in σ^+ polarization at 1.5 K. Vertical line indicates the wavelength at which the variation of optical signal is traced under pulsed magnetic field.

wells, all measurements in pulsed magnetic field were performed in the same setup and in the same conditions (see previous section). Typical spectra of the ensemble of quantum dots with and without magnetic field are shown in Figure 7.16. As described in section 1.3.1, these spectra show a broad band consisting of many of lines, each related to a specific quantum dot. The temporal evolution of the magnetization of the Mn^{2+} ions embedded in the quantum dots is monitored by recording the photoluminescence intensity at indicated energy in selected circular polarization. The results of the measurement of the magnetization relaxation after the magnetic pulse are shown in Figure 7.17.

The result of the experiment on quantum dots in zero field is basically the

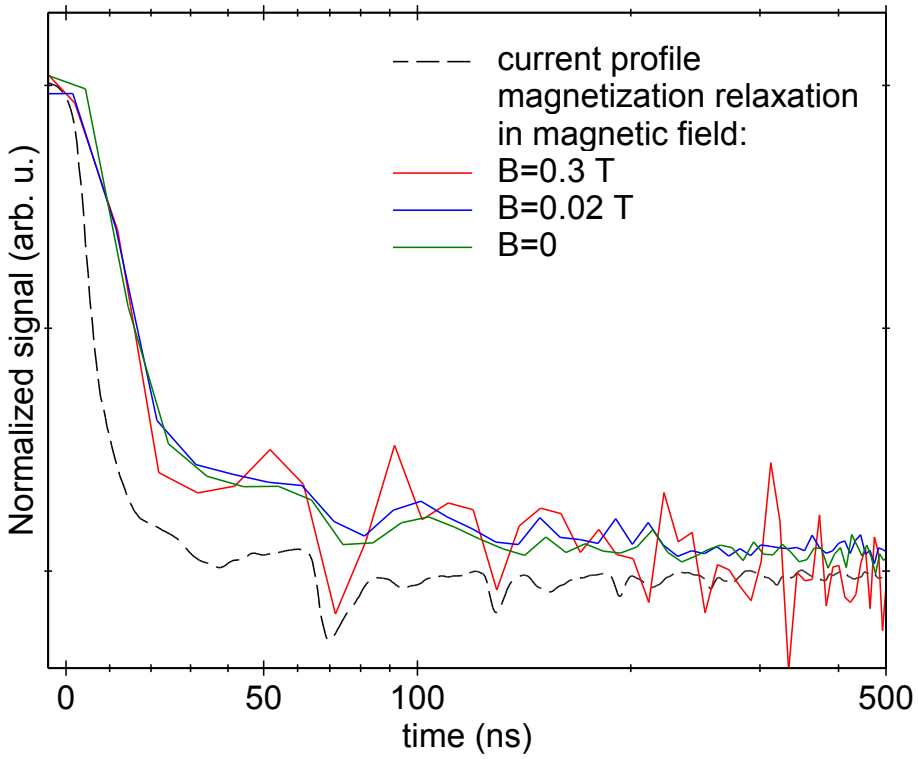

Figure 7.17: Magnetization dynamics of an ensemble of quantum dots at indicated values of external, constant magnetic field at 1.5 K, compared with the profile of the current in the coil (grey line). Note, that for non-zero values of external field the zero point on vertical axis does not correspond to vanishing magnetization but to the equilibrium state after the magnetic pulse. Non-linear time scale chosen to show both fast and slow components of decays clearly.

same as on quantum well. We observe a fast relaxation with characteristic time equal to the previous one within experimental accuracy. However there is a huge difference observed between quantum dots and quantum well in non-zero magnetic field. In quantum dots, in contrast to quantum well, there is no visible slowing down of relaxation after applying external field up to 0.5 T. It is clearly visible in Figure 7.17. The experimental studies in higher field were not possible - the photoluminescence spectrum of ensemble of quantum dots was completely circularly polarized at field of about 1 T and no polarization variation could be observed upon applying small magnetic pulses.

The fact that the magnetization relaxation does not slow down in external field of a few tenths of Tesla is surprising when compared with the experiment described in section 7.1. The relaxation of a single Mn^{2+} ion which do not interact with other magnetic moments was several orders of magnitude slower than the one observed in present experiment. This indicates that one of the origins of the fast relaxation in quantum dots with many Mn^{2+} ions might be the spin-spin interaction between the ions. The interaction is not expected to be strong, as the nominal concentration of the magnetic ions is low (equal to 1%). However, no data is available on the distribution uniformity of the ions inside the dot. Agglomeration of the Mn^{2+} ions in certain parts of the dot (in the dot centre, for instance) would lead to much stronger spin-spin interaction when compared to the case of uniform distribution. Further studies are needed on this field, however they remain beyond the scope of this work.

Chapter 8

Conclusions

The spin dynamics of magnetic ions embedded in semiconductor crystal attracted attention of scientists for years. Although many aspects of the magnetic ions behaviour in a semiconductor crystal were already well understood, there were still a lot of open questions. This work reports new experimental results in this field. It presents experiments related to the mechanisms governing the spin dynamics - orientation and relaxation - of the manganese ions embedded in the CdTe crystal. Large part of the work is devoted to single quantum dots with single Mn^{2+} ions, which give a peerless insight into the interactions of magnetic ion with semiconductor environment. Phenomena occurring in low and zero magnetic field in larger systems of magnetic ions, which have not been investigated before, are also addressed.

The experiments on single CdTe quantum dots with single Mn^{2+} ions have shown, that the random spin flips of the Mn^{2+} spin are strongly enhanced by injection of randomly polarized excitons into the quantum dot. This suggested a procedure of the Mn^{2+} polarization by spin polarized excitons. The experiment exploiting exciton spin transfer from a neighbour non-magnetic quantum dot indeed demonstrated that the information can be written on the spin state of a single Mn^{2+} ion. The magnetic field of 1 T strongly enhances the orientation efficiency. Dynamics of the Mn^{2+} spin under resonant excitation with circularly polarized light was measured in a time-resolved experiment and described with a simple rate equation model. The orientation time varied between 20 and 100 ns over the used range of excitation power. The storage time of information on

the Mn^{2+} spin depends mainly on the spin-lattice relaxation time and reaches almost 0.5 ms in low magnetic field and liquid helium temperature. One of possible orientation mechanisms of the Mn^{2+} spin has been investigated. The dark excitons optical recombination, usually not observable in non-magnetic quantum dots in the absence of magnetic field, is partially allowed in dots with magnetic ions. Each event of such recombination takes place with a simultaneous spin flip of the Mn^{2+} ion. Thus a series of these events can create significant polarization of the Mn^{2+} spin. This mechanism can be particularly efficient for dots with high in-plane anisotropy, thus with significant heavy hole-light hole mixing. However, the experimental results show that it is not the only mechanism which should be taken into account. In particular the dominant mechanism of the Mn^{2+} spin orientation in the dots with low heavy hole-light hole mixing remains unclear.

The Mn^{2+} spin relaxation has been investigated for systems of both single and many magnetic ions. In case of single Mn^{2+} spin in a quantum dot two methods of measurement have been demonstrated. Both gave the same results within the experimental accuracy. However, the time-resolved method allowed measurements with better accuracy and in a broader range of magnetic fields. The measured dependence of the spin-lattice relaxation rate on the magnetic field is qualitatively similar to the one measured previously in bulk material. However, there is a relevant quantitative difference between results of these and previous experiments, especially in high magnetic field. Possible origins of much faster relaxation observed in the experiments on quantum dots include slightly higher temperature of the sample as well as strain fields, usually high in structures containing quantum dots. Confirmation of this hypothesis requires further studies.

The spin relaxation in systems with many Mn^{2+} ions - quantum wells and quantum dots - were performed with the use of new experimental technique. It allowed investigation of the magnetization relaxation in the absence of magnetic field, with temporal resolution down to a few nanoseconds, which was not possible before.

In case of diluted magnetic quantum wells, we analyzed the evolution of the giant Zeeman splitting of the photoluminescence, transmission and reflectivity lines after a pulse of magnetic field. At zero magnetic field, a fast dynamics was observed, with a dominant component being of order of tens of nanoseconds.

This dynamics is driven by hyperfine coupling with the nuclear spin of the Mn^{2+} ion. It is highly sensitive to the presence of the anisotropy, particularly the one introduced by holes and by strain. Due to a thermal distribution of nuclear spins the fast decay of the magnetization is observed when the field is swept down to zero. When applying an additional, static magnetic field, a much slower relaxation (by about 3 orders of magnitude) was observed, with a characteristic time up to tens of microseconds at 1 T for 0.2% - 1.5% Mn. This slow relaxation agrees with previous measurements of the spin-lattice relaxation time. The influence of two dimensional hole on magnetization relaxation is also visible. In relatively large magnetic field (1 T) the presence of hole gas enhances the relaxation rate, due to additional relaxation channel. At B=0, the introduction of holes results in appearance of slow relaxation component, which can be ascribed to stabilization of relaxation caused by the interaction between holes and Mn^{2+} ions.

In experiments with quantum dots with many magnetic ions, we analyzed the degree of circular polarization of photoluminescence spectrum after a pulse of magnetic field. In the absence of magnetic field the magnetization relaxation is very fast, with dominant component of characteristic time equal to about 20 ns. This value is comparable with the one obtained in similar experiment with quantum wells. After applying an additional, static magnetic field of order of 0.5 T, the relaxation does not slow down, contrary to the case of quantum wells. One of the possible origins of the fast relaxation in magnetic field is the spin-spin interaction between the ions. This interaction could be significantly enhanced if the Mn^{2+} ions distribution inside the dot would be highly non-uniform. This aspect requires further studies.

8.1 Perspectives

Although the experiments discussed in this work brought answers to many questions concerning the Mn^{2+} spin dynamics in a CdTe crystal, they also raised new unresolved problems which remain open. One of the most important but not firmly conducted issue concerns the mechanism of the optical spin orientation in quantum dots with single Mn^{2+} ions. Several mechanisms have been proposed

so far, including the one involving dark excitons recombination presented in this work. However a complete explanation of this phenomenon is still missing.

All experiments discussed in this work concern a non-coherent control and evolution of the spin state of magnetic ions embedded in a semiconductor crystal. A completely new emerging field of research is related to coherent phenomena, especially those involving single magnetic ions, as they hold promise for single atom-based qubits. Future experiments in this area will probably focus on investigation of the coherence time and possibility of coherent control over the spin state of a single magnetic ion inside a quantum dot. Hopefully, experimental work presented here will turn out to be helpful in this new, fascinating field.

Appendix A

Parameters used in calculations

- Chapter 6

  Parameters of the Hamiltonian 6.1 used to reproduce energies of excitonic transitions observed for quantum dot QD2 from Figure 6.1(b):

  g_{Mn} = 2.0; g_e = -0.55; g_h = 0.43;

  I_e = -0.09 meV; I_h = 0.19 meV;

  $a_x = a_y = 0$; a_z = -0.025 meV;

  b_x = -b_y = 0.13 meV; b_z = -0.28 meV;

  γ = 15 meV; β = 1.9 meV;

  γ_2 = 0.0022 meV/T^2 (diamagnetic coefficient of the diamagnetic shift: $\Delta E = \gamma_2 B^2$)

- Chapter 7

  Parameters of the Hamiltonian 7.4 and D (equation 7.5) used to reproduce magnetization temporal profile shown in Figure 7.10:

  g_{Mn} = 2.0; A = 680 neV; D = 4.16·10$^-$7 eV; a = 320 neV;

  G_{11} = 46 m^{-1}; G_{11} = 2.7·10$^-$9 Pa^{-1}m^{-1};

Appendix B

List of publications related to this work

- M. Koperski, M. Goryca, T. Kazimierczuk, P. Kossacki, P. Wojnar, J.A. Gaj, *Magnetoluminescence of a CdTe Quantum Dot with a Single Manganese Ion in Voigt Configuration*, Acta Physica Polonica A **119**, 618 (2011).

- M. Goryca, P. Pochocka, T. Kazimierczuk, P. Wojnar, G. Karczewski, J. A. Gaj, M. Potemski, and P. Kossacki, *Brightening of dark excitons in a single CdTe quantum dot containing a single Mn^{2+} ion*, Phys. Rev. B **82**, 165323 (2010).

- M. Goryca, T. Kazimierczuk, M. Nawrocki, A. Golnik, J. A. Gaj, P. Wojnar, G. Karczewski, P. Kossacki, *Optical manipulation of a single Mn spin in a CdTe quantum dot*, Physica E **42**, 2690 (2010).

- M. Goryca, P. Kossacki, A. Golnik, T. Kazimierczuk, P. Wojnar, and M. Nawrocki, *Spin Dynamics of a Single Mn Ion in a CdTe/(Cd, Mg, Zn)Te Quantum Dot*, AIP Conf. Proc. **1199**, 453 (2010).

- M. Goryca, T. Kazimierczuk, M. Nawrocki, A. Golnik, J. A. Gaj, P. Kossacki, P. Wojnar, and G. Karczewski *Optical Manipulation of a Single Mn Spin in a CdTe-Based Quantum Dot*, Phys. Rev. Lett. **103**, 087401 (2009).

- A. Lipińska, C. Simserides, K. N. Trohidou, M. Goryca, P. Kossacki, A. Majhofer, and T. Dietl, *Ferromagnetic properties of p-(Cd,Mn)Te quantum wells: Interpretation of magneto-optical measurements by Monte Carlo simulations*, Physical Review B **79**, 235322 (2009).

- M. Goryca, D. Ferrand, P. Kossacki, M. Nawrocki, W. Pacuski, W. Maślana, J.A. Gaj, S. Tatarenko, J. Cibert, T. Wojtowicz, and G. Karczewski, *Magnetization Dynamics Down to a Zero Field in Dilute (Cd,Mn)Te Quantum Wells*, Phys. Rev. Lett. **102**, 046408 (2009).

- J. Kobak, M. Goryca, P. Kossacki, A. Golnik, G. Karczewski, T. Wojtowicz, and J. A. Gaj, *Magnetization dynamics of (Cd,Mn)Te quantum well in pulsed magnetic field*, Acta Physica Polonica A **116**, 907 (2009).

- J. Papierska, M. Goryca, P. Wojnar, and P. Kossacki, *Temperature of a Single Mn Atom in a CdTe Quantum Dot*, Acta Physica Polonica A **116**, 899 (2009).

- J. A. Gaj, T. Kazimierczuk, M. Goryca, M. Koperski, A. Golnik, P. Kossacki, M. Nawrocki, P. Wojnar, and G. Karczewski, *Spin-related Spectroscopy of CdTe-based Quantum Dots*, Acta Physica Polonica A **116**, 795 (2009).

- M. Goryca, P. Kossacki, M. Nawrocki, P. Wojnar, G. Karczewski *Nanosecond spin dynamics in (Cd,Mn)Te quantum dots and quantum wells*, Journal of the Korean Physical Society **53**, 2963- 2966 (2008).

- M. Goryca, D. Ferrand, P. Kossacki, M. Nawrocki, W. Pacuski, W. Maślana, S. Tatarenko, T. Wojtowicz, G. Karczewski, and J. Cibert *Influence of carriers on magnetization relaxation in (Cd,Mn)Te quantum wells*, Physica Status Solidi (c) **4**, 307-310 (2007).

- J. A. Gaj, J. Cibert, A. Golnik, M. Goryca, E. Janik, T. Kazimierczuk, . Kopotowski, P. Kossacki, J. Kossut, K. Kowalik, O. Krebs, A. Lemaitre, S. Makowski, W. Maślana, M. Nawrocki, P. Płochocka, B. Piechal, P. Selenart, J. Suffczyński, S. Tatarenko, and P. Voisin *Semiconductor heterostructures for spintronics and quantum information*, Comptes Rendus Physique **8**, 243-252 (2007).

- M. Goryca, P. Kossacki, D. Ferrand, M. Nawrocki, W. Pacuski, W. Maślana, S. Tatarenko, J. Cibert *Anisotropy dependent relaxation dynamics of mag-*

netization in (Cd,Mn)Te quantum wells, Physica Status Solidi (c) **3**, 4094-4097 (2007).

- P. Kossacki, D. Ferrand , M. Goryca, M. Nawrocki, W. Pacuski, W. Maślana, S. Tatarenko, J. Cibert *Relaxation dynamics of ferromagnetic domains in (Cd,Mn)Te quantum wells*, Physica E **32**, 454-457 (2006).

- J. A. Gaj, J. Cibert, D. Ferrand, A. Golnik, M. Goryca, G. Karczewski, P. Kossacki, J. Kossut, K. Kowalik, O. Krebs, A. Kudelski, M. Kutrowski, A. Lemaitre, W. Maślana, M. Nawrocki, W. Pacuski, P. Płochocka, P. Senellart, S. Tatarenko, P. Voisin, and T. Wojtowicz, *Optical probing of spin-dependent interactions in II-VI semiconductor structures*, Physica Status Solidi (b) **243**, 906-913 (2006).

- M. Goryca, D. Ferrand, P. Kossacki, M. Nawrocki, W. Pacuski, W. Maślana, S. Tatarenko, J. Cibert *Magnetization dynamics in (Cd,Mn)Te quantum wells*, Physica Status Solidi (b) **243**, 882-886 (2006).

References

[1] S. A. Wolf, D. D. Awschalom, R. A. Buhrman, J. M. Daughton, S. von Molnr, M. L. Roukes, A. Y. Chtchelkanova, and D. M. Treger, *Spintronics: A Spin-Based Electronics Vision for the Future*, Science **294**, 1488 (2001). 1

[2] I. Žutić, J. Fabian, and S. Das Sarma, *Spintronics: Fundamentals and applications*, Rev. Mod. Phys. **76**, 323 (2004). 1

[3] J. Furdyna and J. Kossut, *Diluted magnetic semiconductors,* volume 25 of *Semiconductors and Semimetals* (Academic Press, New York, 1988). 2, 3

[4] J. Gaj, R. Planel, and G. Fishman, *Relation of Magneto-optical Properties of Free Excitons to Spin Alignment of Mn^{2+} Ions in $Cd_{1-x}Mn_xTe$*, Solid State Commun. **29**, 435 (1979). 3, 7, 8, 39

[5] O. Madelung, M. Schulz, and W. Weiss, editors, *Landolt-Börnstein, Numerical Data and Functional Relationships in Science and Technology, New Series*, Group III Vol. 17b (Springer-Verlag, Berlin, 1982). 3

[6] H. Boukari, P. Kossacki, M. Bertolini, D. Ferrand, J. Cibert, S. Tatarenko, A. Wasiela, J. A. Gaj, and T. Dietl, *Light and Electric Field Control of Ferromagnetism in Magnetic Quantum Structures*, Phys. Rev. Lett. **88**, 207204 (2002). 3, 20, 108

[7] Y. Léger, L. Besombes, J. Fernández-Rossier, L. Maingault, and H. Mariette, *Electrical Control of a Single Mn Atom in a Quantum Dot*, Phys. Rev. Lett. **97**, 107401 (2006). 3, 17, 19

[8] S.-H. Wei and A. Zunger, *Alloy-Stabilized Semiconducting and Magnetic Zinc-Blende Phase of MnTe*, Phys. Rev. Lett. **56**, 2391 (1986). 4

[9] R. Triboulet, A. Heurtel, and J. Rioux, *Twin-free (Cd, Mn)Te substrates*, Journal of Crystal Growth **101**, 131 (1990). 4

[10] M. Kutrowski, *Magnetooptyczne własności profilowanych studni kwantowych opartych na związkach $Cd_{1-x}Mn_xTe$ i $Cd_{1-y}Mg_yTe$.*, PhD thesis, Institute of Physics, Polish Academy of Sciences, 2001. 4, 27

[11] J. Kossut and J. Gaj, editors, *Introduction to the Physics of Diluted Magnetic Semiconductors* (Springer-Verlag, Berlin, 2010). 5

[12] J. Kossut and W. Dobrowolski, editors, *Diluted magnetic semiconductors,* in *Handbook of Magnetic Materials,* Vol. 7 (Elsevier B.V., Amsterdam, 1993). 6

[13] J. A. Gaj, W. Grieshaber, C. Bodin-Deshayes, J. Cibert, G. Feuillet, Y. Merle d'Aubigné, and A. Wasiela, *Magneto-optical study of interface mixing in the CdTe-(Cd,Mn)Te system*, Phys. Rev. B **50**, 5512 (1994). 7

[14] W. Grieshaber, A. Haury, J. Cibert, Y. M. d'Aubigné, A. Wasiela, and J. A. Gaj, *Magneto-optic study of the interface in semimagnetic semiconductor heterostructures: Intrinsic effect and interface profile in CdTe-$Cd_{1-x}Mn_xTe$*, Phys. Rev. B **53**, 4891 (1996). 7

[15] W. Maślana, *Carrier induced ferromagnetism in (Cd,Mn)Te quantum wells: a spectroscopic study.*, PhD thesis, University of Warsaw, 2007. 7, 25

[16] R. R. Galazka, S. Nagata, and P. H. Keesom, *Paramagnetic¯spin-glass¯antiferromagnetic phase transitions in* $Cd_{1-x}Mn_xTe$ *from specific heat and magnetic susceptibility measurements*, Phys. Rev. B **22**, 3344 (1980). 7

[17] M. Escorne and A. Mauger, *Spin-glass versus antiferromagnetic clustering in* $Cd_{1-x}Mn_xTe$, Phys. Rev. B **25**, 4674 (1982). 7

[18] S. B. Oseroff, *Magnetic susceptibility and EPR measurements in concentrated spin-glasses:* $Cd_{1-x}Mn_xTe$ *and* $Cd_{1-x}Mn_xSe$, Phys. Rev. B **25**, 6584 (1982). 7

[19] M. A. Novak, O. G. Symko, D. J. Zheng, and S. Oseroff, *Spin glass behavior of* $Cd_{1-x}Mn_xTe$ *below the nearest-neighbor percolation limit*, Journal of Applied Physics **57**, 3418 (1985). 7

[20] K. Kheng, R. T. Cox, M. Y. d' Aubigné, F. Bassani, K. Saminadayar, and S. Tatarenko, *Observation of negatively charged excitons* X^- *in semiconductor quantum wells*, Phys. Rev. Lett. **71**, 1752 (1993). 10

[21] V. Huard, R. T. Cox, K. Saminadayar, A. Arnoult, and S. Tatarenko, *Bound States in Optical Absorption of Semiconductor Quantum Wells Containing a Two-Dimensional Electron Gas*, Phys. Rev. Lett. **84**, 187 (2000). 10

[22] P. Płochocka, P. Kossacki, W. Maślana, J. Cibert, S. Tatarenko, C. Radzewicz, and J. A. Gaj, *Femtosecond Study of the Interplay between Excitons, Trions, and Carriers in (Cd,Mn)Te Quantum Wells*, Phys. Rev. Lett. **92**, 177402 (2004). 10

[23] R. T. Cox, R. B. Miller, K. Saminadayar, and T. Baron, *Trions, excitons, and scattering states in multiple quantum wells with a variable-concentration electron gas*, Phys. Rev. B **69**, 235303 (2004). 10

[24] P. Kossacki, *Optical studies of charged excitons in IIVI semiconductor quantum wells*, Journal of Physics: Condensed Matter **15**, R471 (2003). 10

[25] J. M. Moison, F. Houzay, F. Barthe, L. Leprince, E. André, and O. Vatel, *Self-organized growth of regular nanometer-scale InAs dots on GaAs*, Applied Physics Letters **64**, 196 (1994). 11

[26] R. Nötzel, *Self-organized growth of quantum-dot structures*, Semiconductor Science and Technology **11**, 1365 (1996). 11

[27] A. Babiński, J. Jasiński, R. Bożek, A. Szepielow, and J. M. Baranowski, *Rapid thermal annealing of InAs/GaAs quantum dots under a GaAs proximity cap*, Applied Physics Letters **79**, 2576 (2001). 11

[28] S. Fafard, Z. Wasilewski, J. McCaffrey, S. Raymond, and S. Charbonneau, *InAs self-assembled quantum dots on InP by molecular beam epitaxy*, Applied Physics Letters **68**, 991 (1996). 11

[29] A. Yoffe, *Semiconductor quantum dots and related systems: Electronic, optical, luminescence and related properties of low dimensional systems*, Advances in Physics **50**, 1 (2000). 11

[30] G. Karczewski, S. Maćkowski, M. Kutrowski, T. Wojtowicz, and J. Kossut, *Photoluminescence study of CdTe/ZnTe self-assembled quantum dots*, Applied Physics Letters **74**, 3011 (1999). 11

[31] F. Tinjod, B. Gilles, S. Moehl, K. Kheng, and H. Mariette, *II-VI quantum dot formation induced by surface energy change of a strained layer*, Applied Physics Letters **82**, 4340 (2003). 11, 23

[32] S. H. Xin, P. D. Wang, A. Yin, C. Kim, M. Dobrowolska, J. L. Merz, and J. K. Furdyna, *Formation of self-assembling CdSe quantum dots on ZnSe by molecular beam epitaxy*, Applied Physics Letters **69**, 3884 (1996). 11

[33] V. D. Kulakovskii, G. Bacher, R. Weigand, T. Kümmell, A. Forchel, E. Borovitskaya, K. Leonardi, and D. Hommel, *Fine Structure of Biexciton Emission in Symmetric and Asymmetric CdSe/ZnSe Single Quantum Dots*, Phys. Rev. Lett. **82**, 1780 (1999). 11

[34] J. Suffczyński, T. Kazimierczuk, M. Goryca, B. Piechal, A. Trajnerowicz, K. Kowalik, P. Kossacki, A. Golnik, K. P. Korona, M. Nawrocki, J. A. Gaj, and G. Karczewski, *Excitation mechanisms of individual CdTe/ZnTe quantum dots studied by photon correlation spectroscopy*, Phys. Rev. B **74**, 085319 (2006). 12, 13, 34, 35, 63, 81

[35] L. Besombes, Y. Leger, L. Maingault, D. Ferrand, H. Mariette, and J. Cibert, *Carrier-induced spin splitting of an individual magnetic atom embedded in a quantum dot*, Phys. Rev. B **71**, 161307 (2005). 12, 13, 17, 81

[36] T. Kazimierczuk, T. Smoleński, M. Goryca, L. Kłopotowski, P. Wojnar, K. Fronc, A. Golnik, M. Nawrocki, J. A. Gaj, and P. Kossacki, *Magne-*

tophotoluminescence study of intershell exchange interaction in CdTe/ZnTe quantum dots, Phys. Rev. B **84**, 165319 (2011). 12, 13, 34

[37] T. Kazimierczuk, *Mechanizmy wzbudzenia i relaksacji w kropkach kwantowych CdTe/ZnTe*, PhD thesis, University of Warsaw, Faculty of Physics, Institute of Experimental Physics, to be published in 2012. 12, 13, 68

[38] A. L. Efros, E. I. Rashba, and M. Rosen, *Paramagnetic Ion-Doped Nanocrystal as a Voltage-Controlled Spin Filter*, Phys. Rev. Lett. **87**, 206601 (2001). 13

[39] G. Bacher, A. A. Maksimov, H. Schömig, V. D. Kulakovskii, M. K. Welsch, A. Forchel, P. S. Dorozhkin, A. V. Chernenko, S. Lee, M. Dobrowolska, and J. K. Furdyna, *Monitoring Statistical Magnetic Fluctuations on the Nanometer Scale*, Phys. Rev. Lett. **89**, 127201 (2002). 13

[40] D. Loss and D. P. DiVincenzo, *Quantum computation with quantum dots*, Phys. Rev. A **57**, 120 (1998). 13

[41] C. Bennett and D. DiVincenzo, *Quantum information and computation*, Nature **404**, 247 (2000). 13

[42] M. Leuenberger and D. Loss, *Quantum computing in molecularmagnets*, Nature **410**, 789 (2001). 13

[43] L. V. Titova, J. K. Furdyna, M. Dobrowolska, S. Lee, T. Topuria, P. Moeck, and N. D. Browning, *Magnetic CdSe-based quantum dots grown on Mn-passivated ZnSe*, Applied Physics Letters **80**, 1237 (2002). 13

[44] T. Gurung, S. Mackowski, G. Karczewski, H. E. Jackson, and L. M. Smith, *Ultralong spin memory of optically excited single magnetic quantum dots*, Applied Physics Letters **93**, 153114 (2008). 13

[45] C. Le Gall, L. Besombes, H. Boukari, R. Kolodka, J. Cibert, and H. Mariette, *Optical Spin Orientation of a Single Manganese Atom in a Semiconductor Quantum Dot Using Quasiresonant Photoexcitation*, Phys. Rev. Lett. **102**, 127402 (2009). 13, 21, 65

[46] M. Goryca, T. Kazimierczuk, M. Nawrocki, A. Golnik, J. A. Gaj, P. Kossacki, P. Wojnar, and G. Karczewski, *Optical Manipulation of a Single Mn Spin in a CdTe-Based Quantum Dot*, Phys. Rev. Lett. **103**, 087401 (2009). 13, 65, 68, 78, 84, 86

[47] P. Wojnar, J. Suffczyński, K. Kowalik, A. Golnik, M. Aleszkiewicz, G. Karczewski, and J. Kossut, *Size-dependent magneto-optical effects in CdMnTe diluted magnetic quantum dots*, Nanotechnology **19**, 235403 (2008). 14, 15, 24, 28, 68

[48] A. K. Bhattacharjee and J. Pérez-Conde, *Optical properties of paramagnetic ion-doped semiconductor nanocrystals*, Phys. Rev. B **68**, 045303 (2003). 17

[49] L. Besombes, Y. Léger, L. Maingault, D. Ferrand, H. Mariette, and J. Cibert, *Probing the Spin State of a Single Magnetic Ion in an Individual Quantum Dot*, Phys. Rev. Lett. **93**, 207403 (2004). 17, 19, 78

[50] Y. Léger, L. Besombes, L. Maingault, D. Ferrand, and H. Mariette, *Geometrical Effects on the Optical Properties of Quantum Dots Doped with a Single Magnetic Atom*, Phys. Rev. Lett. **95**, 047403 (2005). 17

[51] J. Fernández-Rossier, *Single-exciton spectroscopy of semimagnetic quantum dots*, Phys. Rev. B **73**, 045301 (2006). 17

[52] A. H. Trojnar, M. Korkusiński, E. S. Kadantsev, P. Hawrylak, M. Goryca, T. Kazimierczuk, P. Kossacki, P. Wojnar, and M. Potemski, *Quantum Interference in Exciton-Mn Spin Interactions in a CdTe Semiconductor Quantum Dot*, Phys. Rev. Lett. **107**, 207403 (2011). 17

[53] A. Kudelski, A. Lemaître, A. Miard, P. Voisin, T. C. M. Graham, R. J. Warburton, and O. Krebs, *Optically Probing the Fine Structure of a Single Mn Atom in an InAs Quantum Dot*, Phys. Rev. Lett. **99**, 247209 (2007). 17

[54] O. Krebs, E. Benjamin, and A. Lemaître, *Magnetic anisotropy of singly Mn-doped InAs/GaAs quantum dots*, Phys. Rev. B **80**, 165315 (2009). 17

[55] S. A. Crooker, D. D. Awschalom, J. J. Baumberg, F. Flack, and N. Samarth, *Optical spin resonance and transverse spin relaxation in magnetic semiconductor quantum wells*, Phys. Rev. B **56**, 7574 (1997). 20

[56] F. Teppe, M. Vladimirova, D. Scalbert, T. Wojtowicz, and J. Kossut, *Optically induced instability of spin precession in magnetic quantum wells*, Phys. Rev. B **67**, 033304 (2003). 20

[57] S. Maćkowski, T. Gurung, T. A. Nguyen, H. E. Jackson, L. M. Smith, G. Karczewski, and J. Kossut, *Optically-induced magnetization of CdMnTe self-assembled quantum dots*, Applied Physics Letters **84**, 3337 (2004). 20

[58] H. Krenn, W. Zawadzki, and G. Bauer, *Optically Induced Magnetization in a Dilute Magnetic Semiconductor:* $Hg_{1-x}Mn_xTe$, Phys. Rev. Lett. **55**, 1510 (1985). 20

[59] C. D. Stanciu, F. Hansteen, A. V. Kimel, A. Kirilyuk, A. Tsukamoto, A. Itoh, and T. Rasing, *All-Optical Magnetic Recording with Circularly Polarized Light*, Phys. Rev. Lett. **99**, 047601 (2007). 21

[60] H. Ohno, D. Chiba, F. Matsukura, T. Omiya, E. Abe, T. Dietl1, Y. Ohno, and K. Ohtani, *Electric-field control of ferromagnetism*, Nature **408**, 944 (2000). 21

[61] Y. Ohno, D. K. Young, B. Beschoten, F. Matsukura, H. Ohno, and D. D. Awschalom, *Electrical spin injection in a ferromagnetic semiconductor heterostructure*, Nature **402**, 790 (1999). 21

[62] L. Kevan and R. Schwartz, editors, *Time Domain Electron Spin Resonance* (Wiley-Interscience, New York, 1979). 21

[63] A. Abragam and B. Bleaney, *Electron Paramagnetic Resonance of Transition Ions* (Oxford University Press, Oxford, 1970). 21, 22, 99, 101

[64] H. A. Sayad and S. M. Bhagat, *Dynamic random fields in diluted magnetic semiconductors:* $Cd_{1-x}Mn_x\,Te$, Phys. Rev. B **31**, 591 (1985). 21

[65] R. E. Kremer and J. K. Furdyna, *Investigation of EPR in* $Cd_{1-x}Mn_xTe$ *by microwave Faraday effect*, Phys. Rev. B **32**, 5591 (1985). 21

[66] D. Scalbert, *Spin-lattice relaxation in diluted magnetic semiconductors*, physica status solidi (b) **193**, 189 (1996). 21, 99

[67] A. V. Scherbakov, A. V. Akimov, D. R. Yakovlev, W. Ossau, G. Landwehr, T. Wojtowicz, G. Karczewski, and J. Kossut, *Spin-lattice relaxation in semimagnetic CdMnTe/CdMgTe quantum wells*, Phys. Rev. B **62**, R10641 (2000). 21, 22, 99

[68] A. V. Scherbakov, D. R. Yakovlev, A. V. Akimov, I. A. Merkulov, B. König, W. Ossau, L. W. Molenkamp, T. Wojtowicz, G. Karczewski, G. Cywinski, and J. Kossut, *Acceleration of the spin-lattice relaxation in diluted magnetic quantum wells in the presence of a two-dimensional electron gas*, Phys. Rev. B **64**, 155205 (2001). 22

[69] A. Scherbakov, A. Akimov, D. Yakovlev, W. Ossau, L. Molenkamp, S. Tatarenko, and J. Cibert, *Spinlattice relaxation in semimagnetic CdMnTe/CdMgZnTe quantum wells with a two-dimensional hole gas tuned by optical excitation*, Solid State Communications **120**, 17 (2001). 22, 107

[70] D. Scalbert, J. Cernogora, and C. Benoît à la Guillaume, *Spin-Lattice Relaxation in Paramagnetic CdMnTe*, Solid State Commun. **66**, 571 (1988). 22, 38, 99, 101, 106

[71] T. Strutz, A. M. Witowski, and P. Wyder, *Spin-lattice relaxation at high magnetic fields*, Phys. Rev. Lett. **68**, 3912 (1992). 22, 38, 97, 98, 101, 106

[72] S. A. Crooker, J. J. Baumberg, F. Flack, N. Samarth, and D. D. Awschalom, *Terahertz Spin Precession and Coherent Transfer of Angular Momenta in Magnetic Quantum Wells*, Phys. Rev. Lett. **77**, 2814 (1996). 22, 38, 100

[73] A. V. Scherbakov, A. V. Akimov, D. R. Yakovlev, W. Ossau, A. Waag, G. Landwehr, T. Wojtowicz, G. Karczewski, and J. Kossut, *Heating of the spin system by nonequilibrium phonons in semimagnetic (Cd,Mn,Mg)Te quantum wells*, Phys. Rev. B **60**, 5609 (1999). 22, 38, 99

[74] W. Farah, D. Scalbert, and M. Nawrocki, *Magnetic relaxation studied by transient reflectivity in* $Cd_{1-x}Mn_xTe$, Phys. Rev. B **53**, R10461 (1996). 22, 38

[75] C. Camilleri, F. Teppe, D. Scalbert, Y. G. Semenov, M. Nawrocki, M. Dyakonov, J. Cibert, S. Tatarenko, and T. Wojtowicz, *Electron and hole spin relaxation in modulation-doped CdMnTe quantum wells*, Phys. Rev. B **64**, 085331 (2001). 22, 38, 100

[76] I. Stranski and L. Von Krastanow, *Abhandlungen der Mathematisch-Naturwissenschaftlichen Klasse*, Akad. Wiss. Lit. Mainz **146**, 797 (1939). 23

[77] E. Bauer, *Phänomenologische Theorie der Kristallabscheidung an Oberflächen. I*, Zeitschrift für Kristallographie **110**, 372 (1958). 23

[78] W. Maślana, P. Kossacki, M. Bertolini, H. Boukari, D. Ferrand, S. Tatarenko, J. Cibert, and J. A. Gaj, *p-type doping of II-VI heterostructures from surface states Application to ferromagnetic* $Cd_{1-x}Mn_xTe$ *quantum wells*, Applied Physics Letters **82**, 1875 (2003). 24

[79] P. Kossacki, H. Boukari, M. Bertolini, D. Ferrand, J. Cibert, S. Tatarenko, J. A. Gaj, B. Deveaud, V. Ciulin, and M. Potemski, *Photoluminescence of p-doped quantum wells with strong spin splitting*, Phys. Rev. B **70**, 195337 (2004). 25

[80] S. Koshihara, A. Oiwa, M. Hirasawa, S. Katsumoto, Y. Iye, C. Urano, H. Takagi, and H. Munekata, *Ferromagnetic Order Induced by Photogenerated Carriers in Magnetic III-V Semiconductor Heterostructures of (In,Mn)As/GaSb*, Phys. Rev. Lett. **78**, 4617 (1997). 24

[81] N. Paganotto, J. Siviniant, D. Coquillat, D. Scalbert, J.-P. Lascaray, and A. V. Kavokin, *Donor bound or negatively charged excitons in thin* $CdTe/Cd_{1-x}Mn_xTe$ *quantum wells*, Phys. Rev. B **58**, 4082 (1998). 24

[82] J. Siviniant, D. Scalbert, A. V. Kavokin, D. Coquillat, and J.-P. Lascaray, *Chemical equilibrium between excitons, electrons, and negatively charged*

excitons in semiconductor quantum wells, Phys. Rev. B **59**, 1602 (1999). 24

[83] T. Wojtowicz, M. Kutrowski, G. Karczewski, and J. Kossut, *Modulation-doped $Cd_{1-x}Mn_xTe/Cd_{1-y}Mg_yTe$ quantum well structures with spatial in-plane profiling of the well width and the doping intensity*, Applied Physics Letters **73**, 1379 (1998). 26

[84] J. Jasny, J. Sepiol, T. Irngartinger, M. Traber, A. Renn, and U. P. Wild, *Fluorescence microscopy in superfluid helium: Single molecule imaging*, Rev. Sci. Instrum. **67**, 1425 (1996). 31

[85] A. H. Mack, J. Riordon, C. R. Dean, R. Talbot, and G. Gervais, *Local control of light polarization with low-temperature fiber optics*, Opt. Lett. **32**, 1378 (2007). 33

[86] Y. Léger, L. Besombes, L. Maingault, and H. Mariette, *Valence-band mixing in neutral, charged, and Mn-doped self-assembled quantum dots*, Phys. Rev. B **76**, 045331 (2007). 34, 80, 83

[87] H. S. Lee, A. Rastelli, M. Benyoucef, F. Ding, T. W. Kim, H. L. Park, and O. G. Schmidt, *Microphotoluminescence spectroscopy of single CdTe/ZnTe quantum dots grown on Si(001) substrates*, Nanotechnology **20**, 075705 (2009). 34

[88] R. M. Stevenson, R. J. Young, P. Atkinson, K. Cooper, D. A. Ritchie, and A. J. Shields, *A semiconductor source of triggered entangled photon pairs*, Nature **439**, 179 (2006). 35

[89] N. Akopian, N. H. Lindner, E. Poem, Y. Berlatzky, J. Avron, D. Gershoni, B. D. Gerardot, and P. M. Petroff, *Entangled Photon Pairs from Semiconductor Quantum Dots*, Phys. Rev. Lett. **96**, 130501 (2006). 35

[90] R. Hanbury Brown and R. Q. Twiss, *Correlation between Photons in two Coherent Beams of Light*, Nature **177**, 27 (1956). 35

[91] D. Yakovlev, W. Ossau, G. Landwehr, R. Bicknell-Tassius, A. Waag, S. Schmeusser, I. Uraltsev, A. Pohlmann, and E. Gbel, *Dynamics of two-dimensional exciton magnetic polaron in CdTe/(Cd,Mn)Te quantum wells*, Journal of Crystal Growth **117**, 854 (1992). 41

[92] L. Besombes, Y. Leger, J. Bernos, H. Boukari, H. Mariette, J. P. Poizat, T. Clement, J. Fernández-Rossier, and R. Aguado, *Optical probing of spin fluctuations of a single paramagnetic Mn atom in a semiconductor quantum dot*, Phys. Rev. B **78**, 125324 (2008). 56, 62, 73

[93] P. Michler, A. Kiraz, C. Becher, W. V. Schoenfeld, P. M. Petroff, L. Zhang, E. Hu, and A. Imamoğlu, *A Quantum Dot Single-Photon Turnstile Device*, Science **290**, 2282 (2000). 58

[94] C. Santori, M. Pelton, G. Solomon, Y. Dale, and Y. Yamamoto, *Triggered Single Photons from a Quantum Dot*, Phys. Rev. Lett. **86**, 1502 (2001). 58

[95] A. Beveratos, R. Brouri, T. Gacoin, J.-P. Poizat, and P. Grangier, *Non-classical radiation from diamond nanocrystals*, Phys. Rev. A **64**, 061802 (2001). 58

[96] C. Santori, S. Götzinger, Y. Yamamoto, S. Kako, K. Hoshino, and Y. Arakawa, *Photon correlation studies of single GaN quantum dots*, Applied Physics Letters **87**, 051916 (2005). 58

[97] E. Moreau, I. Robert, L. Manin, V. Thierry-Mieg, J. M. Gérard, and I. Abram, *Quantum Cascade of Photons in Semiconductor Quantum Dots*, Phys. Rev. Lett. **87**, 183601 (2001). 58

[98] D. V. Regelman, U. Mizrahi, D. Gershoni, E. Ehrenfreund, W. V. Schoenfeld, and P. M. Petroff, *Semiconductor Quantum Dot: A Quantum Light Source of Multicolor Photons with Tunable Statistics*, Phys. Rev. Lett. **87**, 257401 (2001). 63, 71

[99] T. Kazimierczuk, J. Suffczyński, A. Golnik, J. A. Gaj, P. Kossacki, and P. Wojnar, *Optically induced energy and spin transfer in nonresonantly*

coupled pairs of self-assembled CdTe/ZnTe quantum dots, Phys. Rev. B **79**, 153301 (2009). 65, 66, 68

[100] M. Goryca, P. Plochocka, T. Kazimierczuk, P. Wojnar, G. Karczewski, J. A. Gaj, M. Potemski, and P. Kossacki, *Brightening of dark excitons in a single CdTe quantum dot containing a single Mn^{2+} ion*, Phys. Rev. B **82**, 165323 (2010). 68

[101] M. Goryca, D. Ferrand, P. Kossacki, M. Nawrocki, W. Pacuski, W. Maślana, J. A. Gaj, S. Tatarenko, J. Cibert, T. Wojtowicz, and G. Karczewski, *Magnetization Dynamics Down to a Zero Field in Dilute (Cd,Mn)Te Quantum Wells*, Phys. Rev. Lett. **102**, 046408 (2009). 69, 71, 78

[102] J. D. Cuthbert and D. G. Thomas, *Fluorescent Decay Times of Excitons Bound to Isoelectronic Traps in GaP and ZnTe*, Phys. Rev. **154**, 763 (1967). 76

[103] P. Palinginis, H. Wang, S. V. Goupalov, D. S. Citrin, M. Dobrowolska, and J. K. Furdyna, *Exciton dephasing in self-assembled CdSe quantum dots*, Phys. Rev. B **70**, 073302 (2004). 76

[104] S. A. Crooker, T. Barrick, J. A. Hollingsworth, and V. I. Klimov, *Multiple temperature regimes of radiative decay in CdSe nanocrystal quantum dots: Intrinsic limits to the dark-exciton lifetime*, Applied Physics Letters **82**, 2793 (2003). 76

[105] O. Labeau, P. Tamarat, and B. Lounis, *Temperature Dependence of the Luminescence Lifetime of Single CdSe/ZnS Quantum Dots*, Phys. Rev. Lett. **90**, 257404 (2003). 76

[106] G. Bacher, R. Weigand, J. Seufert, V. D. Kulakovskii, N. A. Gippius, A. Forchel, K. Leonardi, and D. Hommel, *Biexciton versus Exciton Lifetime in a Single Semiconductor Quantum Dot*, Phys. Rev. Lett. **83**, 4417 (1999). 76

[107] M. Bayer, G. Ortner, O. Stern, A. Kuther, A. A. Gorbunov, A. Forchel, P. Hawrylak, S. Fafard, K. Hinzer, T. L. Reinecke, S. N. Walck, J. P.

Reithmaier, F. Klopf, and F. Schäfer, *Fine structure of neutral and charged excitons in self-assembled In(Ga)As/(Al)GaAs quantum dots*, Phys. Rev. B **65**, 195315 (2002). 76, 82

[108] K. Kowalik, O. Krebs, A. Golnik, J. Suffczyński, P. Wojnar, J. Kossut, J. A. Gaj, and P. Voisin, *Manipulating the exciton fine structure of single CdTe/ZnTe quantum dots by an in-plane magnetic field*, Phys. Rev. B **75**, 195340 (2007). 76, 80, 82

[109] M. Winger, A. Badolato, K. J. Hennessy, E. L. Hu, and A. m. c. Imamoğlu, *Quantum Dot Spectroscopy Using Cavity Quantum Electrodynamics*, Phys. Rev. Lett. **101**, 226808 (2008). 76

[110] D. Gammon, E. S. Snow, B. V. Shanabrook, D. S. Katzer, and D. Park, *Homogeneous linewidths in the optical spectrum of a single gallium arsenide quantum dot*, Science **273**, 87 (1996). 78

[111] L. Besombes, L. Marsal, K. Kheng, T. Charvolin, L. S. Dang, A. Wasiela, and H. Mariette, *Fine structure of the exciton in a single asymmetric CdTe quantum dot*, Journal of Crystal Growth **214**, 742 (2000). 79

[112] M. Bayer, A. Kuther, A. Forchel, A. Gorbunov, V. B. Timofeev, F. Schäfer, J. P. Reithmaier, T. L. Reinecke, and S. N. Walck, *Electron and Hole g Factors and Exchange Interaction from Studies of the Exciton Fine Structure in $In_{0.60}Ga_{0.40}As$ Quantum Dots*, Phys. Rev. Lett. **82**, 1748 (1999). 80

[113] A. V. Koudinov, I. A. Akimov, Y. G. Kusrayev, and F. Henneberger, *Optical and magnetic anisotropies of the hole states in Stranski-Krastanov quantum dots*, Phys. Rev. B **70**, 241305 (2004). 80

[114] K. Brunner, G. Abstreiter, G. Böhm, G. Tränkle, and G. Weimann, *Sharp-Line Photoluminescence and Two-Photon Absorption of Zero-Dimensional Biexcitons in a GaAs/AlGaAs Structure*, Phys. Rev. Lett. **73**, 1138 (1994). 81

[115] H. W. van Kesteren, E. C. Cosman, W. A. J. A. van der Poel, and C. T. Foxon, *Fine structure of excitons in type-II GaAs/AlAs quantum wells*, Phys. Rev. B **41**, 5283 (1990). 82

[116] E. L. Ivchenko, A. Y. Kaminski, and U. Rössler, *Heavy-light hole mixing at zinc-blende (001) interfaces under normal incidence*, Phys. Rev. B **54**, 5852 (1996). 82

[117] A. A. Toropov, E. L. Ivchenko, O. Krebs, S. Cortez, P. Voisin, and J. L. Gentner, *Excitonic contributions to the quantum-confined Pockels effect*, Phys. Rev. B **63**, 035302 (2000). 82

[118] S. J. Cheng and P. Hawrylak, *Controlling magnetism of semi-magnetic quantum dots with odd-even exciton numbers*, EPL **81**, 37005 (2008). 82

[119] B. E. Larson and H. Ehrenreich, *Anisotropic superexchange and spin-resonance linewidth in diluted magnetic semiconductors*, Phys. Rev. B **39**, 1747 (1989). 99

[120] T. Dietl, P. Peyla, W. Grieshaber, and Y. M. d'Aubigné, *Dynamics of Spin Organization in Diluted Magnetic Semiconductors*, Phys. Rev. Lett. **74**, 474 (1995). 99, 102

[121] J. Lambe and C. Kikuchi, *Paramagnetic Resonance of CdTe: Mn and CdS: Mn*, Phys. Rev. **119**, 1256 (1960). 101

[122] M. Quazzaz, G. Yang, S. Xin, L. Montes, H. Luo, and J. Furdyna, *Electron Paramagnetic Resonance of Mn2+ in strained-layer semiconductor superlattices*, Solid State Commun. **96**, 405 (1995). 101, 103

[123] W. Low, *Paramagnetic resonance in solids,* in *Solid State Physics,* Vol. 2: Supplement (Academic Press, New York, 1967). 103

[124] G. Yang, *Electron Paramagnetic Resonance in II-VI Semiconductor Heterostructures*, PhD thesis, University of Notre Dame, 1993. 103

[125] M. Causa, M. Tovar, S. Oseroff, R. Calvo, and W. Giriat, *Spin-lattice coefficients of Mn2+ in IIVI compounds*, Physics Letters A **77**, 473 (1980). 103, 106

[126] E. R. Feher, *Effect of Uniaxial Stresses on the Paramagnetic Spectra of* Mn^{3+} *and* Fe^{3+} *in MgO*, Phys. Rev. **136**, A145 (1964). 106

[127] C. Bodin, R. André, J. Cibert, L. S. Dang, D. Bellet, G. Feuillet, and P. H. Jouneau, *Optical linewidth and field fluctuations in piezoelectric quantum wells*, Phys. Rev. B **51**, 13181 (1995). 106

[128] L. Bogani and W. Wernsdorfer, *Molecular spintronics using single-molecule magnets*, Nature Mater. **7**, 179 (2008). 108

[129] A. Haury, A. Wasiela, A. Arnoult, J. Cibert, S. Tatarenko, T. Dietl, and Y. Merle d'Aubigné, *Observation of a Ferromagnetic Transition Induced by Two-Dimensional Hole Gas in Modulation-Doped CdMnTe Quantum Wells*, Phys. Rev. Lett. **79**, 511 (1997). 108

[130] T. Dietl, A. Haury, and Y. Merle d'Aubigné, *Free carrier-induced ferromagnetism in structures of diluted magnetic semiconductors*, Phys. Rev. B **55**, R3347 (1997). 108

[131] K. V. Kavokin, *Coherent dynamics of localized spins coupled with a two-dimensional hole gas in diluted-magnetic quantum wells*, Phys. Rev. B **59**, 9822 (1999). 108

[132] P. Kossacki, D. Ferrand, M. Goryca, M. Nawrocki, W. Pacuski, W. Malana, S. Tatarenko, and J. Cibert, *Relaxation dynamics of ferromagnetic domains in (Cd,Mn)Te quantum wells*, Physica E: Low-dimensional Systems and Nanostructures **32**, 454 (2006). 108

[133] D. Scalbert, F. Teppe, M. Vladimirova, S. Tatarenko, J. Cibert, and M. Nawrocki, *Softening of spin resonance at low temperature in p-doped* $Cd_{1-x}Mn_xTe$ *quantum wells*, Phys. Rev. B **70**, 245304 (2004). 108